Design and Analysis of Woven Shape Memory Alloy Fabric

by

Amanda Marie Skalitzky

A thesis submitted to the Graduate Faculty of
Auburn University
in partial fulfillment of the
requirements for the Degree of
Master of Science

Auburn, Alabama
December 15, 2018

Approved by

David Beale, Chair, Professor of Mechanical Engineering
Royall Broughton Jr, Professor Emeritus of Polymer and Fiber Engineering
Ramsis Farag, Manager of Research and Testing Facilities, Center for Polymers and Composites

Abstract

Shape Memory Alloys (SMA) are smart materials that can memorize a shape and return to that shape after deformation upon the application of stress or heat. The most commonly used SMA is Nitinol (NiTi) which consists of equal parts nickel and titanium. Nitinol has two primary crystalline phases, Martensite and Austenite. The crystalline phase of Martensite occurs at lower temperatures and higher stresses whereas the crystallization of Austenite occurs at higher temperatures and lower stresses. These phases cause the material to experience two different properties: super elastic (Austenite at room temperature) and shape memory (Martensite at room temperature). Nitinol comes in many forms including wire, tubes, plates, and springs. A literature review indicates that the author has woven Nitinol wire into the first ever known Nitinol woven fabric.

The main objective of this thesis is to establish a relationship between a single Nitinol wire and woven Nitinol fabric to predict the apparent elastic modulus of the fabric. First, the wire and fabric were heat treated and aged for various temperatures and times. The heat treatment showed that as the heat treatment temperature increased, the transformation temperature(s) increased during heating and decreased during cooling. Upon the heat treatment, both single wire and fabric were experimentally tested at various temperatures, and their elastic modulus derived. Modeling for woven Nitinol fabric is initially derived from both composite analysis and fabric weaving. From the model, an equation is derived that predicts the woven fabric's characteristic, specifically the apparent elastic modulus. The analytical and experimental data were examined, and the results show that the model has a 6.45% error on average. This demonstrates that the proposed analytical model offers a useful tool for design and simulation of woven Shape Memory Alloy fabrics.

Acknowledgments

I would like to express my gratitude to my advisor Dr. David Beale for the countless hours of support, suggestions, recommendations, and encouragement throughout this master's thesis. I would like to thank Dr. Ramsis Farag for all the laboratory equipment and help with use of the machines. Additionally, I would like to thank Dr. Austin Gurley for the countless hours of support on this topic and for consistently providing feedback whenever it was needed. I would like to personally thank Anna Bozeman, Jordan Crutchfield, and Jack Glendinning for their support throughout the duration of my thesis. Finally, I would like to thank my family who has supported me throughout this process and always pushed me to be my best and to achieve my dreams.

Table of Contents

List of Tables

List of Figures

List of Abbreviations

SMA: Shape Memory Alloy

NiTi: Nitinol

SMASH: Smart Materials Actuators Sensors and Hardware

SME: Shape Memory Effect

at.%: Atomic Percentage

PM: Powder Metallurgy

HIP: Hot Isostatic Pressing

CS: Combustion Synthesis

SMP: Shape Memory Polymer

RUC: Repetitive Unit Cell

SAM: Slice array model

ANN: Artificial neural network

Nomenclature

Abbreviation	Name
M, A	Martensite/Austenite
M_s, A_s	Martensite/Austenite-start-temperature
M_f, A_f	Martensite /Austenite-finish-temperature
M_d	Martensite deformation temperature
C_M, C_A	Slope of M, A line on phase diagram
L	Total Length between yarn intersection
p	Reciprocal of the number of threads per inch
c	Yarn crimp
h	Perpendicular displacement of center line of yarn out of the fabric plane
α	Angle of inclination of that length of yarn which is out of the fabric plane
D	Sum of the warp and weft diameters
l_f	Non-stretched yarn length
l_y	Stretched yarn length
w	Warp yarns per inch
f	Weft yarns per inch
d_w	Warp Diameter
C	Cover factor
E_w, E_f	Elastic modulus of warp/weft yarn
A_w, A_f	Cross-sectional area of warp/weft yarn
A_A	Apparent cross-sectional area of unit-cell
ξ	Phase fraction
σ	Stress
T	Temperature
θ	Coefficient of thermal expansion
Ω	Transformation tensor
ε	Strain
E_M, E_A	Elastic modulus of purely Martensite/Austenite
σ_M, σ_A	Martensite/Austenite stress
A_c	Wire cross-sectional area
L_0, d_0	Initial length/diameter of the wire
υ_A	Poisson's ratio of the Austenite phase
υ_M	Poisson's ratio of the Martensite phase
$\xi_{M\to A}$	Material moving from Martensite to Austenite
$\xi_{A\to M}$	Material moving from Austenite to Martensite
K_M, K_A	Distribution of the transformation load in Martensite/ Austenite
$x_{M\to A}$	Distance from Austenite center line
$x_{A\to M}$	Distance from Martensite center line
ν	Inflection point of transformation
k	Distribution Factor

Chapter 1
Introduction & Outline

Introduction

Shape Memory Alloys (SMA) are smart materials that can memorize a shape and return to that shape after deformation upon the application of stress or heat. SMAs are often used for robotic, biomedical, and aerospace applications (Table 1) because of their unique ability to undergo large amounts of stress and strain during thermo-mechanical loading when compared to traditional metals [1, 2].

Table 1: Specific Applications of SMA's

Aerospace Applications	Robotic Applications	Biomedical Applications
Wing: [3]	Sensors: [4]	Vessels: [5]
Landing Gear: [6]	Flying: [7] [8]	Valves: [9]
Composite Body: [10]	Climbing: [11]	Catheters: [12]

The most commonly used SMA is Nitinol (NiTi) which consists of equiatomic nickel and titanium. Nitinol is the most commonly used SMA because it boasts a relatively large and controllable range of strain between the Martensite and Austenite phases which allows its use as an actuator. Nitinol actuators (single Nitinol wires) can “self-sense”, thus eliminating the need for a separate sensor to determine actuator displacement [13, 14, 15]. The Auburn Smart Material Actuators Sensors and Hardware (SMASH) lab has completed extensive research on straight Nitinol wire’s capabilities as stated above. Nitinol can be purchased off-the-shelf in many different forms besides a single wire (Figure 1) to include springs (Figure 2), tubes (Figure 3), and plates (Figure 4).

Figure 1:Nitinol Wire [16]

Figure 2: Nitinol Spring [17]

Figure 3: Nitinol Tubing [18]

Figure 4: Nitinol Plates [19]

Springs are used in optics and fire safety devices, tubes are used in catheters and stents, and plates are used to displace current aluminum and steel formed sheets [20]. At the SMASH lab, the author has woven Nitinol wire into the first known Nitinol woven fabric (Figure 5). The woven fabric form demonstrates pliability (because of its uniquely low elastic modulus and high strain to failure) and the ability to warm/heat and therefore heal the material to its original shape after damage. Applications of SMA fabric as a "passive" material could include shields, seatbelts, watchbands, and screens. Its applications as an "active" material could include robotic actuators, wearable medical and therapy devices, and self-healing shields and screens.

Figure 5: Nitinol Fabric

Outline

The main objective of this thesis is to establish a relationship between a single Nitinol wire and woven Nitinol fabric to predict the elastic modulus when the wire/fabric is both below and above its transformation temperature(s). Another objective is to determine which heat treatment temperature and aging time provides the most accurate results to the model established above. Finally, compare the results of the model when using a proof of concept experimental heating system to the results using an industry grade thermal chamber. To achieve this, the following were completed:

1. A literature review of shape memory alloys, the phase transformation, the properties of the SMA Nitinol, and the material's hysteresis (Chapter 2).
2. The impacts of the materials transformation temperature(s) based on atomic percentage of nickel and titanium in the alloy, the annealing impacts to the materials transformation

temperature(s), aging and heat treatments of the material, and the thermal cycling effects to the material.

3. A review of weaving and micromechanical, meso-mechanical and macro-mechanical modeling of fabrics.
4. A review of other SMA textiles.
5. Modeling of a single SMA wire to include an overview of the phase diagram. Both mechanical modeling and phase kinetic modeling are presented (Chapter 3).
6. Modeling for a woven SMA fabric at the macro-mechanical level initially derived from both composite analysis and fabric weaving. From the model an equation is derived that predicts the woven fabric's characteristic, specifically the apparent elastic modulus. The fabric model is based on actual weave geometry, to include the presence of open gaps and consideration of wire cross-sectional area. For simplicity, the same diameter and alloy in the warp and weft is used (Chapter 4).
7. The progression of creating woven Nitinol fabric to include the initial weaving process, hand weaving, and the use of machinery needed to create the fabric (Chapter 5).
8. A discussion of the heat treatment used in this thesis and an overview of Differential Scanning Calorimeter analysis. The heat treatment performed to both a single wire and the fabric is displayed and the results of the transformation temperature(s) of the material are presented after being calculated using a DSC instrument. After determination of the proper heat treatment needed for both a single wire and woven fabric, the heat treatment is performed, and the exact transformation temperature(s) are then calculated (Chapter 6). The proof of concept experimental heating system and industry grade thermal chamber are displayed as well as the tensile testing machine used throughout the experiments.

9. The experimental set-up for both a single wire and woven Nitinol fabric. The apparent elastic modulus is calculated using a tensile test for both the wire and the fabric when the material begins in the Martensite phase (shape-memory effect) and Austenite phase (super-elastic effect). These results are then used in the model developed in Chapter 4 and the predicted elastic modulus of the woven Nitinol fabric is found. The predicted and experimental results are compared (Chapter 7). Furthermore, a comparison using a proof of concept experimental heating system to an industry grade thermal chamber are compared and the error is calculated.
10. A discussion of the research results shows the fabric model presented in this thesis and the experimental data have approximately an average error of 6.45% across all temperatures (Chapter 8). The results when using the proof of concept experimental heating system verse the industry grade thermal chamber show an average error of 23.14%. Sources of error are discussed, and a path forward for future research is described.

Chapter 2

Background and Literature Review

Introduction

A literature review of Shape Memory Alloys (SMA) show that Nitinol, which is equiatomic nickel and titanium is the most commonly used SMA. The two different crystalline phases of Nitinol, Martensite and Austenite are discussed in detail as well as the two different properties of the material, shape memory effect and super-elastic effect. The special R-phase, which is to be avoided for this application, is described and the transformation between Martensite to Austenite which causes hysteresis to occur is detailed. Furthermore, impacts to the materials transformation temperature(s), which include the atomic percentage of nickel and titanium in the alloy, the manufacturing process, the annealing affects that occur during the manufacturing process, aging and heat treatment performed by the user, and thermal cycling effects are presented. It is found that the processes can either raise or lower the transformation temperature(s) of the alloy and determine which property the material will display at room temperature (shape memory or super-elastic).

Next, an overview of weaving and the different types of weaving processes are discussed to include the five basic motions that must occur to weave a material: warp let-off, warp shedding, weft insertion, weft beat-up, and fabric take-up. A review of micro, meso, and macro-mechanical modeling of fabrics is presented to include an overview of the oldest and most utilized model: the Peirce model. Finally, a review of other SMA textiles that exist are detailed. Upon conclusion of the literature review presented above, it is determined that this work is the first known on woven Nitinol fabric and the author has produced the first known woven Nitinol fabric.

Overview of Shape Memory Alloys

Shape Memory Alloys (SMA) are characterized by unique crystalline solid phases that can be interchanged through application of stress or heat. For example, large deformations can be recovered after slight heating induces a phase change, which returns the materials to its original memorized shape. SMA's were first discovered by Arne Ölander in 1932, but it was not until 1942 that Vernon defined the term "shape-memory" [21, 22]. Shape Memory Alloys are lightweight and great alternatives to conventional actuators. There are applications of Shape Memory Alloys used in robotic, automotive, aerospace and biomedical industries. In 1962, Frederick Wang discovered the Shape Memory Effect (SME) while working under Buehler [23]. In the shape memory effect, the alloy returns to its memorized shape through a transformation process between the materials two phases, Martensite and Austenite.

The two most common SMA's are copper-aluminum-nickel and nickel-titanium (Nitinol). However, SMAs can be created using a variety of alloys such as copper, gold, iron, and zinc. When evaluating SMAs from a price standpoint, the cheaper alloys lack stability and practicability when compared to Nitinol. When evaluating SMAs from a practical standpoint, Nitinol offers the highest number of benefits as an SMA. Therefore, the most commonly used SMA is Nitinol, which consists of equiatomic nickel and titanium. Nitinol was first discovered by William Buehler in 1959 at the Naval Ordnance Laboratory. Nitinol is the most commonly used SMA because of its low cost, strain-heat recovery, energy conversion, and ease of changing the memory-recovery temperature through alloying variation.

Nitinol has two primary crystal phases, Martensite (M) and Austenite (A) and there are three different crystalline structures of Nitinol: detwinned Martensite, twinned Martensite, and Austenite. The crystalline phase of detwinned Martensite occurs at lower temperatures and

higher stresses whereas the crystallization of Austenite occurs at higher temperatures and lower stresses [24]. The Martensite phase exhibits a tetragonal crystalline structure ($B19$ structure) and it is stable at lower temperatures (Figure 6-left). The Austenite phase exhibits a cubic crystalline structure ($B2$ structure) and is stable at higher temperatures (Figure 6-right) [25]. The twinned Martensite phase occurs at lower temperatures and lower stresses and occurs when the Nitinol cools from the Austenite phase at a relatively low stress which allows for the shifting of the Martensite crystalline lattices. When the Martensite structure realigns, it is said to be detwinned and has a high value of engineering strain when compared to the twinned Martensite phase [26]. The material can only return to the twinned Martensite crystalline structure after completely transforming to the Austenite phase and cooling without the application of stress.

A special phase that occurs upon cooling at lower stresses is called the R-phase. This phase is rhombohedral in structure (R structure) (Figure 6-middle). This structure is a distortion of the Austenite structure but does not allow for large strain transformation. The Martensite phase is desired, but the R-phase initially forms because it is kinetically superior since it has a lower activation energy. The R-phase is not desired in actuator applications because it has an extremely small recovery strain. However, the R-phase is stable once thermally cycled and has a very high fatigue life, both qualities are desired when utilizing the two-way shape-memory effect which will be discussed in detail later in this chapter [27]. The R-phase has been found to be eliminated when the material is annealed at 600 ℃ or above [28]. Another way to eliminate the R-phase is to thermally cycle the material above a certain stress level [29, 30, 31]. It should be noted that in fully annealed wires (conducted by the manufacturer), the R-phase is not present.

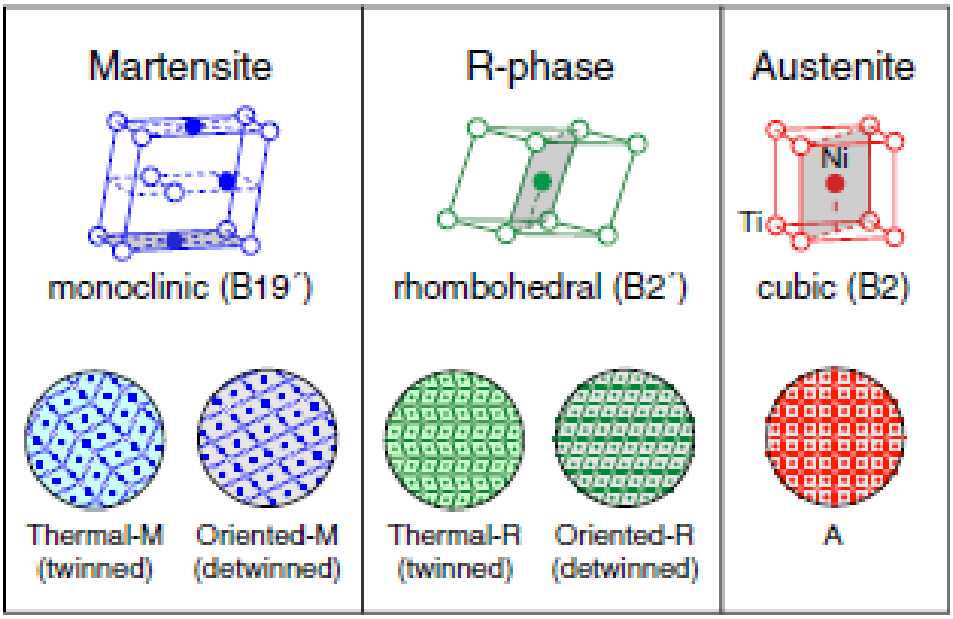

Figure 6: Crystal and microstructure of Nitinol [32]

Phase transformations between Martensite and Austenite can occur either by changing the temperature or by applying stress, regardless if the Martensite phase is twinned or detwinned. The temperature at which the phase change occurs during both heating and cooling is called the "transformation temperature(s)." When the material is heated, the Austenite-start-temperature (A_s) is eventually reached. The A_s temperature is where the transformation from Martensite to Austenite begins. As the heating induced phase transformation continues, the Austenite-finish-temperature (A_f) is reached. This is the temperature when the heating induced transformation is complete [33]. As the material is cooled, the material begins to transform back to the Martensite phase therefore resulting in the Martensite-start-temperature (M_s). When the cooling induced transformation back to Martensite is complete, the Martensite-finish-temperature (M_f) is found. The temperature in which Martensite can no longer be stress induced is the Martensite deformation temperature (M_d) and the material is permanently deformed above this temperature [34]. Two other potential transformation temperature(s) that may be found during the materials

cooling process are the R-phase start temperature (R_s) and the R-phase finish temperature (R_f). These temperatures occur before the transformation to the Martensite phase and may or may not be present in the material. The general conditions where the various Nitinol crystal phases exist are shown in Figure 10 on the Nitinol Phase Diagram.

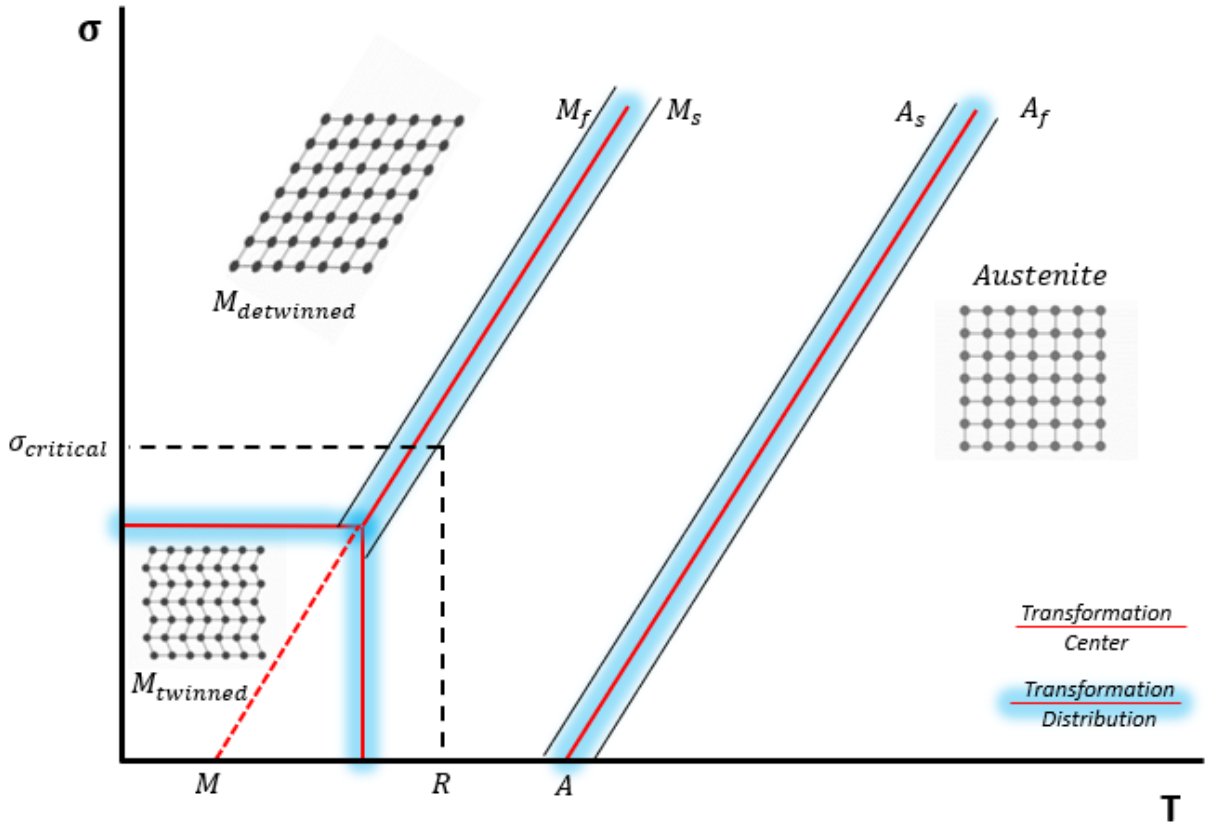

Figure 7: Nitinol Phase Diagram

Hysteresis

The gap in between the two transformation bands is called the hysteresis and occurs during cycling between the two crystalline phases. It is the measure of the difference in the transformation temperature(s) between cooling and heating and is found using:

$$\Delta T = A_p - M_p$$

A_p is the temperature at which the material is 50% transformed to Austenite upon heating and M_p is the temperature at which the material is 50% transformed to Martensite upon cooling [35]. To properly calculate the materials hysteresis, Differential Scanning Calorimeter analysis must be performed on the material. This test determines the materials' transformation temperature(s) as well as identifies if there is any presence of the R-phase in the material. Furthermore, this test can determine the amount of energy absorbed/released during heating and cooling. The test heats the material to find the A_s and A_f temperatures and cools the material to find the M_s and M_f temperatures (as well as the R_s and R_f temperature if present).

To calculate the instant at which the material is 50% transformed to the Martensite phase upon cooling, the follow equation is used:

$$M_p = M_s - M_f$$

To calculate the instance at which the material is 50% transformed to Austenite upon heating, the following equation is used:

$$A_p = A_f - A_s$$

Using DSC analysis, the tangent of the peaks during heating and cool find the transformation temperature(s): M_s, M_f, A_s, A_f R_s and R_f. The typical hysteresis range for a binary Nitinol alloy is 25-50℃ and the solid grey line in Figure 8 is the major hysteresis path. This path is a non-linear path the material follows when it is cycled between the Martensite and Austenite finishing temperatures. The arrows in Figure 8 detail the path the material takes with the red arrows describing the heating cycle and the blue arrows describing the cooling cycle.

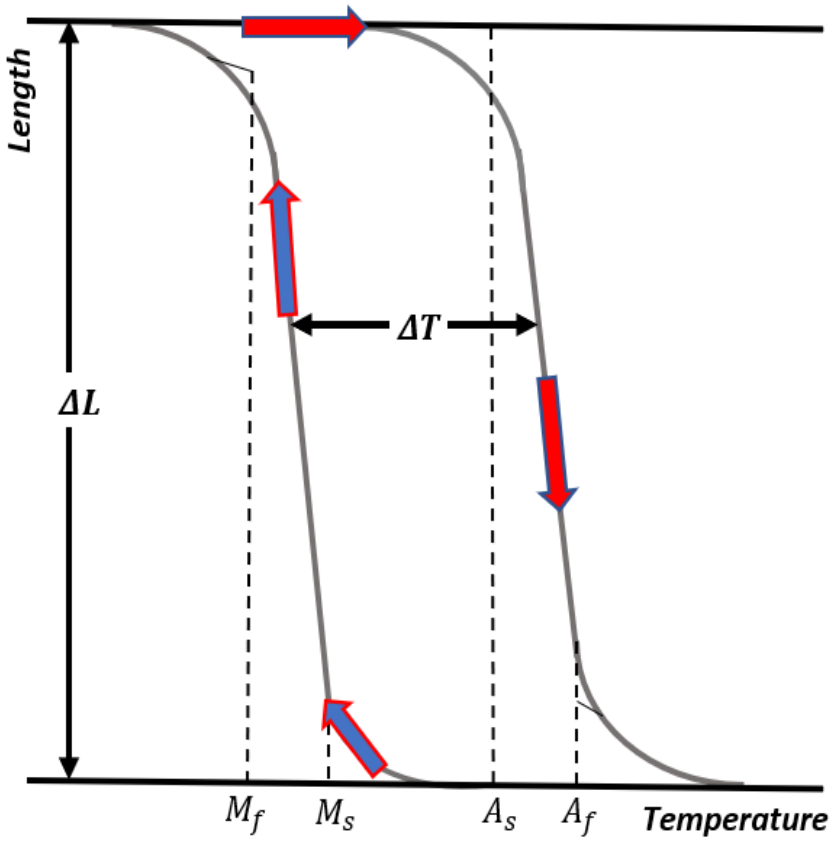

Figure 8: Length vs. Temperature in Constant Load Test for Nitinol

The hysteresis of the material is an important property because different applications may require activation properties and the hysteresis defines those properties. For an actuation application, a smaller hysteresis is desired, so the material can actuate quickly. However, for applications where the memorized shape needs a large temperature range, the hysteresis desired is much larger. The hysteresis behavior of an SMA is influenced by the transformation temperature(s), the alloy composition, and the working environment of the material.

Nitinol Properties

There are two different properties that SMA possess: shape memory and super elasticity (pseudo-elastic). Shape Memory Alloys, specifically Nitinol, are said to be super-elastic when the Nitinol is in the Austenite phase at room temperature and zero stress is applied. This property allows the Nitinol to exhibit a reversible response to applied stress without a heat source. When a stress is applied to a SMA exhibiting the super-elastic property, it transformations from the Austenite phase to the Martensite phase. When this transformation occurs, it appears as if the SMA has plastically deformed. In most materials, when a material plastically deforms, it fails. However, due to the super-elastic property of Nitinol, this deformation is not permanent and disappears upon the release of the applied stress, in which the material transformations from the detwinned Martensite phase to the Austenite phase [36]. It is important to note that the Nitinol is not actually plastically deforming, rather only going through a phase change with a super-elastic deformation.

The shape memory effect occurs when Nitinol is in the Martensite phase. While holding stress constant and cycling heat, the wire expands and contracts with the shape memory effect. When stress is applied and released to an SMA yielding this effect, it appears to have undergone permanent strain displacement. However, when the SMA is heated above its A_f temperature and then cooled at little stress, the strain is recovered. The variation in temperature causes a change in the material's crystals which leads to a large strain displacement. This shape memory effect allows Nitinol to act as an actuator. Recent research at Auburn University has shown that it is possible to control Nitinol wires as they undergo a phase change to allow for precise position control [13, 14, 15]. An overview of the shape memory effect cycle can be seen in Figure 9.

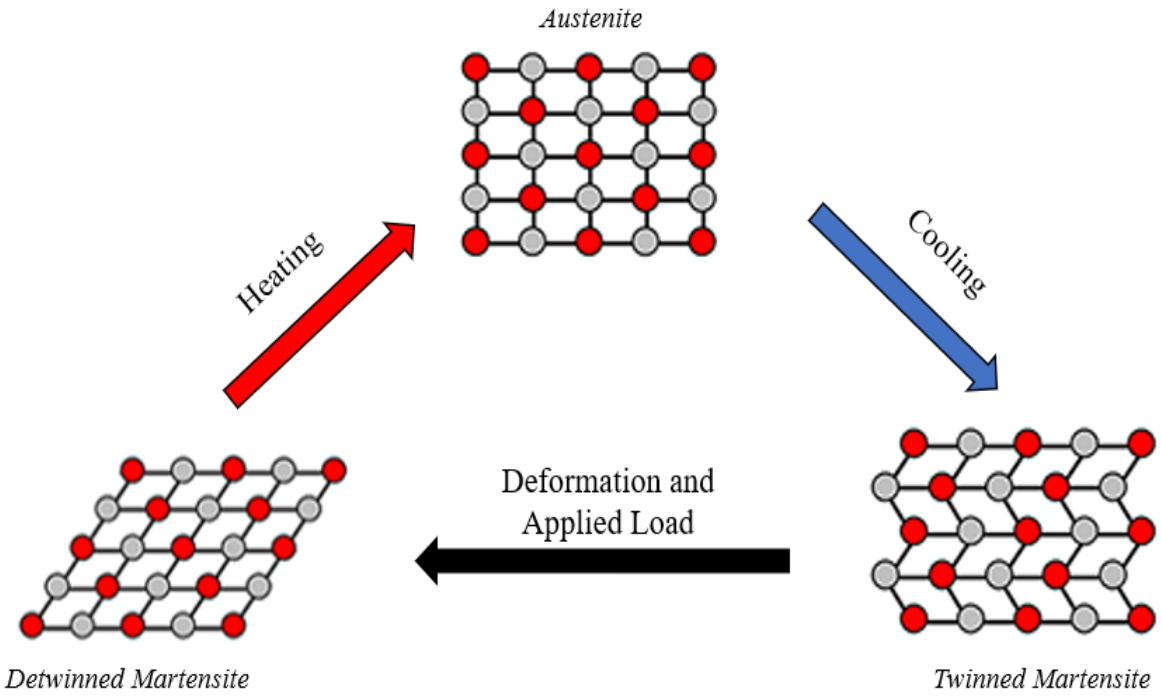

Figure 9: Shape Memory Effect of Nitinol

If the material exhibits the super-elastic effect, it will remain in the fully Austenite state until the material is loaded to its critical stress level in which the strains will no longer be recoverable. When this occurs, the transformation to detwinned Martensite will be induced. The "end use" temperature of a super-elastic material must be lower than the materials' A_s temperature or the material will begin transforming to the Martensite phase and therefore, possess shape memory properties. If this occurs, the material may not be suitable for the proposed end use. The super-elastic effect will allow the material to have reverse deformation without the use of temperature.

The shape memory effect is where the material's transformation temperature(s) is above the environmental temperature that the material will be used in. When exhibiting the shape memory effect, the material remains in the Martensite phase until stress or heat is applied. The material can transform to the Austenite phase if stress or heat is applied and when in this phase, it exhibits super-elastic characteristics. There are two different causes of transformation and they

are stress and temperature induced. Super-elasticity is stress induced and shape memory is temperature induced and the loading paths can be seen in Figure 10 and Figure 11 respectfully. It should be noted that these loading paths are not the exact ones an SMA follows but demonstrate the general path in which an SMA will take when exhibiting the super-elastic and shape memory effect.

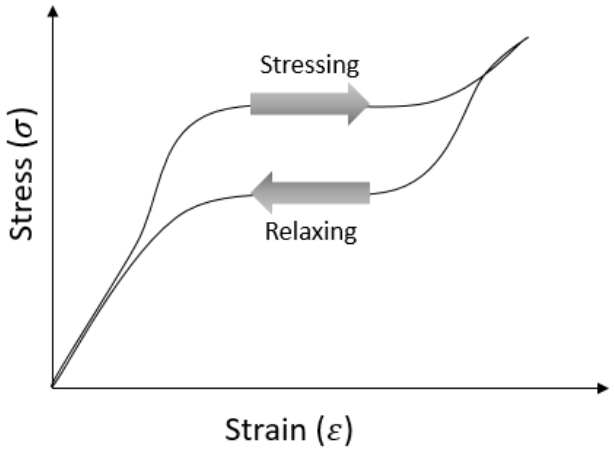

Figure 10: Stress induced loading path for the super-elastic effect

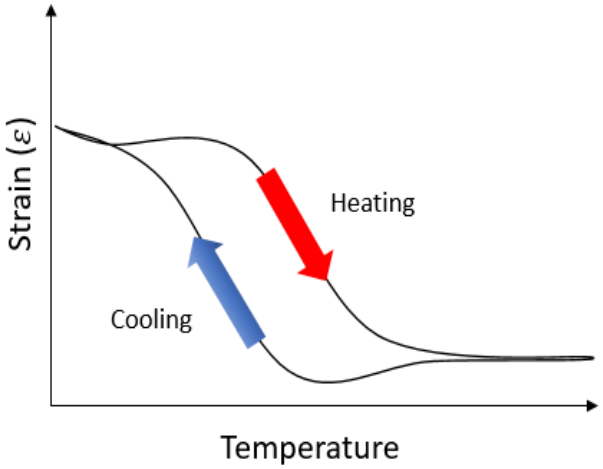

Figure 11: Temperature induced loading path for the Shape Memory Effect

The shape memory effect and super-elastic effect can be categorized into three different shape memory characteristics: one-way shape memory effect, two-way shape memory effect, and super-elasticity.

The one-way shape memory effect occurs when the material is below the A_s temperature and is deformed [37]. For the one-way shape memory effect to occur, the loading path must be considered. The loading path for the one-way shape memory effect usually follows the steps below in the following order:

1. The material is heated above the A_f temperature and cooled below the M_f temperature with zero stress to transform the material to twinned Martensite.

2. The material is loaded at a temperature in which T<M_f which causes the alloys of the material to reorient, known as detwinned Martensite. Inelastic strains are developed during this stress-induced detwinning.
3. The material is then unloaded in which T<M_f and remains in the detwinned Martensite state. The inelastic strains developed while loading the material are not recovered.
4. The material is then heated above its A_f temperature and cooled below its M_f temperature, which causes the material to transform from detwinned Martensite to Austenite and finally twinned Martensite if a low enough stress is applied. During this transformation, the inelastic strains are recovered. This change is observed macroscopically as depicted in Figure 12.

During the one-way shape memory effect, no transformation strains are induced during the cooling of the material. When using the material as an actuator, this effect requires a residual strain to be created before actuation.

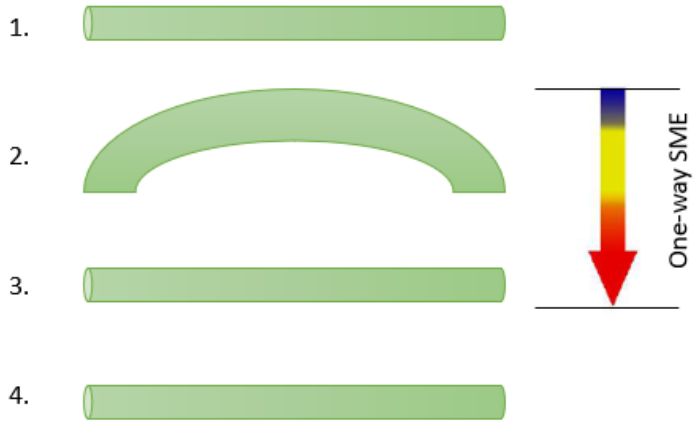

Figure 12: One-way shape memory effect: (1) Twinned Martensite, (2) Loaded and Deformed in Martensite T≤ Mf, (3) Austenite, (4) Cooled to twinned Martensite T ≤Mf

During the two-way shape memory effect, transformation strains are generated when the material is heated and when it is cooled. This allows the material to memorize two different shapes, one at high temperatures (above A_f) and one at low temperatures (below M_f) [38]. For the material to experience this effect, the material must go through a training process. There are many different training processes that can be used to for the material to experience the two-way shape memory effect. The training processes include: aging under applied stress in either the Martensite or Austenite phase, isothermal mechanical loading, or thermal cycling. The training process for the material to experience this effect is rather difficult as repeated transformations between Martensite and Austenite must occur. The effect causes the SMA to have a lower total recovery strain and changes the materials transformation temperature(s). Optimal conditions for this effect to occur requires an understanding of the amount of training cycles it takes to induce this effect. Insufficient cycling will cause the SMA to have a non-stable two-way shape memory effect and too many cycles will cause unwanted effects that reduce the efficiency of the training procedure [39, 40]. The two-way shape memory effect is desired when using the SMA for actuation because this effect does not require a residual strain to be created before actuation (Figure 13). The SMA begins in the Martensite phase. As the SMA is deformed an irreversible amount, dislocations are introduced into the material. It is at this stage where the two-way shape memory effect begins to take place. As the SMA is heated, it deforms to a certain shape. As the material is cooled, it has another trained shape in which it deforms.

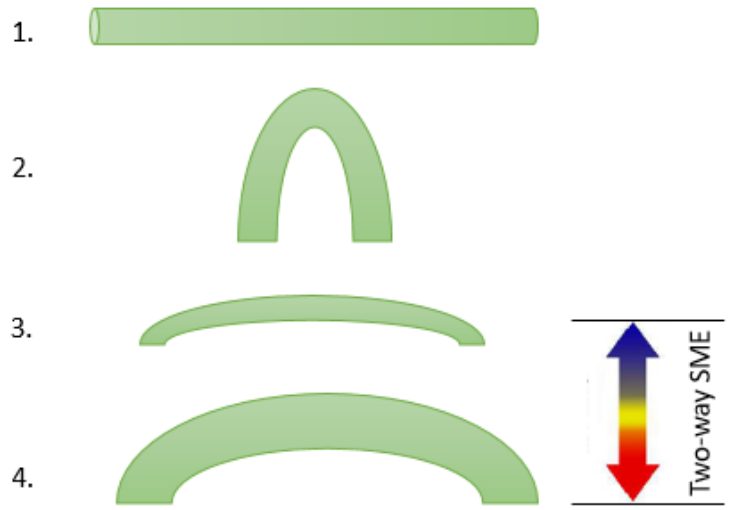

Figure 13: Two-way shape memory effect: (1) Martensite, (2) Deformation with an irreversible amount, (3) Heated, (4) Cool

In practice, the two-way memory effect can only produce strains of 1% to 2%, whereas the one-way effect can produce strains of 6% or more. The behavior exhibited by the one-way shape memory effect occurs when the material has been untrained while the behavior exhibited by the two-way shape memory effect occurs when the material has been trained. The untrained and trained SMA effects display different thermomechanical behavior [41, 42, 43]. As a result, the one-way shape memory effect is more reliable and more widely utilized in industry and the two-way shape memory effect allows for more precise actuation and is utilized in robotic applications.

Finally, super-elasticity is where the SMA will return to its memorized shape once an applied load is released. However, thermal activation is not needed with this effect. The super-elastic effect is observed when the Martensite phase transformation is induced by applying a stress or load to the material. The temperature must adhere to $A_f < T < M_d$ to ensure the inelastic strains produced are recovered upon unloading. The detwinned Martensite phase is the phase the material enters during loading. When the material is unloaded, the phase

transformation that occurs is detwinned Martensite to Austenite. The loading path for the SMA exhibiting the super-elastic effect is as follows (Figure 14).

1. The material begins in the Austenite region with zero stress.
2. Upon loading, the material transforms to detwinned Martensite so long as $A_f < T < M_d$.
3. Upon unloading, the material returns to Austenite.

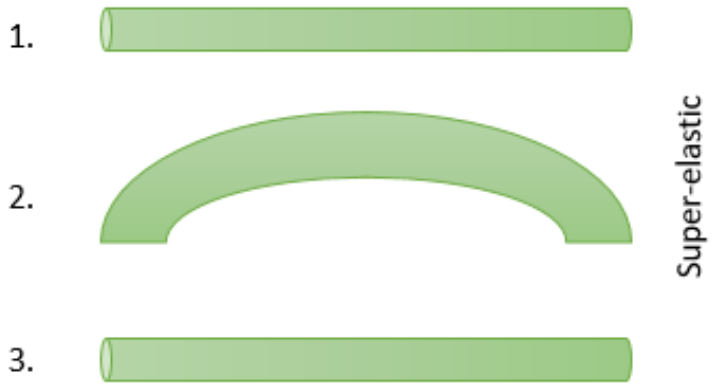

Figure 14: Super-elastic effect: 1. Austenite, 2. Loading and transformation to detwinned Martensite, 3. Unloading and transformation to Austenite

Current research conducted on single Nitinol wire exhibiting the shape memory and super-elastic effect has resulted in their properties being estimated by numerous researchers and companies [44, 45]. It has been determined that free-recoverable strain, applied stresses, and recoverable stresses are properties that are peculiar for SMA's. Nitinol, for example, can reach an 8% recoverable strain. However, if a full recovery is desired, 6% is the maximum allowable recovery strain [46]. The recovery stress for Nitinol depends upon the amount of cold-work, annealing, and overall composition of the material. The materials properties play a large role in the various effects that the material can exhibit.

Review of Nitinol Processes that affect Transformation temperature(s)

There are several factors that affect the transformation temperature(s) of Nitinol:

1. The atomic percentage (at.%) of nickel and titanium in the alloy
2. The production process for creating Nitinol
3. The annealing process of the material during the manufacturing process
4. The aging effect and heat treatment that occurs by the user
5. Thermal cycling under a constant load

The transformation temperature(s) can be measured using electrical resistivity, differential scanning calorimetry, elastic modulus, yield strength and strain, or monitoring the strain during cooling on a constant load and to measure the recovery during heating [34]. Many researchers have conducted various tests to estimate the transformation temperature(s) of Nitinol wire, plates, springs, and tubes. Although the research varies, the overall processes utilized remain the same [47, 48, 49, 50].

First, a detailed overview of the impacts of the atomic percentages of nickel and titanium have on the materials transformation temperature(s) is discussed. Next, the production process of creating Nitinol and the various techniques that can be utilized will be detailed as all impact the transformation temperature(s) of the material. The manufacturing of Nitinol into its various forms is detailed as the different forms each require different steps (as listed above) to obtain the shape-memory property, and furthermore to determine the material's transformation temperature(s). Next, the annealing process that occurs during manufacturing is detailed. Following the annealing process, once the material is purchased, the user may choose to perform an initial or additional heat treatment to the material for varying amounts of time. This process is called aging. The heat treatment performed by several researchers is examined and the results of aging and temperature are reviewed. After all the processes above are complete, the user may

need to thermally cycle the material to achieve stabilization. The stabilization in the material allows the user to determine the correct transformation temperature(s) of the material. It has been found that these transformation temperature(s) generally decrease throughout the cycling. Each process impacts the overall properties of the material and furthermore dictates the material's transformation temperature(s). All are important because the transformation temperature(s) of the material varies depending on the application of the material and must be able to be altered to some degree by the user.

Impacts to transformation temperature(s) based on Atomic Percentage

The precise amount of Nickel and Titanium is extremely important in initially setting the transformation temperature(s) range and determining if the material poses the super-elastic or shape memory effect. The atomic percentage (at.%) of nickel ranging from 49.3 to 50.3 at.% are generally shape memory, while ranges of 49.4 to 51 at.% are generally super-elastic [34]. As the percentage of nickel increases, the ductility of the material significantly decreases [51]. As the at.% of nickel is increased, the transformation temperature(s) of cold-worked wire is drastically decreased [52, 53, 54]. Figure 15 is an example of how the at.% of nickel affects the M_s temperature.

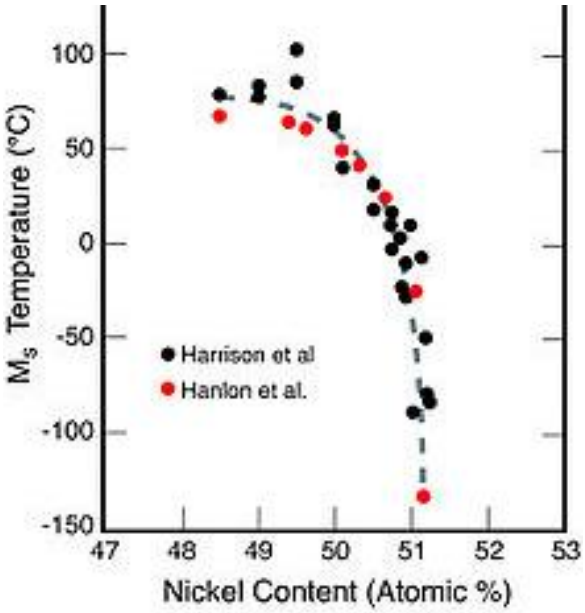

Figure 15: At.% of Ni vs. to M_s temperature [51]

Production of Nitinol and the impacts on its transformation temperature(s)

Shape Memory Alloys have been created using many techniques, but Powder Metallurgy (PM) is the most common. It is a metal processing technique that creates different metals through raw metal powders. The PM process involves using pre-alloyed powders which allows for extremely complex part geometries to be produced with extreme precision. The PM techniques that can be used until the material reaches its desired size and shape are: conventional sintering, Hot Isostatic Pressing (HIP) [55], and Combustion Synthesis (CS) [54].

Conventional sintering diffuses the elements, in this case nickel and titanium, at near melting temperatures, but it requires a long heating procedure [56]. This long heating procedure creates many voids which lowers the overall density of the material. Continuous furnaces, which are mainly used during conventional sintering, have three stages of the manufacturing process: preheat, sinter, and cool down (Figure 16). A belt that is moving carries the material through various chambers, and heat doors rapidly open and close to ensure the material passes through

successfully while maintaining accurate temperatures. The belt moves at a specific speed for each specific material to ensure the material gets ample time in each chamber.

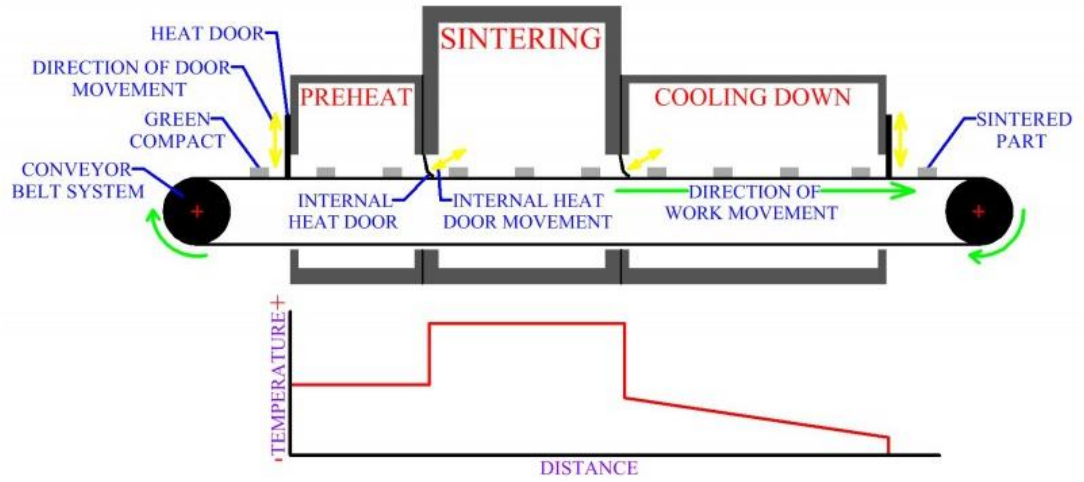

Figure 16: Conventional Sintering [57]

Hot Isostatic Pressing is a sintering technique that uses pressure and a high temperature (below the melting temperature of the material) which does not cause a decay in the overall density of the material. The material is placed inside of the work piece and the chamber is heated, causing the pressure of the vessel to increase. Depending upon the material composition, gas pumping is sometimes needed to achieve the desired pressure. This system can be seen in detail in Figure 17. It should however be noted that gas pumping does cause undesired contaminants in the alloys.

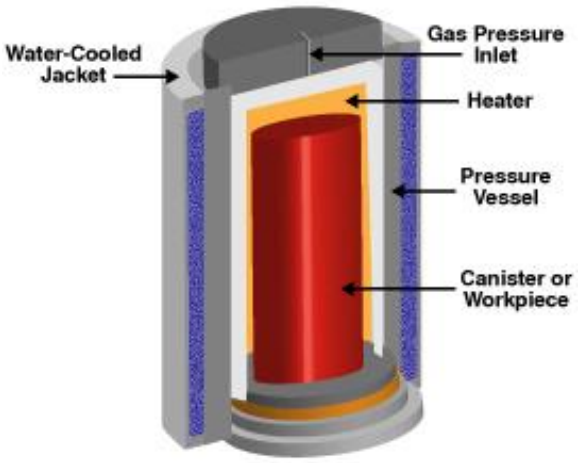

Figure 17: Hot Isostatic Pressing [58]

Combustion Synthesis is the most useful and desired method when producing Nitinol. It utilizes a chemical reaction during which heat is released through electron transfer [59]. This process is characterized by high-temperatures, fast heating rates, the ability to form any size or shape, and extremely short reaction times. These characteristics of CS result in the CS process being affordable and reliable to use during the production of Nitinol. This process in general can be seen in Figure 18.

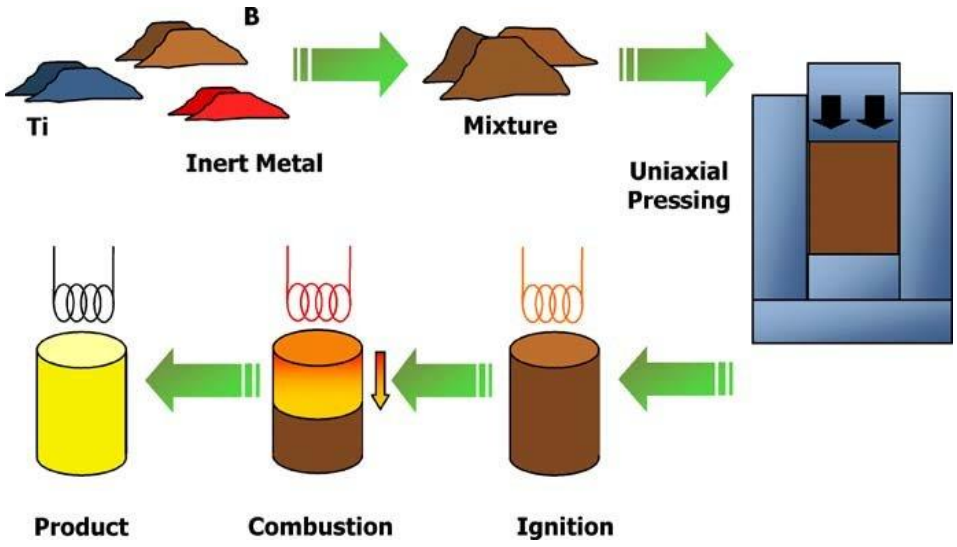

Figure 18: Combustion Synthesis [60]

Wang *et. al* states that the transformation temperature(s) is strongly dependent upon the composition of the material and the manufacturing process of the material as stated above [61]. Depending on the production method of the Nitinol sample, the transformation temperature(s) may increase or decrease with the annealing, aging, or cyclic-temperature [54].

Annealing impacts to Transformation temperature(s)

The annealing process of the material is affected by the percentage of nickel and titanium in the wire. The composition percentage of the wire is critical to know for the manufacturer to anneal the wire properly. Nickel-rich (unstable) compositions cause the M_s temperature to increase throughout the annealing process, as nickel is leached from the material [54] and titanium-rich compositions cause the opposite to happen. When the Nitinol wire exhibits the shape memory effect, the process which causes the material to memorize a shape is called a shape-set and is achieved by deforming the wire into its desired shape and then annealing the material well above its recrystallization temperature, all while maintaining the deformation. If the wire exhibits the shape memory effect, deforming it in any sort of direction and applying a heat source will bring the wire back to its "set" or annealed shape. The temperature at which the material must be annealed is a function of the alloys composition and any prior processing by the manufacturer (i.e. amount of cold work). Annealing the material at a certain temperature maximizes the amount of plastic deformation the material can tolerate and still return to its original shape [62].

Nitinol that exhibits the shape memory effect is available in many different forms such as: cold-worked, as-drawn, actuator wire, and pre-determined transformation temperature(s) and much research has been conducted on all [63] . Cold-worked is the most common as it is easily accessible and relatively inexpensive. However, a heat treatment performed by the end user must

be applied to the material to "set" the transformation temperature(s). The amount of cold work and alloy composition determines the recrystallization temperature of the alloy, which can be as low as 275 ℃ [34]. This temperature is important because during the heat treatment process, the temperature of the alloy must reach a temperature over the recrystallization temperature to properly shape-set and acquire the shape memory behavior and transformation temperature(s). The effect that the heat treatment has on cold-worked wire is the same as the thermal cycling- it lowers the transformation temperature(s) of the wire [64].

In a literature review of the most common SMA manufacturers, it is rare for manufacturers to release the details of their annealing processes due to their proprietary nature. It is known that the annealing process is conducted during the manufacturing process and can be either a full anneal in which the wires have a pre-determined transformation temperature(s), like Dynalloy Flexinol® Actuator Wire or cold-worked as-drawn which means the wire was not annealed or shape-set. If the wire is cold-worked as-drawn, the wire does not exhibit any shape memory properties [65].

Shabalovskaya *et. al* conducted an experiment on Nitinol wire that was manufactured with equal parts nickel and titanium and found that temperatures ranging from 800-1000 ℃ are required to anneal wire during its drawing process to have the material demonstrate the shape memory effect [66]. However, when a Nitinol wire is not equiatomic, the annealing process differs and is dependent on the diameter of the wire, the process used to create the wire, and the cold-work performed on the wire. It has been discovered that during production of the Nitinol, controlling the temperature at which the alloy begins to return to its previous shape is of upmost importance, but little research has been conducted on the effects of the aging process. The shape memory properties for as-drawn wire are not exhibited when the wire is initially produced. The

end user needs to either specify or perform the proper heat treatment and aging process to induce these characteristics.

Aging and Heat treatment

For this application, aging refers to the secondary process after annealing and is the amount of time a wire is heat treated, which is usually longer periods of time than the annealing cycle performed by the manufacturer. Heat treatment refers to the temperature used to introduce the shape memory properties of a wire and induce a full shape-set of the wire. Heat treatment is the same concept as annealing, however it is performed by the end user instead of the raw material manufacturer. The term "heat treatment" will be utilized if the process has been conducted by the end user and the term "annealing" will be used if the process was conducted by the raw material manufacturer.

A full shape-set to a shape memory wire means the wire will return to its memorized shape once deformed and heated and has a Martensite and Austenite start and finish temperature. Aging is where the material remains at a certain temperature for a pre-determined amount of time and once complete, the material is cooled by either quenching the material in water or another liquid or allowed to cool to room temperature on its own. The temperature at which the material is heat treated is dependent on the aging time and material's size. It has been discovered that an increased ageing time decreases the hysteresis between the R and M transformations [67]. For the material to display its transformation temperature(s) and for the elimination of the R-phase to occur, the material must be heat treated above the materials recrystallization temperature (which is determined using DSC analysis). Researchers have conducted studies on aging of Nitinol and different heat treatments and discovered that the aging time effects the M_s temperature [68, 43]. It should be noted that although most researchers have agreed upon the

general effects heat treatment and aging has on a material, the exact SMA properties differ and the results of the transformation temperature(s) differ depending on the experiment conducted.

Sadrnezhaad *et. al* conducted an experiment on Nitinol wire with 50.2 at.% nickel by aging the material for a certain period of time, varying the heat treatment from 300-600 ℃ for various durations, and quenching the material in water upon the completion of the heat treatment [54]. Their results showed that at a constant temperature, as the aging duration increased, the M_s temperature decreased. However, they only observed the M_s temperature and not all the transformation temperature(s). Therefore, their results are not considered for this literature review.

Losertova *et. al* conducted a study in which they increased the aging duration of the material and varied the heat treatment temperature from a range of 400-600 ℃ [69]. Their results concluded that the transformation temperature(s) of the material increased as the aging time increased. Eggeler *et. al* concluded that the transformation temperature(s) of the material increased as the aging time increased [70], which is consistent with Losertova's *et. al* results. During their experiment, a Nitinol wire was heat treated to 450℃. The material was aged from 0 minutes to 200 hours and DSC analysis was performed to prove the affects aging had on the materials' M_s and M_f temperature (Figure 19).

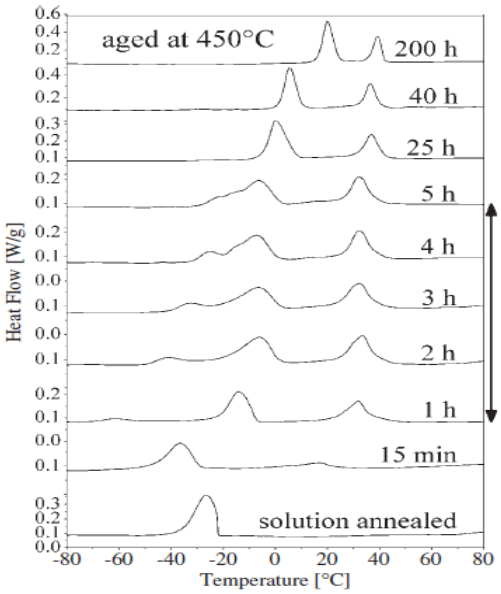

Figure 19: DSC test results for a (50.8 at.% Ni) Nitinol wire at various aging times [70]

Sadiq *et. al* performed an experiment on a Nitinol wire and concluded that the ultimate strain increased significantly as the heat treatment temperature was increased (Figure 20) [28]. They also concluded that the transformation temperature(s) generally increased as the heat treatment temperature increased (Figure 21).

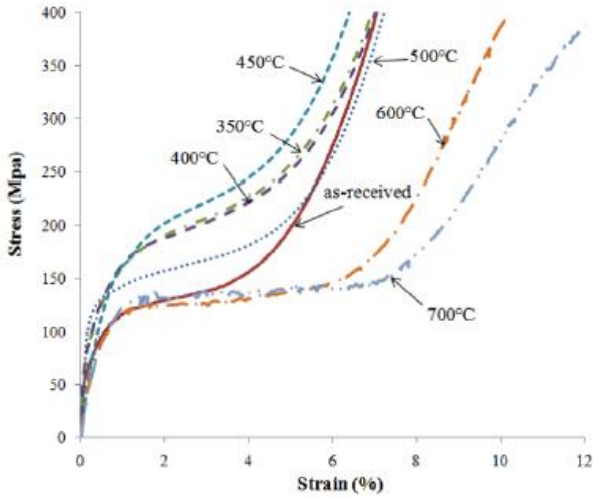

Figure 20: Ultimate Strain of Nitinol vs. Stress as the heat treatment temperature of the material increases and the aging time remains the same [28]

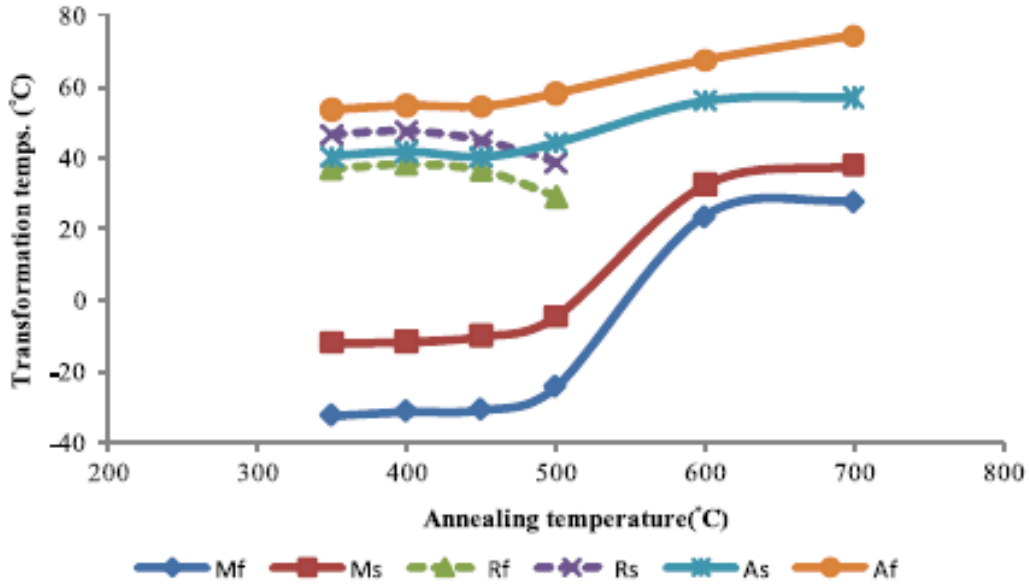

Figure 21: Effect of heat treatment temperature of Nitinol vs. the materials transformation temperature(s) [28]

Kaieda conducted an experiment in which various Nitinol wires were used that varied in the at.% of nickel [71]. He aged the various wires for two different durations and two temperatures. This aging had an impact on the transformation temperature(s) of the Nitinol with respect to both time and alloy composition. Also, when the material was aged, and heat treated at a lower time and temperature, the material was water quenched. However, when the material was aged, and heat treated at a higher temperature, it was solution treated (the specific solution was not detailed). Table 2 details his DSC analysis results of the transformation temperature(s). The aging time, heat treatment temperature, atomic percentage of nickel, and process after heat treatment all play major roles in the transformation temperature(s) of the material. It is worth noting during his work that as the atomic percentage (at.%) of nickel increased, in general the transformation temperature(s) of the material decreased (Figure 22).

Table 2: Nitinol Transformation temperature(s) Changes with various heat treatments and alloy composition [71]

Heat Treatment	Aging time	Process	at.% Ni	Mf	Ms	As	Af
510 °C	25 min	Quenched	48.9%	57°C	70°C	94°C	109°C
510 °C	25 min	Quenched	49.4%	55°C	70°C	92°C	108°C
510 °C	25 min	Quenched	49.7%	29°C	49°C	72°C	90°C
510 °C	25 min	Quenched	49.9%	4°C	15°C	49°C	64°C
510 °C	25 min	Quenched	50.1%	-18°C	-10°C	34°C	45°C
510 °C	25 min	Quenched	50.5%	-68°C	-48°C	0°C	18°C
510 °C	25 min	Quenched	50.7%	-73°C	-52°C	0°C	19°C
920 °C	40 min	Solution Treatment	48.9%	59°C	79°C	92°C	114°C
920 °C	40 min	Solution Treatment	49.4%	56°C	80°C	87°C	110°C
920 °C	40 min	Solution Treatment	49.7%	44°C	62°C	77°C	97°C
920 °C	40 min	Solution Treatment	49.9%	27°C	43°C	56°C	77°C
920 °C	40 min	Solution Treatment	50.1%	14°C	27°C	38°C	57°C
920 °C	40 min	Solution Treatment	50.5%	-23°C	-3°C	7°C	17°C
920 °C	40 min	Solution Treatment	50.7%	-53°C	-33°C	-23°C	-3°C

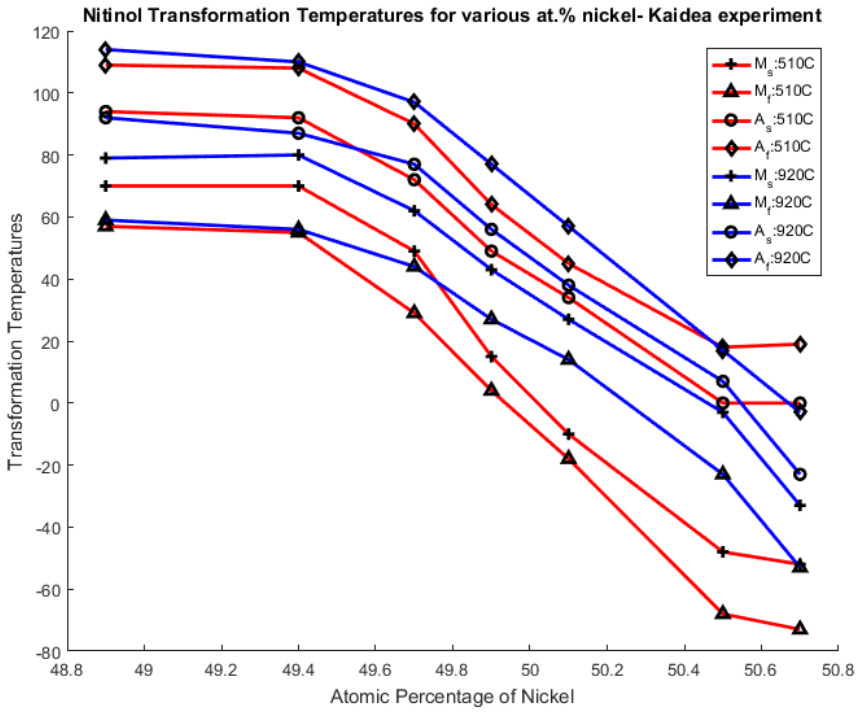

Figure 22: Nitinol Transformation temperature(s) vs. Alloy Composition and Temperature for Kaidea's experiments

Thermal cycling impacts to Transformation temperature(s)

Another important aspect in determining the transformation temperature(s) of Nitinol is thermal cycling. Thermal cycling is used to stabilize the range of motion achieved during later shape memory actuation. To perform a complete thermal cycle, the M_s and A_f temperature of the material must be known and the specimen must be cycled between these two temperatures to achieve a complete thermal cycle [55]. When performing a complete thermal cycle, it is ideal to cycle the wire under a fixed load until stabilization has been reached. However, the number of cycles it takes to stabilize a wire is dependent upon the wire's heat treatment, alloy composition, aging, and precipitates that occur in the material. In fact, the wire never really stabilizes because of the functional fatigue effect, but gets extremely close to stabilizing and therefore, the exact instance in which stabilization occurs for a single Nitinol wire has not been agreed upon [72, 73, 74]. Todoroki has found that the transformation temperature(s) of Nitinol depended on the amount of external stress applied [75]. Lagoudas and Bo found the relationship between the transformation temperature(s) and external stress was not linear [72] and is because of the variation of transformation strain with applied stress. This non-linearity causes difficulty in predicting the transformation temperature(s) therefore, the transformation temperature(s) can be measured using the techniques discussed earlier [76]. Padula performed a cycling test under fixed loads and found that approximately 100 cycles stabilized the material he was using. However, he stated that in some cases it can take up to 5,000 thermal cycles to achieve the same stabilization [77]. Although the exact number of cycles needed is dependent upon many factors, it is known that through thermal cycling, the transformation temperature(s) generally decreases throughout the cycles and eventually stabilizes. Once the material is cooled to the twinned Martensite phase and a stress is applied to it, the material elongates. This elongation gradually increases throughout the thermal cycling process until the material stabilizes [78]. In general, the

effects related to thermal cycling occur in the earlier cycles and stabilize at the completion of these cycles [79, 80]. Figure 23 demonstrates the effect of thermal cycling Nitinol wire and the effect it has on the recoverable stress.

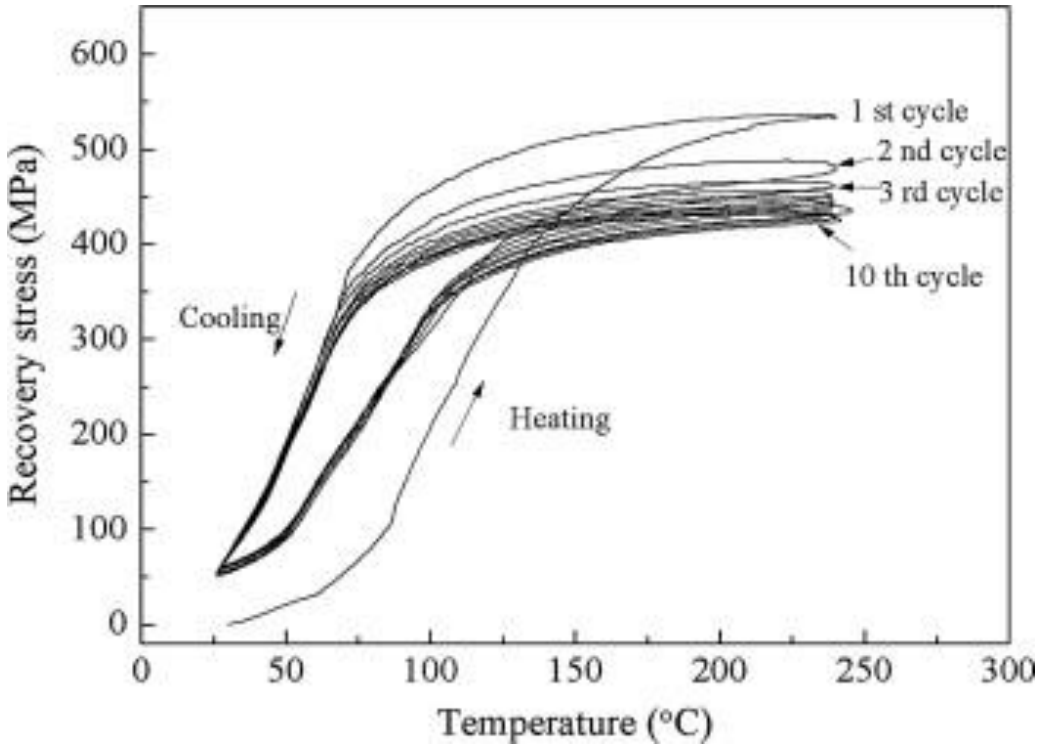

Figure 23: Effect of thermal cycling on stress of Nitinol [81]

Review of Woven Fabrics

While the textile industry has developed many different fabric manufacturing techniques such as knitting, braiding, tufting, slashing, nonwovens, and woven fabrics, the focus here is on woven fabrics and the other manufacturing techniques will not be discussed. A woven fabric is created by interlacing two directional yarns called the warp and weft yarn. The warp yarns run longitudinally throughout the length of the fabric and the weft yarns run transversely and remain there throughout the fabric-making process [82]. There are many different types of weaves [83], however the most common are the plain, twill, satin, and basket weave (Figure 24) . These types of weaves differ from one another by the amount of wires the warp skips over in the weft and vice versa.

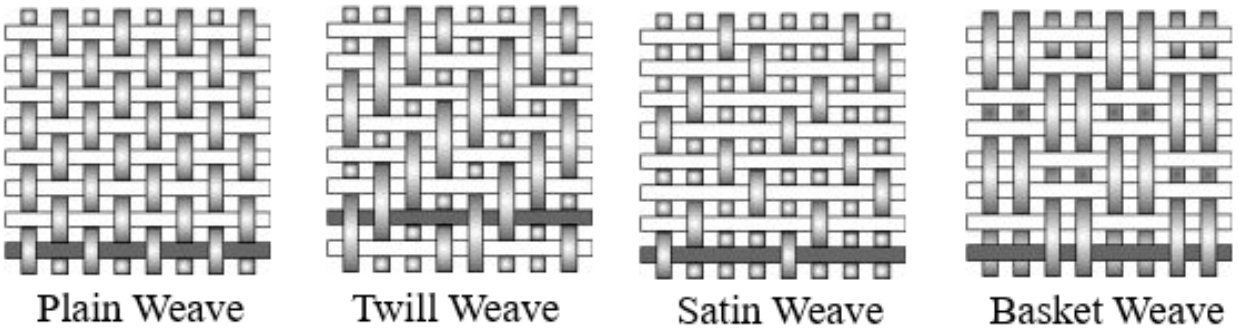

Figure 24: Various Weave Patterns

The plain weave is the simplest due to its repeating unit of interlacement. Plain weaves are extremely firm and prevent the yarn from slipping. The weave pattern for a plain weave is one weft yarn going over one warp yarn and under the next. This sequence continues to repeat until the fabric is completed. A plain weave usually utilizes yarns of the same weight in both the warp and weft direction to create a uniform appearance (Figure 25). The plain weave usually has the same fabric properties in both directions. Some benefits of a plain weave are that the weave is uniform and can be oriented in either direction and it is flexible and can produce the tightest

weave structure. The plain weave is the base-line for all other weaves as all other weaves are a modified version of the plain weave.

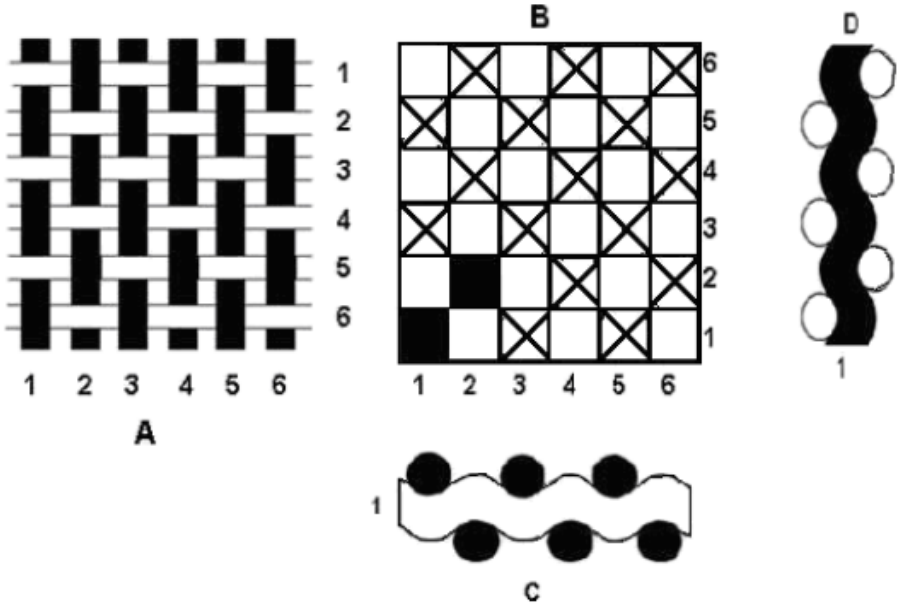

Figure 25: Plain Weave (A), Weave Representation (B), Cross-sectional view along weft (C), Cross sectional view along warp (D)

Weaving Motions

For weaving to occur, five basic motions must occur: warp let-off, warp shedding, weft insertion, weft beat-up, and fabric take-up [84]. The warp let-off is where the tension in the warp direction is controlled by a feed roller or other tensioning device in which the warp yarns extend (Figure 26) [85]. Increasing the tension of the warp causes it to lie flatter which effects the overall thickness of the fabric. The overall thickness is controlled by the crimp, which is the bending of the yarn during interlacing. The fabric is at its thinnest when the warp and weft crimp are equal and anytime they are not equal, it will increase the thickness of the fabric.

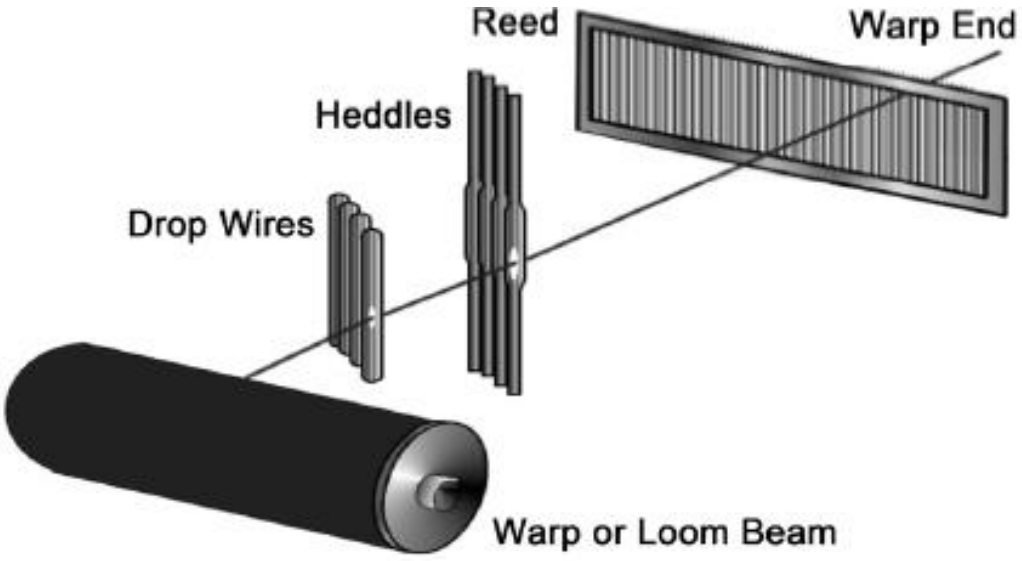

Figure 26: Warp Beam that controls tension of the warp yarns [77]

The warp shedding mechanism (Figure 27) moves the warp yarns up and down to dictate the weaving pattern that is desired [86]. Every warp yarn must be controlled throughout the weaving process using a device called a heddle. Heddles can be connected, or all be separated, but every weft yarn must be in the small eye in the middle of the heddle to ensure the weaving pattern remains the same throughout the weaving process.

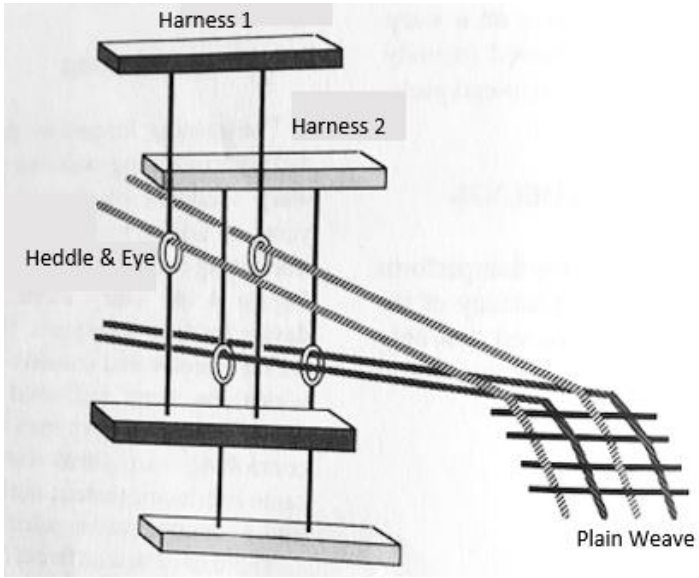

Figure 27: Elements of Warp Shedding Motion [84]

The weft insertion is where the weft yarn is placed in between all the warp yarns that have been raised and all the warp yarns that have been lowered (Figure 28). For a plain weave, every other yarn in the warp direction will be raised.

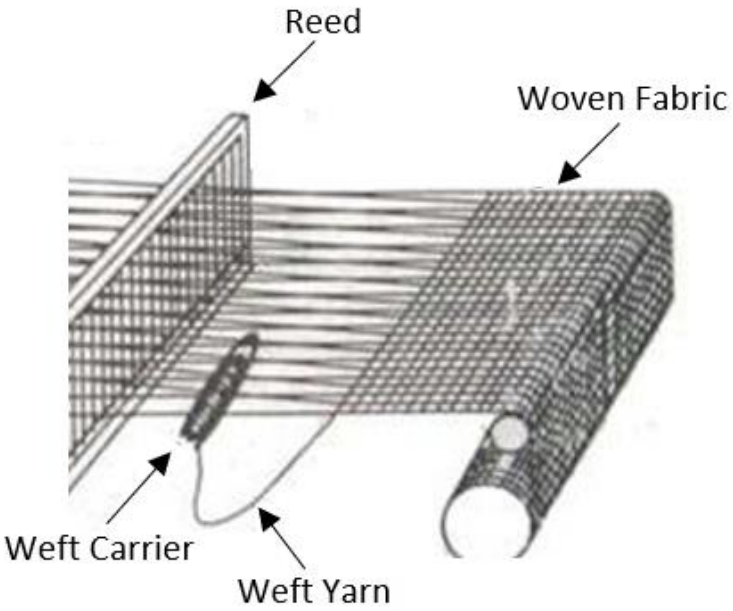

Figure 28: Weft Insertion [84]

There are many different types of weft insertions and these types factor into how weaving machines are classified. There are several different systems: shuttle, rapier, projectile, needle and jet looms [87]. The narrow fabric weaving machine is of focus here (Figure 29).

Figure 29: Narrow Fabric Weaving Machine

The weft-beat up is the next motion to define (Figure 30). The weft-beat up is where the reed pushes the weft yarns closer to each other. The spacing of the weft yarns is dependent on the picks per inch (the amount of weft wires per inch of the fabric) [88]. Also, the reed controls how close the warp wires are to one another which is expressed as ends per inch. The reed has spaced out wire blades and the number of spaces and their distances is called dents per inch.

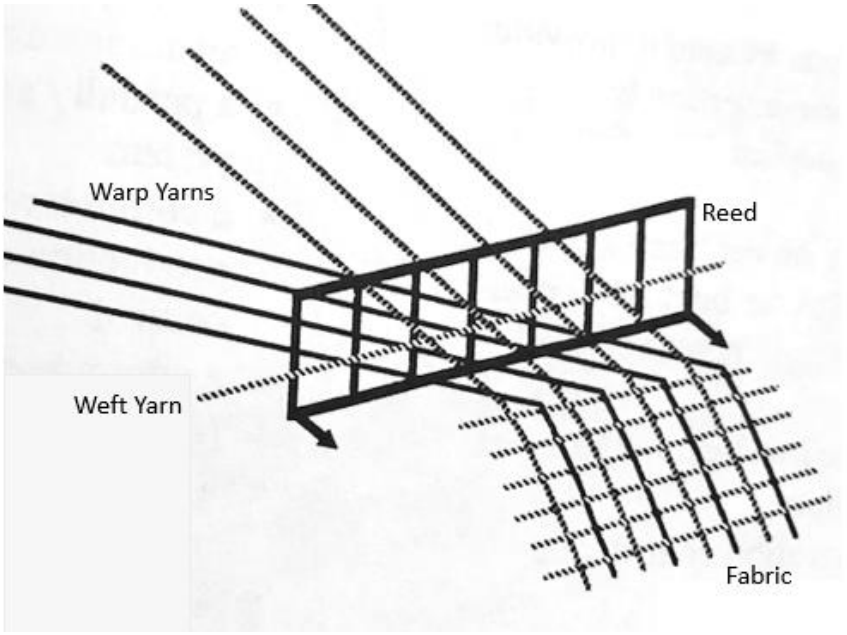

Figure 30: Weft beat-up motion [84]

Finally, the fabric take-up is where the machine removes the already created weave and moves at a speed that is determined by the number of picks per inch (Figure 31). Although these are the five main functions needed to complete a weave, there are many sub-systems associated with each that are needed depending on the machine chosen and the weave desired.

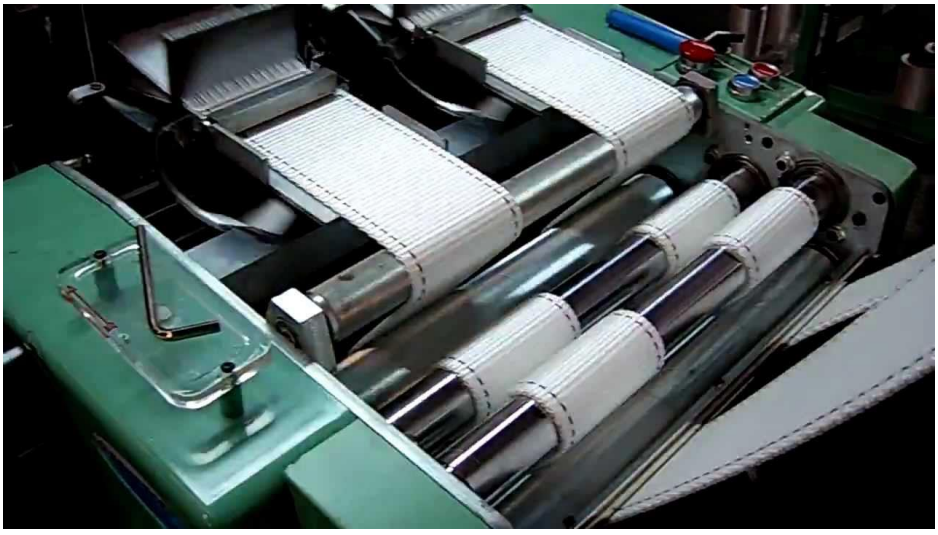

Figure 31: Fabric Take Up for a Narrow Fabric Weaving Machine [89]

Modeling Woven Fabrics

A woven fabric is a two-dimensional plane formation and it is important to know the fabrics characteristics and properties to predict behavior and potential problems with the fabric. These modeling techniques are dependent upon which properties of the fabric are known, unknown, what the model is solving for, and how precise the model needs to be. The ability to calculate the resistance a fabric has to deformation, such as extension, bending, or shear, is one reason that mechanical modeling is useful. Like many composite materials, woven fabric can be analyzed on the micro-mechanical, meso-mechanical, and macro-mechanical scales [90].

One of the first known analytical models was proposed by Peirce who assumed that the yarns were infinitely flexible and had a circular cross-section (Figure 32). Peirce's model is based on the following factors: total length of yarn between yarn intersections (L), reciprocal of the number of threads per inch (p), yarn crimp (c), perpendicular displacement of the center line of a yarn out of the fabric plane (h), angle of inclination of that length of yarn which is out of the fabric plane (θ), and the sum of the warp and weft diameters (D) [91].

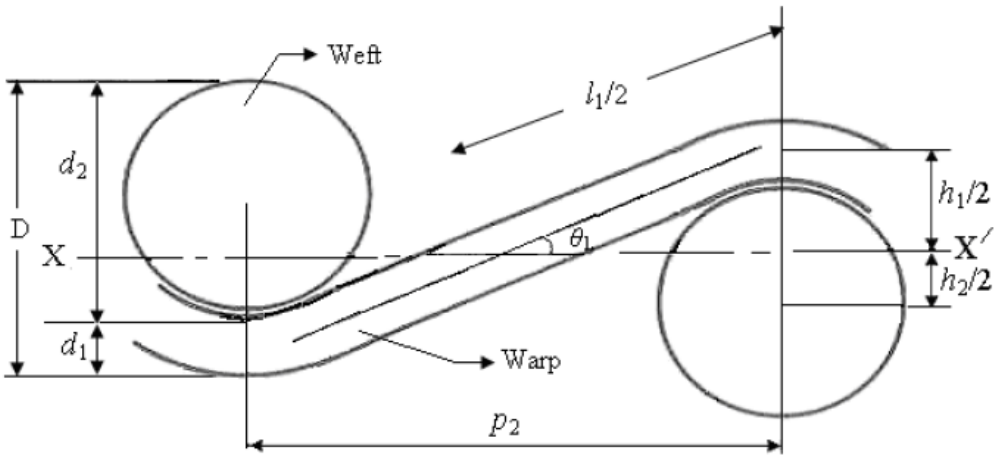

Figure 32: Peirce's unit cell for a plain weave

Micro-mechanical modeling involves using the fiber properties and yarn structure to calculate the yarn properties. The fiber properties are determined by geometric factors such as cross-sectional area, shape, length, amount of crimp, stiffness of the material and suface characteristics [84]. The yarn properties are determined by the yarn diameter, twist, cross-sectional shape, and degree of fiber compactness. Since the material utilized throughout this thesis is a single fiber, what is of importance is the cross-sectional area, length, and yarn crimp. Woven fabrics consist of various weave patterns in which the warp and weft yarn interlace and therefore one, or both of the yarns have a wavy path. The yarn crimp for both the warp and weft yarns is calculated by using the non-stretched yarn length (l_f) and the stretched yarn length (l_y) to solve for the total crimp percent ($c(\%)$) [92]:

$$c(\%) = \frac{l_y - l_f}{l_f} * 100$$

The yarn crimp is of importance because it can impact the fabrics overall geometry and result in positive or negative changes to the breaking strength, elongation, and energy absorption of the fabric. As the crimp is increased, the fabric shrinks less, is softer, and is more expensive. However, this does not happen with wire due to the stiffness of the wire.

The yarn/wire properties are then used in the meso-mechanical model to calculate the fabrics properties and appropriate unit cell. The fabric properties are determined by the fabric's weave, number of threads per inch, degree of thread packing, and the yarn crimp which are governed by the yarn properties calculated in the micro-mechanical modeling. In calculating the number of warp and weft yarns per inch, the cover factor must be calculated using:

$$C = (w * d_w) + (f * d_f) - (w * f * d_w * d_f)$$

Where the warp yarns per inch (w), weft yarns per inch (f), warp diameter (d_w), and weft diameter (d_f) all impact the cover factor (C). When the cover factor is equal to one, this means

that the maximum number of yarns have been woven into the fabric. If any more yarns are added, the yarns will begin piling on top of each other and therefore result in multiple layers of yarn in certain areas of the fabric. This is obviously not ideal and should be avoided.

The macro-mechanical model predicts the mechanical performance of the fabric [93, 94]. What is of interest is the apparent elastic modulus of the fabric which can be found using a modified version of fabric composite analysis performed by Morozov [95]. The apparent elastic modulus of the fabric is expressed in terms of the moduli of the warp (E_w) and weft yarns (E_f), cross-sectional area of the warp (A_w) and weft yarns (A_f), and apparent cross-sectional area of the unit cell (A_A):

$$E_a = \frac{E_f A_f + E_w A_w}{A_a}$$

This model becomes more complex and takes into account the angle of the slope in the warp direction. Also, the shear modulus and Poisson's ratio must be known in order to successfully utilize this model. Overall, modeling woven fabrics can be extremely complex if modeling from the micro to macro-mechanical level. In general, modeling usually only occurs at one level and this thesis utilizes the macro-mechanical model which is detailed in Chapter 4.

Shape Memory Alloy Textiles

This work is not the first SMA textile that has been studied. SMA textile actuators have been studied for medical and consumer applications. Those applications include braided heart stents, SMA yarn, and knitted SMA. This section will review the SMA textiles that have been studied and give an in-depth explanation for each.

Heart stents are braided SMA's that are used in the medical industry. Braiding is formed by the diagonal intersection of yarns. Braiding does not require any warp or weft yarns, beat-up, heddles, or reeds. It is the simplest form of textile creation. Braided heart stents are placed in veins and arteries inside of the heart to re-open them if they are clogged (Figure 33). These SMA heart stents are made up of Nitinol and are in the super-elastic form at body temperature. They have excellent bending flexibility and do not kink when forced into a tight radius, such as an artery or vein [96].

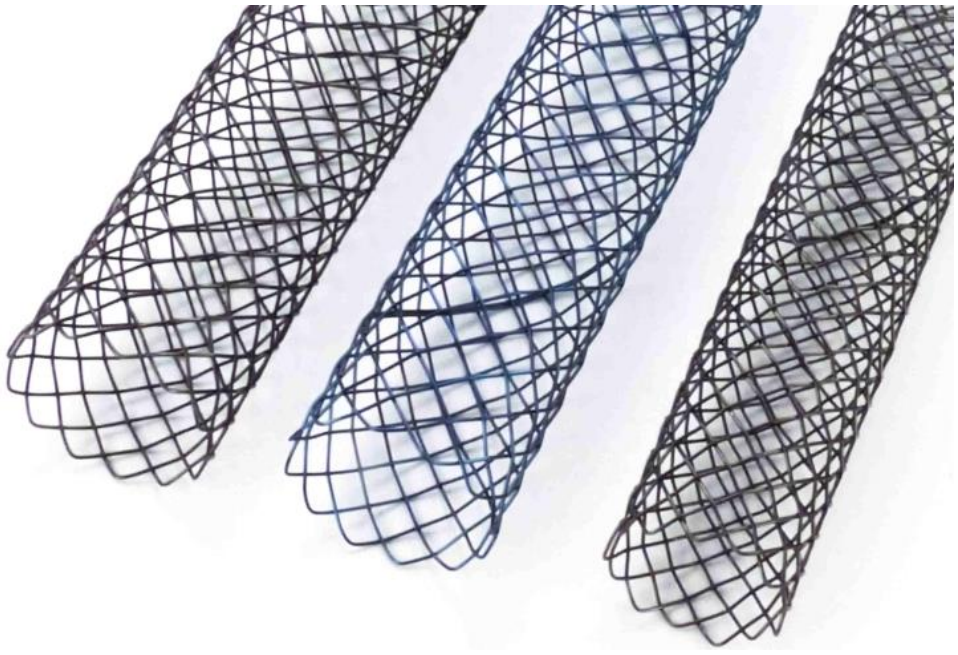

Figure 33: Braided Heart Stents [96]

Another SMA textile that has been studied is the SMA yarn [97]. This yarn takes a single Nitinol wire, heat treats and ages the wire to produce a full shape-set before applying the yarn to the desired structure. In this case many SMA, wires and natural fibers were intertwined (Figure 34). This allows for a normal fabric look with enhanced capabilities. These smart woven textiles can move into desired shapes when stimulated (Figure 35), however the transformation temperature(s) of the material matters as most materials could catch fire if the transformation temperature(s) is too high.

Figure 34: Yarn SMA

Figure 35: Interlaced SMA into Normal Fabric

The last SMA textile is a knitted SMA textile. Knitting is a process where a single fiber is interlaced into various rows of loops pulled from a spool of wire. Knitting creates loops that are bound together by other loops [98]. Knits and weaves are often found in the same textile product applications and have some major differences. The stability of a weave is far greater than a knit and the weave is more durable than a knit [99]. Therefore, knitting is preferable when a pliable material is desired, while weaving is preferred when a tight interlacing material is required for strength and stability.

It was concluded that there have been no studies or research completed on woven SMA fabric. The following chapters will detail the modeling, creation, and experimentation that occurred to weave the first ever SMA fabric.

Conclusion

As discussed above, Shape Memory Alloys, specifically Nitinol can memorize a shape and return to that shape upon the application of heat or stress. There are two different phases of Nitinol, Austenite and Martensite with three different crystalline structures: twinned Martensite, detwinned Martensite and Austenite. These phases cause the material to experience two different properties: super elastic (Austenite at room temperature) and shape memory (Martensite at room temperature). The transition temperature(s) of the material are dependent upon the materials atomic percentage of nickel and titanium as well as the Powder Metallurgy process in which they were created. Furthermore, the amount of cold work, annealing process, heat treatment, and aging all affect the transformation temperature(s) of the Nitinol. It has been shown that when Nitinol is thermal cycled enough times, it can become stable and its transformation temperature(s) remains the same once stabilized.

An overview of woven fabrics, specifically the plain weave, was presented and modeling from a micro, meso, and macro-mechanical level were shown. These are all initially based off Peirce's woven fabric model created in the 1930's and are still used today. A review of other SMA textiles was presented. Ultimately, it was concluded that the author has created the first known woven Nitinol fabric.

Chapter 3
Modeling of Single SMA Wire

Introduction

Although modeling of a single SMA wire is used for actuator applications, it is imperative to detail the process in which a Nitinol wire can be model. Modeling of a single SMA wire includes mechanical modeling and phase kinetic modeling. The models can estimate the single wires elastic modulus and other properties when the Martensite phase fraction (ξ) is known or calculated using data from DSC analysis. A discussion of the phase diagram used to depict the various properties of Nitinol is discussed in depth. Ultimately, these models will not be used to predict a single wire's elastic modulus for this thesis since wire being tested is either purely Martensite or purely Austenite meaning the phase fraction is 0 or 1.

Overview of SMA Modeling

Shape memory alloys can transform between two different crystalline phases, Austenite and Martensite depending upon the application of stress or temperature. As seen in the phase diagram (Figure 36), there are two bands referred to as transformation bands and are the active regions for transformation. These transformation bands denote the region between M_s and M_f temperatures as well as A_s and A_f temperatures. By cooling or applying stress, a SMA can transform by crossing the Martensite transformation band. If stress is relieved or heat is applied, the material can cross the Austenite transformation band. Lines M and A define the midpoint of transformation (50%) between Martensite and Austenite. The slope in which the Martensite and Austenite lines occur are denoted by C_M and C_A respectively, and C_R is the slope of the R-phase. There is a large gap in between the two bands in which the material can be a mixture of the two

phases. If stress is not applied or the temperature is extremely low, the material can enter the Martensite twinned state.

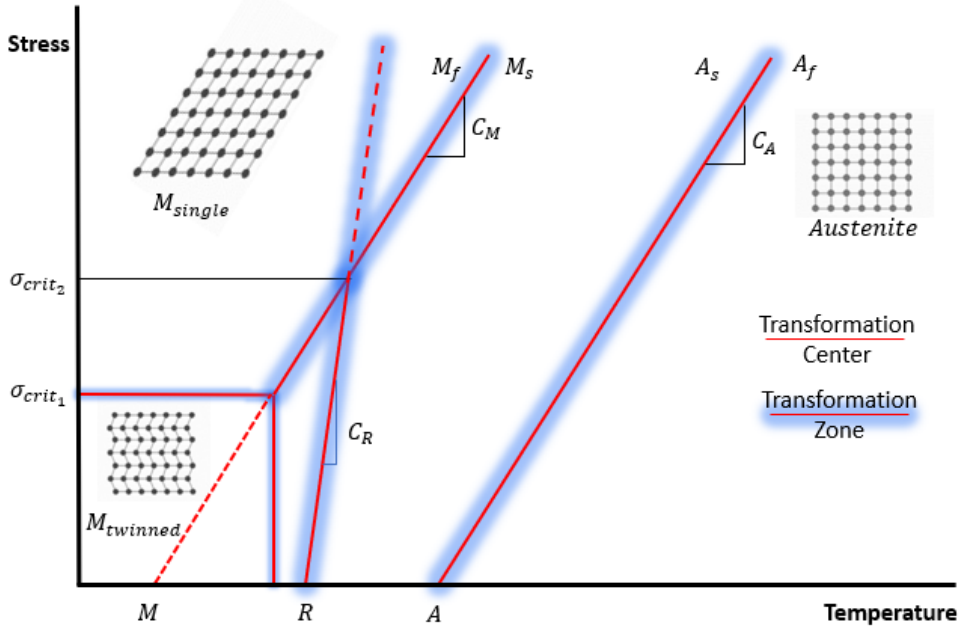

Figure 36: Phase Diagram of Nitinol with the transformation bands

A single SMA wire does not instantly transform from one phase to the next. Therefore, the percentage of each phase at any given instance is denoted by the phase fraction, ξ, which is the detwinned Martensite phase fraction bound by $0 \leq \xi \leq 1$. When stress is cycled, and temperature is held constant (below the transformation temperature(s) of the material), the material moves from twinned Martensite to de-twinned Martensite. However, when the stress is released from the material, it seems to have plastically deformed. This is because the material did not return to twinned Martensite, but rather detwinned Martensite. When temperature is applied, the material transformations to the Austenite phase and once cooled back to the twinned Martensite phase. This complete cycle is defined as the shape memory effect. As seen in Figure 37, as the material is heated from Martensite to Austenite, the temperature increases while the

phase fraction decreases. As the material is cooled from Austenite to Martensite, the temperature decreases while the phase fraction increases.

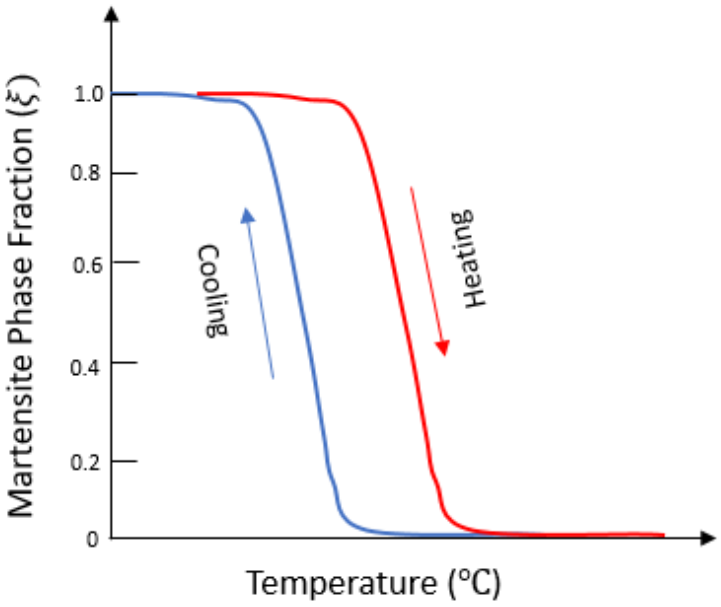

Figure 37: Variations in the Martensite Phase Fraction vs. Temperature

Although the models discussed below are for actuators, the wire utilized throughout this thesis is high-temperature actuator wire. Therefore, the models presented are useful in estimating the wires elastic modulus if the wire will be transforming in between phases. The work completed in this thesis keeps the wire in purely Martensite or purely Austenite form. Therefore, the phase fraction remains 0 or 1 respectfully. However, it is appropriate to examine the models used to predict the wires elastic modulus if the phase fraction is between 0 and 1.

Mechanical Modeling

Tanaka [100] presented the earliest form of a mechanical model for a super-elastic SMA expressed as:

$$\dot{\sigma} = E(\xi)\dot{\varepsilon} + \theta(\xi)\dot{T} + \Omega(\xi)\dot{\xi}$$

This describes the wires stress (σ) as a function of the temperature (T), coefficient of thermal expansion (θ), transformation tensor (Ω), phase fraction (ξ), and strain (ε). The proposed model above is a thermodynamic model. Liang and Rogers [101] state that the model above is only consistent if the transformation tensor is the stress associated with the phase transformation:

$$\Omega(\xi) = -\varepsilon_L E(\xi)$$

This model neglects the stress applied from the mechanical system. It also states that the strain (ε_L) associated with the phase transformation has no elastic deformation. The elastic modulus, coefficient of thermal expansion, and the transformation tensor are constant for each individual phase; however, they differ as the phase fraction changes. It has been noted that this model does not differentiate between the twinned and detwinned Martensite phase, but for simplicity this will not be investigated further.

The modeling choice impacts the elastic modulus of the wire. However, there are two other ways of modeling the problem:

1. Modeling the two crystalline phases as springs in parallel
2. Modeling the two crystalline phases as springs in series

If the phases are modeled in parallel they will have identical strain whereas in series, they have identical stresses. Gurley has shown that the choice of the parallel or series model only has a small impact on the system inside of the transformation region, therefore the parallel model will be looked at more closely [102].

The parallel model, also known as the Voigt model, proposed by Ikuta [103] views the two crystalline phases as springs in parallel where:

$$\sigma = (1-\xi)\sigma_A + \xi\sigma_M = (E_A(1-\xi) + E_M\xi)\varepsilon$$

The elastic modulus of the purely Austenite phase is denoted by E_A and the elastic modulus of the purely Martensite phase is denoted by E_M. Furthermore, the stress of the Austenite phase is denoted by σ_A and the stress of the Martensite phase is denoted by σ_M.

A model was developed by Brinson and Huang [104] that represented the above model by solving for the wires overall strain with respect to its elastic deformation, transformation strain, and thermal expansion such that:

$$\varepsilon = \frac{\sigma}{E(\xi)} - \varepsilon_L E(\xi) + \frac{\theta(\xi)}{E(\xi)}(T_0 - T)$$

The overall strain of the actuator can be represented by the equation above where T_0 is a reference temperature.

The elastic modulus must be allowed to change with respect to the phase fraction to obtain accurate results. Representing the phases as springs in parallel, the Voigt model yields an effective elastic modulus denoted by:

$$E = (1 - \xi)E_A + \xi E_M$$

By taking the equation above, the phase fraction can be found:

$$\xi = \frac{E - E_M}{E_M - E_A}$$

To incorporate small wire diameters, it is accurate to convert the model to an actuator model. This model utilizes the cross-sectional area (A_c), wire length (L), and wire diameter (d). The wire's geometry is a function of the Poisson's ratio (υ) and strain of the material (ε) [105]:

$$A_c = \frac{\pi}{4} d^2$$

$$L = L_0(1 + \varepsilon)$$

$$d = d_0(1 + \upsilon\varepsilon)$$

The subscript "$_0$" indicates the initial condition of the material. The Poisson's ratio is dependent on the crystalline structure of the material and therefore has been found to vary from 0.41 for the crystalline structure of the Martensite phase to 0.30 for the crystalline structure of the Austenite phase. Due to the different phases, the Poisson's ratio can be found as a function of the Martensite phase fraction using the Voigt model:

$$\upsilon = (1 - \xi)\upsilon_A + \xi\upsilon_M$$

The Poisson's ratio for Austenite is denoted by υ_A and the Poisson's ratio for Martensite by υ_M.

Phase Kinetic Modeling

Phase kinetic modeling explains how the phase fraction changes over the transformation period as a function of temperature and stress. The phase diagram is used to determine when the transformation is going to occur in a model. Many models exist that model the transformation conditions by the start and end transformation temperature(s) [104, 106]. If the assumption is made that the transformation temperature(s) are viewed as endpoints of a transformation region, then a simplistic model can be used so that the transformation conditions of a SMA are based on directionality of temperature and stress which are perpendicular to the transformation boundaries [101] such that:

$$if \begin{Bmatrix} \dot{T} - \dfrac{\dot{\sigma}}{C_A} > 0 \\ \dot{T} - \dfrac{\dot{\sigma}}{C_M} < 0 \end{Bmatrix} then \begin{Bmatrix} \xi_{M\to A} \\ \xi_{A\to M} \end{Bmatrix}$$

The term $\xi_{M\to A}$ denotes the material moving from Martensite to Austenite and $\xi_{A\to M}$ denotes the material moving from Austenite to Martensite.

Models can be explicitly bound within the transformation region to the distance of the transformation boundaries and are called bounded models:

$$x_{A\to M}^{bounded} = \frac{(T - \frac{\sigma}{C_M} - M_s)}{M_s - M_f}$$

$$x_{M\to A}^{bounded} = \frac{(T - \frac{\sigma}{C_A} - A_f)}{A_f - A_s}$$

The bounded model that is most simplistic is where the Martensite phase fraction is the distance across the boundary [107]:

$$\xi_{A\to M} = x_{A\to M}^{bounded}$$

$$\xi_{M\to A} = x_{M\to A}^{bounded}$$

Models that view the transformation as a smooth distribution throughout are called distribution models. The distribution from the Martensite center line ($x_{A\to M}$) and the distribution from the Austenite center line ($x_{M\to A}$) can be found where K_M and K_A are calculated using DSC analysis as they determine the distribution of the transformation load [108]:

$$x_{A\to M}^{distributed} = K_M(T - \frac{\sigma}{C_M} - M)$$

$$x_{M\to A}^{distributed} = K_A(T - \frac{\sigma}{C_A} - A)$$

The boundaries of transformation are denoted on Figure 38 with all parameters measured at zero stress. Both the bounded and distributed transformation load are labeled as well as the slope of the Martensite and Austenite finish temperatures.

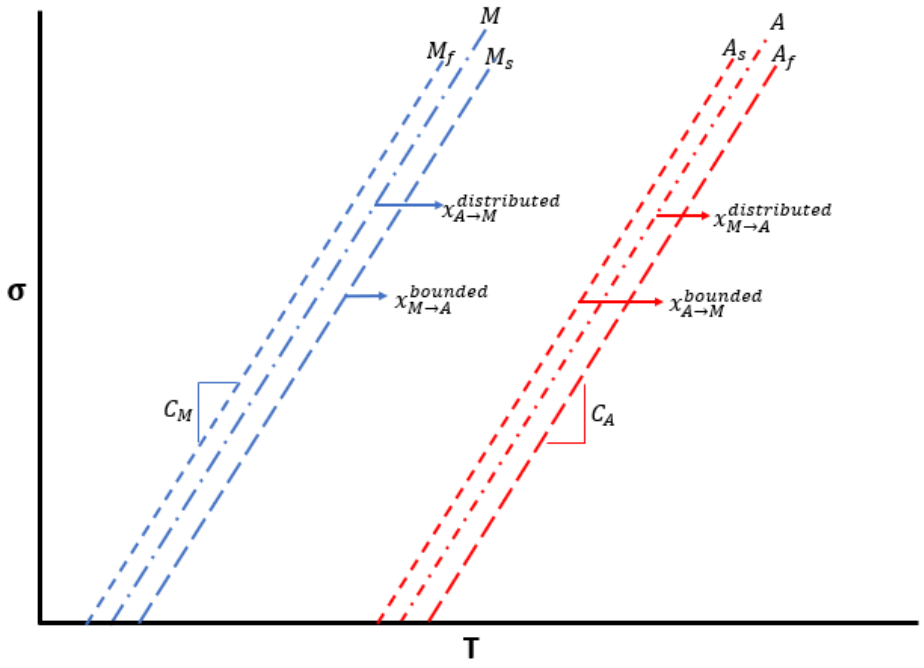

Figure 38: Temperature-Stress Phase Diagram denoting the transformation boundaries

Furthermore, Zotov *et. al* found that Martensite to Austenite transformation can be modeled and Gurley found the same modified exponential model would work for the Austenite to Martensite transformation [109, 15]. The logistic function, which is commonly used in population growth modeling, is bounded between 0 and 1 for all values of stress and temperature and phase fraction can be modeled as:

$$\xi_{M\to A} = \frac{\xi_M}{(1 + v_A \exp(k x_{M\to A}^{distributed}))^{\frac{1}{v_A}}}$$

$$\xi_{A\to M} = \frac{1 - \xi_A}{(1 + v_M \exp(k x_{A\to M}^{distributed}))^{\frac{1}{v_M}}} + \xi_A$$

The transformation center offset parameters v_A and v_M can be solved using data gathered from DSC analysis. The hysteresis parameters are ξ_M and ξ_A, which store the phase fractions as the temperature reverses direction.

$$\xi_{M\to A}, \xi_A = \xi$$

$$\xi_{A\to M}, \xi_M = \xi$$

The constant k can be calculated by the A_f and A_s boundaries. For simplicity, the assumption that $k = \frac{\nu}{2}$ is sufficient. The inflection point of transformation can be solved for ν using the following equations:

$$\frac{A_f - A_s}{A - A_s} = (v_A + 1)^{\frac{1}{v_A}}$$

$$\frac{M_s - M_f}{M - M_f} = (v_M + 1)^{\frac{1}{v_M}}$$

It should be noted that there are empirical models that relate the phase fraction to temperature and stress have been developed experimentally. The experiments performed were a tensile test and thermal cycling test for more precise modeling [110]. However, the models presented are more than accurate to explain how the Martensite phase fraction changes during the transformation period based on the temperature and stress applied.

Conclusion

Modeling of a single SMA wire was shown and it was determined that the wires elastic modulus can be predicted when the Martensite phase fraction is known or calculated through DSC analysis. An overview of the Nitinol phase diagram was presented and the phase's impacts on the Martensite phase fraction were shown. Ultimately, it was concluded that the modeling presented above will not be used to estimate the wire utilized throughout the experimental testing in this thesis since the material remains fully Martensite or fully Austenite throughout testing, which makes the phase fraction 0 or 1 respectfully.

Chapter 4
Modeling Woven SMA Fabric

Introduction

For this thesis, a unit cell model is developed based off many models to include Naik and Ganesh's slice array model (SAM) for a plain weave [111]. The model uses repetitive unit cell (RUC) analysis which takes the smallest repetitive unit of the fabric and models it, so the fabrics properties can be predicted. The fabric model presented makes a few assumptions to include that the elastic modulus of a single wire is the same in the transverse and axial direction, the cross-sectional area of the wire is circular, the weft wire is completely straight throughout the fabric, and the angle at which the warp yarn is in relation to the weft is the same throughout the fabric. These assumptions allow a fabric model to be created which accurately predicts woven Nitinol fabric's elastic modulus. The model considers the area of a single wire, the area of the unit cell, the elastic modulus of a single wire, and the slope of the warp yarn in relation to the weft. Ultimately, the model developed accurately predicts the elastic modulus of the fabric in the warp direction.

Macro-mechanical Modeling

Peirce created the first known geometric fabric model in which he made many assumptions to include that the yarns were infinitely flexible, and they had a circular cross-section [91]. When manufacturing a fabric, Hearle discovered that the shapes of the cross-sections for the yarns were not actually circular and created a model which accounts for the non-circular cross-sections of the individual yarns in both the warp and weft direction [112]. Ishikawa and Chou then developed three different models to predict the elastic moduli of a plain woven fabric: the mosaic, crimp and bridge model [113, 114, 115]. The mosaic model does not

focus on the undulation of the warp or weft yarn. The crimp model considers the undulation of the warp yarn only. The bridging model is used mostly for satin weaves and is a combination of the two models stated above. All three models require the assumption of iso-stress or iso-strain conditions. This means that all materials in the woven fabric will have the same stress or strain. Ito and Chou further developed the model above by considering the phase shift between different layers of a laminate [116, 117].

Even though the plain weave is the least complicated weave, several assumptions are made to create an analytical model that accurately predicts woven fabric textiles characteristics. A few of the assumptions made throughout various fabric models include using circular geometry of the strand, considering the undulation of the strand in only one direction, and modeling the fabric in one or two dimensions [111, 118, 119].

As stated above, Ishikawa and Chou investigated the non-linear behavior of woven fabric composites. Although the Nitinol fabric is not a composite as the definition of a composite is two different materials, the matrix, which is present in composites can be assumed to be "0" in terms of stiffness. They developed three different theoretical models and the fiber undulation model, which considers the effect of yarn continuity provides a two-dimensional analysis for simulating the behavior of plain weave composites

The model developed will utilize the following assumptions and the unit cell for the fabric can be seen in Figure 39:

1. The elastic modulus of a single wire is the same in the transverse and axial direction
2. The cross-sectional area of the wires is circular
3. The weft wire is completely straight and does not affect the overall stiffness of the fabric

4. The angle at which the warp yarn is in relation to the weft is the same for every section of the fabric

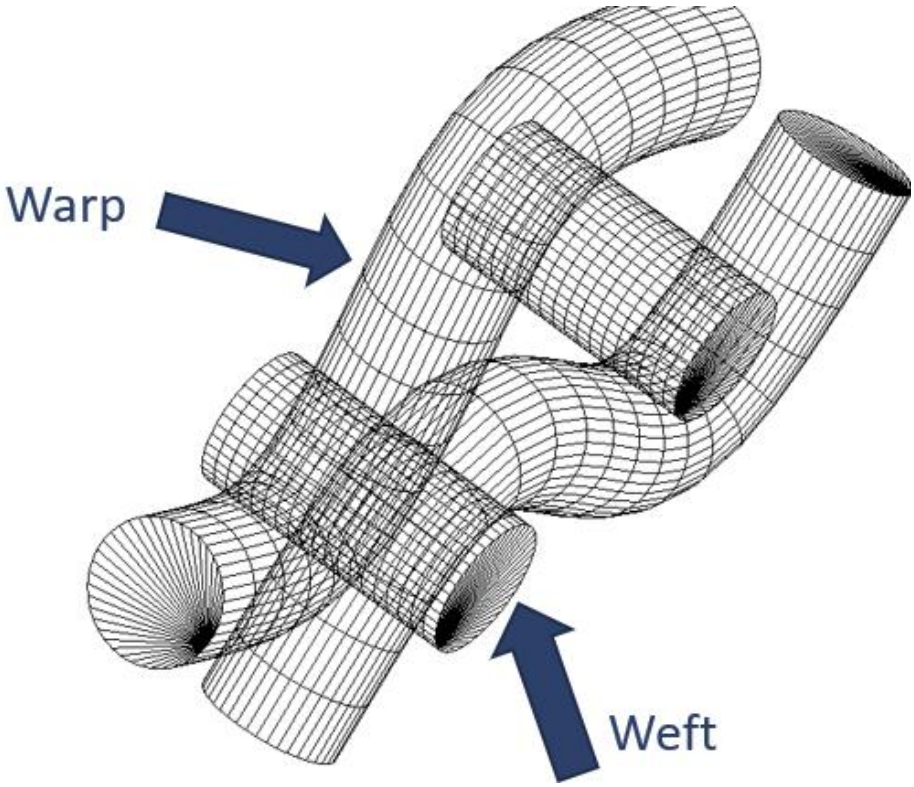

Figure 39: Woven Nitinol fabric unit cell model

The assumption that the wire's elastic modulus is the same in both directions is derived from Ishikawa and Chou's model. The Nitinol fabric has iso-stress conditions and the material used throughout testing is the same in both the warp and weft direction. Also, the fabric is not reinforced with a matrix. The assumption of circular cross-sectional area for the wires is derived from Peirce's model since the wires are not like yarns and have a very high tensile strength and no obvious sign of distortion. The assumption regarding the weft wire being completely straight and having no impact on the stiffness of the fabric is because the fabric that was developed is extremely thin and experimentally, it was not possible to test the fabric in the weft direction (with the equipment available). Finally, the angle being the same throughout the fabric is

derived from Ito and Chou's model because it is not possible to perform unit cell analysis unless the material remains the same throughout.

The objective of this model is to predict the elastic modulus E for the NiTi fabric. This is done by modifying already existing models to account for the absence of a matrix and assumption that the elastic modulus is the same in a single wire for both the transverse and axial direction.

$$E_L = E_T$$

This further means that the Poisson's ratio in both directions is equal as well:

$$\nu_{TL} = \nu_{TT}$$

It has been shown in [120] how the angle affects the stiffness of a fabric and is accurate for this model. It is expressed using the following equation where d is the wires diameter and g is the gap between the wires in the weft direction. Furthermore, the height, length and width of the unit cell can be described as h, L and w, respectively. In Figure 40, the weft yarn can be seen coming out of the paper and the warp yarn is crossing over and under the weft.

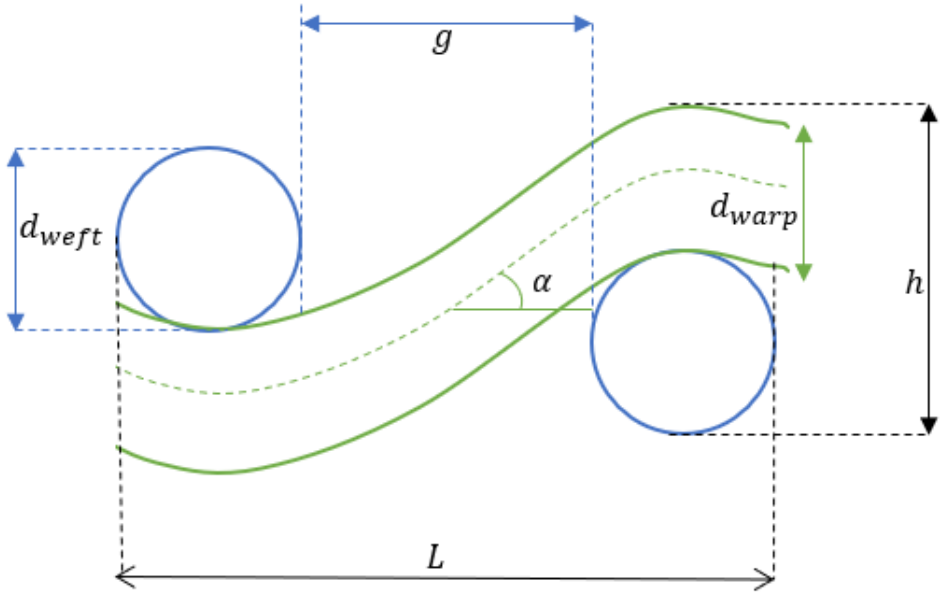

Figure 40: Unit Cell of plain Woven Fabric

The angle is calculated based on the slope of the warp yarn:

$$\alpha = \tan^{-1}(\frac{2d}{g})$$

The elastic modulus corrected for the warp angle is:

$$E_\alpha = E_L cos^2(\alpha)$$

The elastic modulus of the warp yarns is:

$$E_w = \frac{1}{\frac{d}{E_L} + \frac{g}{E_\alpha}}$$

Substituting E_α into the equation above, E_w becomes

$$E_w = \frac{E_L}{d} + \frac{E_L * cos^2(\alpha)}{g}$$

The apparent elastic modulus can be expressed as:

$$E_a = \frac{E_{warp} A_w}{A_a}$$

Where, A_w is the cross-sectional area in the warp direction and A_a is the apparent area of the unit cell.

$$A_w = 2\frac{\pi d^2}{4} \qquad A_a = hw$$

Substituting the equations for area into apparent elastic modulus equation,

$$E_a = \frac{\frac{\pi}{2} * d^2}{6d^2} * E_w$$

Replacing E_w with the equation found above,

$$E_a = \frac{\frac{\pi}{2} * d^2}{6d^2} * (\frac{E_1}{d} + \frac{E_1 * cos^2(\alpha)}{g})$$

The equation above simplifies, and the apparent elastic modulus of the fabric can be predicted using:

$$E_a = \frac{\pi}{12}\left(\frac{E_L}{d} + \frac{E_L cos^2(\alpha)}{g}\right)$$

Conclusion

As shown above, unit cell analysis is used to create a model that accurately predicts the woven Nitinol fabrics elastic modulus. The model uses repetitive unit cell (RUC) analysis which takes the smallest repetitive unit of the fabric and models it, so the fabrics properties can be predicted. This model accurately predicts the elastic modulus of the fabric in the warp direction.

Chapter 5

Woven Nitinol

Introduction

In this section, the progression of creating woven Nitinol fabric is discussed. The process began with hand-weaving using a jig. This provided the insight that it is indeed possible to weave Nitinol together and a wooden hand-weaving machine was acquired. A sample of Nitinol fabric was creating using this machine, however many problems still existed within the weaving process. Therefore, a narrow fabric weaving machine was acquired and multiple samples were made using this machine after modifications were done to the machine. Finally, the final woven Nitinol fabric uses 0.01" wires in the warp and weft direction and a binder cord is used to hold the fabric together and not allow it to unravel. The fabric has 100 dents per inch and 15 picks per inch.

Initial Weaving Procedure

A device was created to help weave Nitinol wire together. The device consisted of a 2"x2" piece of machined aluminum stock (Figure 41). The center was milled out for ease of weaving and 23 one-millimeter holes were places around the edges. A pin was placed in each hole and is pictured below. Four larger holes were drilled and tapped surround the one square inch center to help pull the wires in closer together when the weaving was complete.

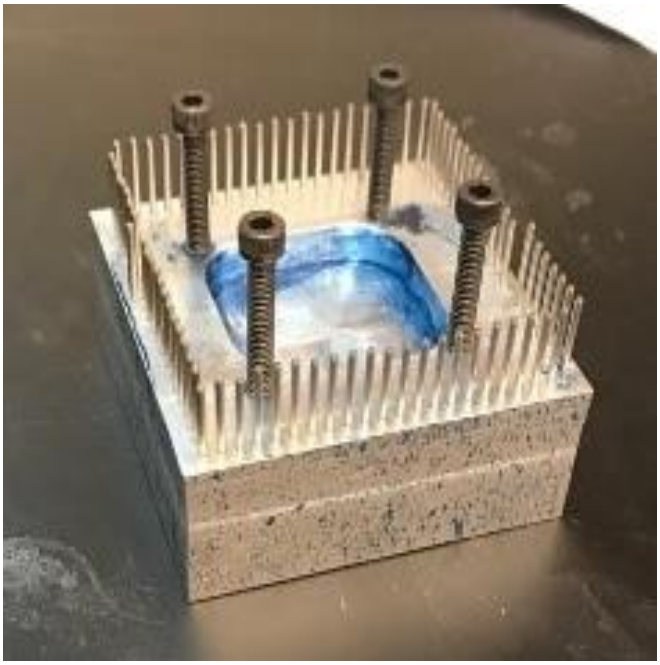

Figure 41: Initial Hand Weaving Device

During the first and second iteration, the wires were zig-zagged over every pin up and down. Side to side, the wire was woven through going above the first wire, below the second and continuing the pattern throughout the rest of the wires (Figure 42). Once a row was completed, the wire was wrapped around the next pin and the process happened again.

Figure 42: Hand Woven Nitinol Fabric

When using super elastic wire, a problem occurred about halfway through the pins and became extremely tight and difficult to weave the wires through. Once this occurred, the wires were pushed as closely together as possible and placed into the oven. Although the wires were not as close as intended, once removed from the furnace, the wires remained in place regardless of how the material was bent (Figure 43).

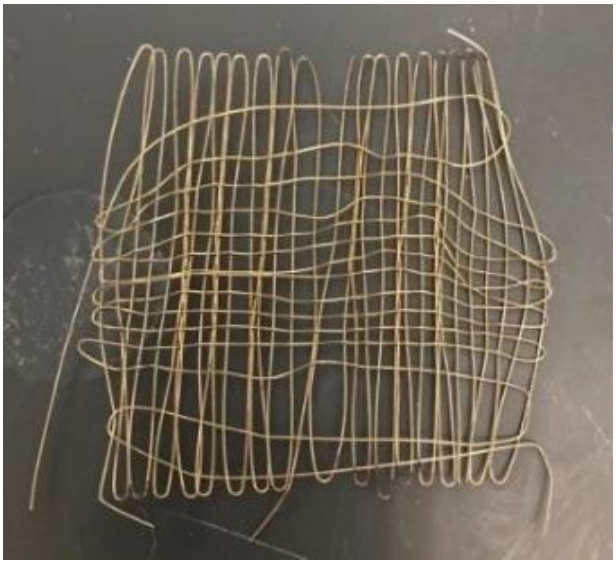

Figure 43: Hand Woven super-elastic Nitinol Fabric

The second iteration utilized shape-memory wire. There was less difficultly when weaving this wire and after it was placed in the furnace, the material would conform to any shape it was bent to. After heating the woven wire, it returned to its memorized flat shape (Figure 44).

Figure 44: Shape-memory hand Woven Nitinol Fabric

The third iteration used a different type of weave called the twill weave. This weave has wires going over two, then under two and continuing throughout the entire fabric. However, after every iteration the wires are offset by one. This weave allowed the wires to become more compact (Figure 45).

Figure 45: Hand Woven Nitinol Fabric using the Twill Weave

Ultimately, this paved a path forward proving it was possible to weave Nitinol wire together to create a fabric.

Wooden Hand Weaving

After successfully hand weaving the material, an off-the-shelf woven hand weaving machine was purchased (Figure 46). This machine provided the capability of "packing" the weft wires closer together and creating a much wider sample.

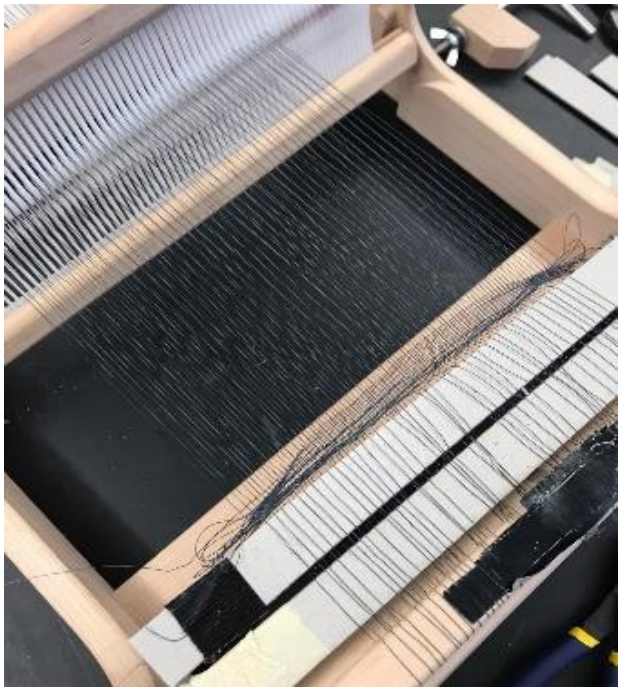

Figure 46: Wooden Hand Weaving Machine

However, this machine only provides one source of tensioning and due to that, individual wires in the warp direction had different tensions. This led to many issues as the material could not be packed as tight. Also, this weaving machine utilizes a plastic reed that also doubled as the heddles. In Figure 47, the wire in the warp direction had to be taped down to try to eliminate some of the tensioning issues that occurred with each individual wire.

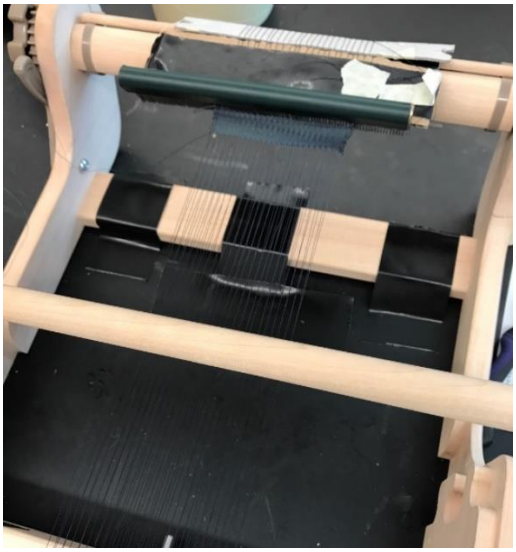

Figure 47: Hand weaving machine tensioning issues

Due to the material being metal, it was extremely difficult to pack the wire into a tight weave. After each iteration of weft wire being ran through the warp, it took approximately 2 minutes to successfully pack the weft wire. Also, there was no way to prevent the weft wire from completely unraveling as the ends were not held down by a binder cord (Figure 48). Upon pulling on the weft strand, the entire fabric can unravel.

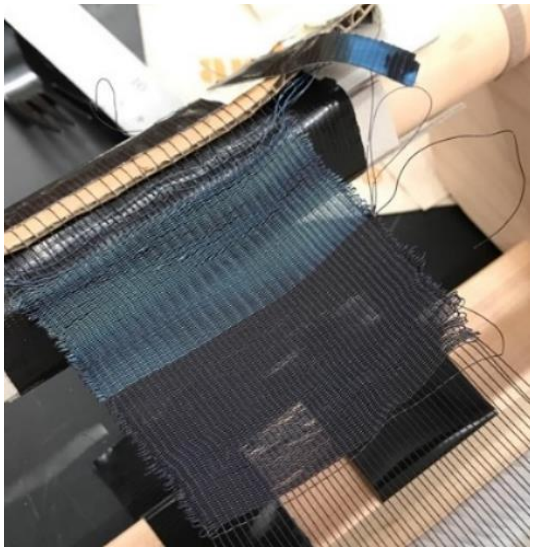

Figure 48: Hand woven fabric without binder cord

Narrow Fabric Weaving Machine

Upon realizing the tensioning issues that were occurring with the hand weaving techniques, a narrow fabric weaving machine was acquired. The intention of this machine is to make elastic waist bands, shoe strings, and clothing logos. Many modifications to the machine had to be done so that wire could be used on the machine. The initial issue with using this machine was that it did not provide enough tension to the wires as it was built for yarn.

Upon the first iteration of utilizing this machine, a wooden frame was made (Figure 49) that held each individual wire with a sandbag attached to each end (Figure 50). Each sandbag weighed 1 pound.

Figure 49: Narrow Fabric Weaving Machine initial tension device

Figure 50: Individual Sandbags used to tension wires for Narrow Fabric Weaving Machine

Once the tension system was complete, wires of the same diameter were running in both the warp and weft direction. At this point, the machine was not capable of utilizing a binder cord

therefore the fabric could still become unraveled, although it was more difficult since one side of the fabric was bound together. As seen in Figure 51, the fabric was not woven very tightly, and the right side of the fabric was not bound by the binder cord. The right-side weft wire could be pulled to unravel the fabric.

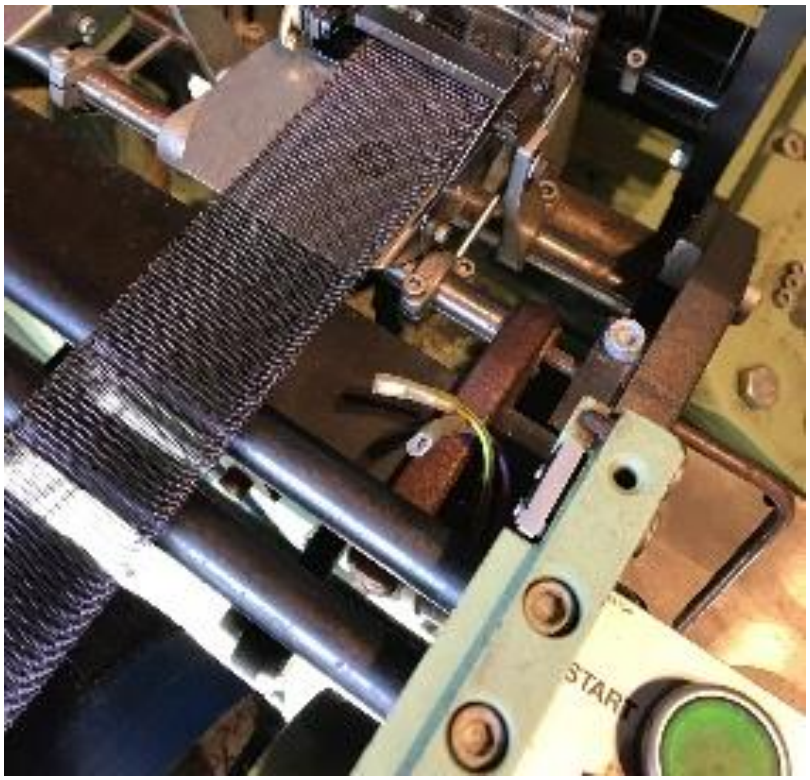

Figure 51: Initial Fabric created from Narrow Fabric Weaving Machine

To gain more control of the tensioning of the warp yarns, a creel was installed that held each individual warp spool. This creel allowed each wire to be tensioned individually and ultimately allowed for the addition of a binder cord. The binder cord bound the other side of the fabric, so it could not become unraveled. However, due to the angle of the spools from the creel to the machine, the fabric was extremely inconsistent when the machine was running. The inconsistencies that occurred were the protrusion of the weft wire, the overall packing of the fabric, and the "tying" of the weft wire and binder cord. The weft wire on the left edge of the fabric differed in the amount it protruded from the fabric. Also, the weft wires were not always

packed together which can be seen in Figure 52. Finally, the right edge of the fabric did not always “tie” together with the weft yarn and binder cord.

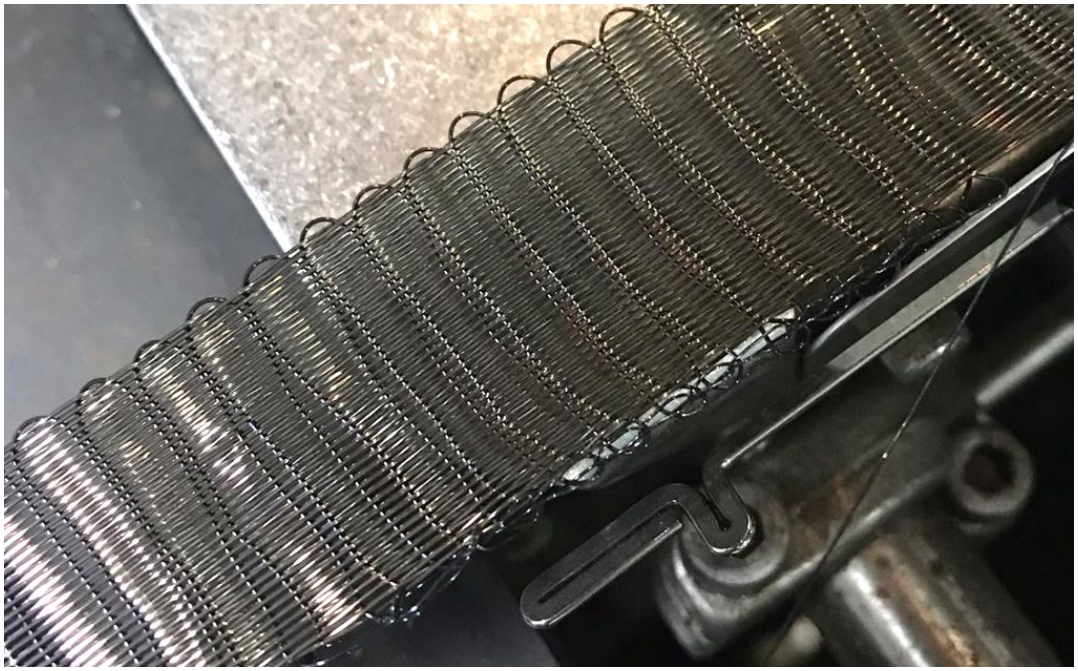

Figure 52: Inconsistencies in Woven Fabric using a creel

After the creel caused inconsistencies in the fabric, a feed-in roller was placed in the front of the machine. This allowed more control of the warp yarns. The final fabric that will be used for testing can be seen in Figure 53. The wire in the warp and weft direction is 0.01” in diameter and the fabric is 1.00” wide. There are 100 dents per inch and 15 picks per inch. Since wire is much stiffer than yarn, the number of picks per inch could not be any higher without removing some of the wires in the warp direction or allowing the wires in the warp to start piling on top of one another. The fabric can be any length since it is continuously running through the machine. The woven Nitinol fabric is extremely strong, yet flexible and it cannot become unraveled along its edges since it is bound by a binder cord.

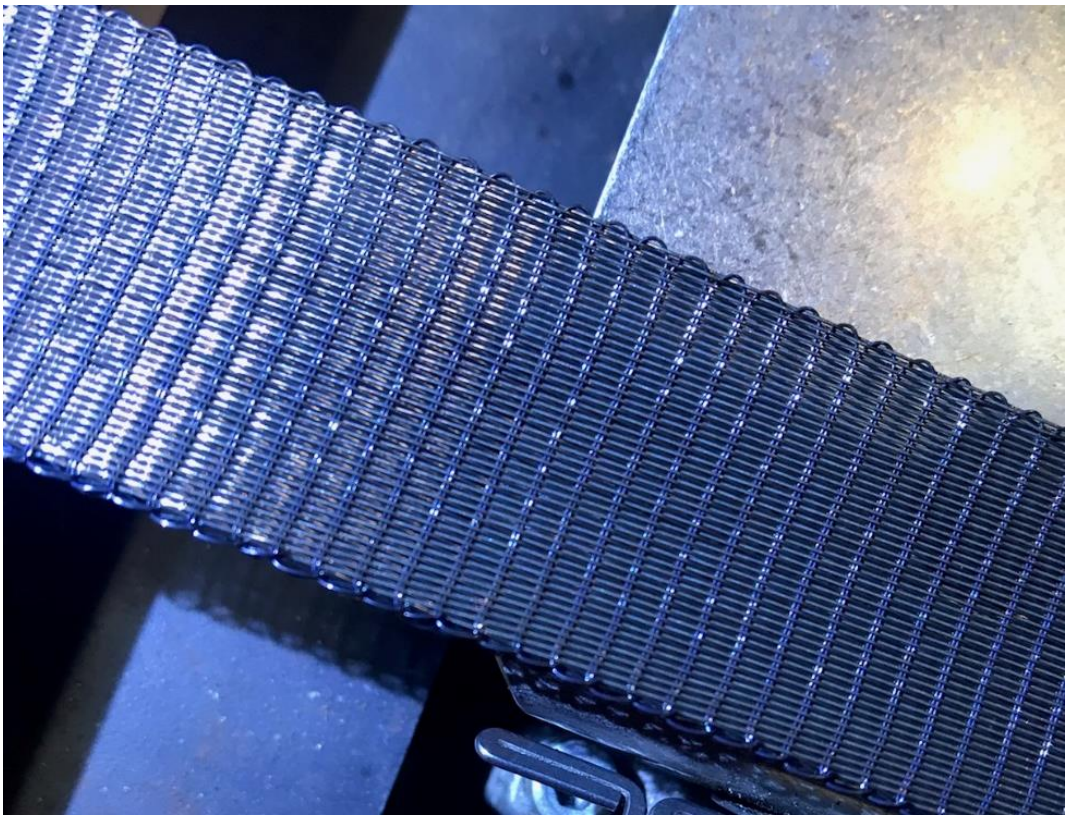

Figure 53: Final Woven Nitinol Fabric

Conclusion

The progression of creating woven Nitinol fabric was shown from the initial attempts using a hand-made jig and wooden hand-weaving machine. Ultimately, a Narrow Fabric weaving machine was used and a fabric that uses 0.01” diameter wire in the warp and weft direction is used and the overall width of the fabric is 1.00”. The fabric has 100 dents per inch and 15 picks per inch.

Chapter 6

Experimental Equipment

Introduction

Various equipment was needed to perform experiments on the Nitinol wire and woven fabric. First, a Differential Scanning Calorimeter was used to determine the transformation temperature(s) of various heat-treated wires. Next, a tensile testing machine was used to determine the wire and fabrics elastic modulus. A proof of concept experimental heating system (hand-made) and thermal chamber (industry purchased) were used with the tensile testing machine to determine the change in elastic modulus as the temperature of the wire and fabric increases. Finally, an overview of the heat-treatment equipment is presented to include the testing jig to hold the wire and fabric flat during heat treatment and the furnace used for the heat treatment.

Differential Scanning Calorimeter Overview

A Differential Scanning Calorimeter is a machine that measures the amount of heat a material gives off or absorbs as it is heated and cooled through its phase transformation temperature(s). For this test, a model DSC Q2000 from TA was used. The test provides data on endothermic and exothermic processes that occur during the solid-solid phase changes. The DSC works by inputting heat into the material at a constant rate as the material goes from low to high temperature and cooling the material at a constant rate as it goes from high temperature to low temperature.

DSC analysis can measure: the melting point, latent heat of melting, latent heat of fusion, crystalline phase transformation temperature(s) and energy, specific heat, and heat flow. The

properties determined to be critical to this research are the crystalline phase transformation temperature(s) and energy, specific heat and the heat flow.

A sample is placed into a DSC testing pan which can be made from Al, Cu, Au, Pt, alumina, and graphite depending on the sample being tested. For this application, an aluminum pan is used, and the sample is encapsulated into the pans using a press. The sample size used per the ASTM F2004-17 standard is 25-45 mg [121]. The sample is placed in the machine holding area. It is then picked up (Figure 54) and placed adjacent to a reference pan (Figure 55). The reference pan utilized in this application is an empty pan.

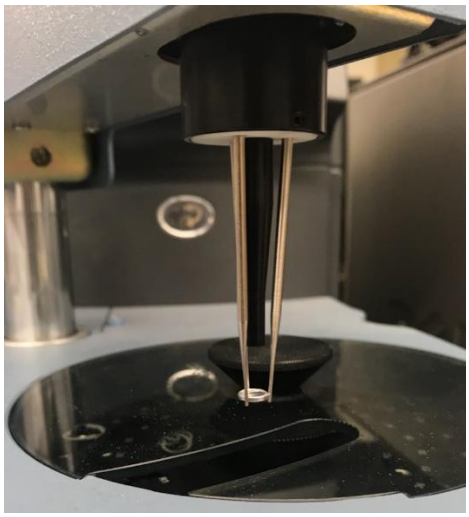

Figure 54: DSC pan moving from reference area to testing chamber

Figure 55: DSC sample and reference pan inside of testing chamber

Per the ASTM standard, a heating and cooling rate of 10℃/min is utilized throughout the test. The test heats the sample and the reference pan to a temperature of at least 30℃ above the A_f temperature. Once the material reaches this temperature, it is then cooled to a temperature of at least 30℃ below the M_f temperature. Data recorded for this test includes: temperature (℃), heat flow (mW), and heat capacity (mJ). This test determines the SMA's M_s, M_f, A_s, and A_f temperatures. It is also able to locate if there is any R-phase present or if any recrystallization occurs.

Tensile Testing Equipment

A testing jig was constructed as a proof of concept experimental heating system for the wire and fabric (Figure 56) in which they were placed inside of the proof of concept experimental heating system and in both jaws of the tensile testing machine.

Figure 56: Woven Nitinol Fabric placed in jaws of tensile testing machine

The proof of concept experimental heating system was monitored by two thermocouples placed inside, one at the top and one at the bottom. A heat gun was used to heat the fabric to the desired temperature and the difference in temperature from the bottom of the fabric to the top was no more than 10˚C (Figure 57). At the time these tests were conducted, little was known about heat treatment or aging. Therefore, the fabric and wire were only heat treated at one temperature, 600 ˚C for 10 minutes. The results of this test are important when comparing this proof of concept experimental heating system to the current thermal chamber and will be discussed in a later section.

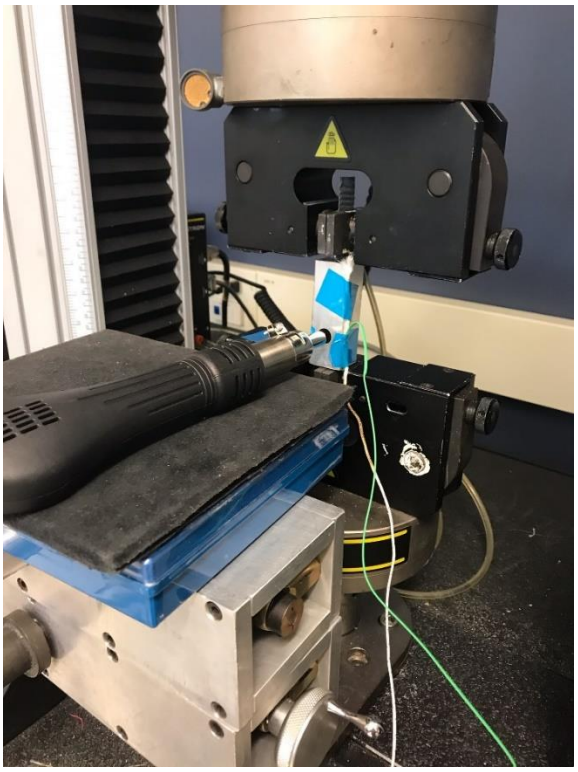

Figure 57: Proof of concept Experimental Heating System for tensile test

What is of extreme importance is an overview of the tensile testing machine and current thermal chamber being utilized. The machine is an Instron-8562 with a 10,000 lbf load cell (the load cell was unable to be changed because a smaller one was not available). A thermal chamber capable of heating up to 600℃ was placed on the machine (Figure 58). The machine can be controlled when cooling, however during the time testing was conducted, that function was not available. Therefore, the samples had to be cooled by opening the chambers' door. The heating temperature was controlled by a hand-held remote (Figure 59), but since the cooling function of the chamber was inactive, the chamber had to be monitored very closely as it would attempt to overshoot the target temperature.

C

Figure 58: Thermal Chamber attached to the tensile testing machine

Figure 59: Thermal Chamber remote used to control the temperature inside of the chamber

Overview of Nitinol Wire Heat Treatment Process

The wire utilized throughout the weaving process is 0.25mm wire with shape-memory properties, but initially it displayed as-drawn wire characteristics. As-drawn means that the wire has not been aged or heat treated but has been cold-worked. The manufacturer published properties for the wire can be seen below in Table 3 [122].

Table 3: Properties of Nitinol Wire used for wire and fabric testing

	Cold Worked			*Shape Memory Effect*		
Product	**A_s (℃)**	**UTS (psi)**	**Elongation (%)**	**UTS (psi)**	**Elongation (%)**	**A_f (℃)**
NiTi #5	$\geq +85$	220,000 min	$> 3\%$	160,000 min	$> 10\%$	$\geq +85$

A device that could hold the wire and fabric during the shape-setting process was created to ensure the wire/fabric would remain completely straight throughout (Figure 60). This device clamps both sides of the wire/fabric and prevents the material to move around during heat treatment.

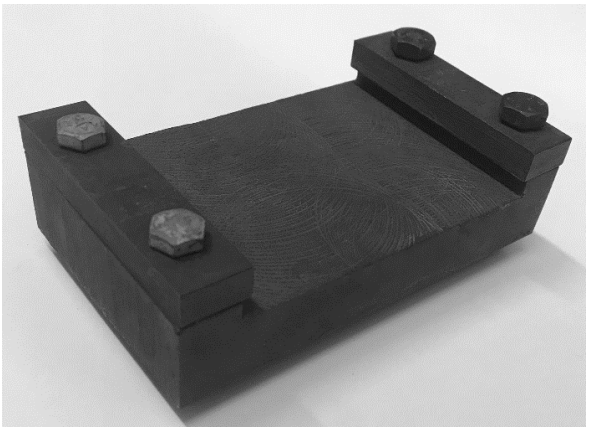

Figure 60: Device to hold wire/fabric straight during heat treatment

For the heat treatment process, a furnace capable of achieving the following temperature was utilized: $50 - 1500℃$ (Figure 61). Initially the furnace was only able to control temperature

with a toggle switch that caused inflections in the temperature range up to 30℃. To correct for this potential error, the SMASH lab disassembled the furnace and re-wired it using neoPLC microcontrollers [123]. A code was written in Arduino to control the temperature within a precision of 0.1 °C. The code can alter the furnaces temperature to any within its range by entering it into the command line.

Figure 61: Furnace used to heat treat wire/fabric

Conclusion

The testing equipment used for the experiments on the Nitinol wire and fabric included a Differential Scanning Calorimeter, tensile testing machine, proof of concept experimental heating system, thermal chamber, testing jig and furnace. All were extremely necessary in performing the correct experiments detailed in Chapter 7 and provide a vital role in determining the elastic modulus of both the wire and fabric.

Chapter 7
Experimentation

Introduction

This chapter discusses heat treatment performed to both the wire and fabric, DSC analysis conducted on the heat-treated wire, stabilization of Nitinol, and the experimental data obtained from tensile testing of Nitinol wire and fabric. Heat treatment was initially performed on single Nitinol wires and DSC analysis was conducted to determine the transformation temperature(s) of each heat-treated wire. Tensile testing was then conducted on the wire and the ones that had the highest energy absorption while having no presence of the R-phase and most recoverable strain were further examined (600℃).

A wire and piece of fabric must undergo multiple tensile tests to stabilize the Nitinol, meaning the stress-strain curve remains the same throughout all cycles after stabilization. Once stabilization occurred, the wire and fabric were tested at various temperatures using a proof of concept experimental heating system and also a thermal chamber (as shown in Chapter 6); the apparent elastic modulus of both were calculated. The dimensions of the wire and fabric used throughout the experiments can be seen in Table 4. An aging time of 10 minutes demonstrated that at room temperature, the elastic modulus of both the wire and fabric had the lowest deviation. The elastic modulus results at room temperature using the fabric model showed an average error of 8.53%. Next, the experimental and predicted elastic modulus results were compared when the material was placed inside of a thermal chamber and the temperature ranged from 100-200℃ (at 50-degree increments) and found to have an average error of 6.53%.

Table 4: Fabric and Wire Specs used throughout experimentation

	Wire Diameter	Wire Count	Thickness	Width	Binding Style
Fabric	**0.01”**	**72**	**0.032”**	**0.75”**	**Plain**
Wire	**0.01”**	**1**	**0.01”**	**0.01”**	**N/A**

The previous experiments were repeated using the proof of concept experimental heating system and the elastic modulus results of the fabric model showed an average error of 19.89% across all temperatures (100-200℃). When comparing the model using the proof of concept experimental heating system to the model using the thermal chamber, there is a 23.01% error overall. Thus, it can be concluded that the use of a thermal chamber provides more accurate results for the model presented above and should be utilized when using the model. Furthermore, these results indicate that higher temperature tensile testing provides more accurate results for the fabric model presented below.

Heat Treatment and DSC Results of a Single Nitinol Wire

The heat treatment initially performed on a 0.01” diameter single straight wire ranged from temperatures of 300-750℃. The aging time for each temperature and each wire was exactly 10 minutes and immediately following, the wire was quenched in room temperature water. The temperature range selected was used to determine which temperature a full shape-set occurred as well as to determine the transformation temperature(s) of each wire. The initial heat treatment process conducted on each wire is detailed in Table 5.

Table 5: Initial Heat treatment of a single wire

Heat Treatment (℃)	Aging Time	Process	Technique Used
300℃	10 minutes	Water Quenched	DSC Test
350℃	10 minutes	Water Quenched	DSC Test
400℃	10 minutes	Water Quenched	DSC Test
450℃	10 minutes	Water Quenched	DSC Test
500℃	10 minutes	Water Quenched	DSC Test
550℃	10 minutes	Water Quenched	DSC Test
600℃	10 minutes	Water Quenched	DSC Test
650℃	10 minutes	Water Quenched	DSC Test
700℃	10 minutes	Water Quenched	DSC Test
750℃	10 minutes	Water Quenched	DSC Test

DSC analysis reveals a full-shape set by showing a peak in the curve during heating and cooling which indicates an Austenite start and finish temperature (heating) and a Martensite start and finish temperature (cooling). It was determined through DSC analysis that the wire heat treated at and below 450℃ did not result in a full shape-set, which is evident by a lack of any peaks in the heat measured (Figure 62). Although the temperatures and times may have been high enough to begin shape-setting the material, 10 minutes of aging was not a long enough duration to achieve a full shape-set.

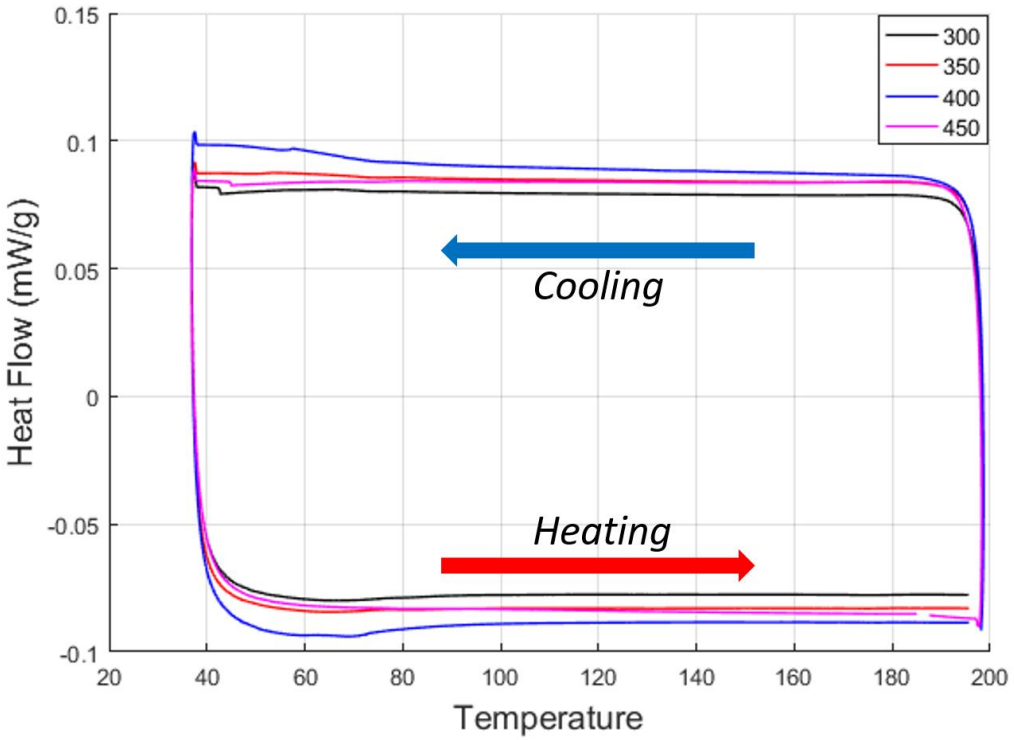

Figure 62: DSC analysis for heat treatment 450C and below aged for 10 minutes

After confirming any wire heat treated at and below 450℃ and aged for 10 minutes did not fully shape-set, a new set of DSC pans were prepared with new wire. A full shape-set will have a Martensite start and finish temperature, Austenite start and finish temperature, and if there is any R-phase present, a start and finish temperature. The test first heats the material and then cools, and an example of the testing procedure and results can be seen in Figure 63.

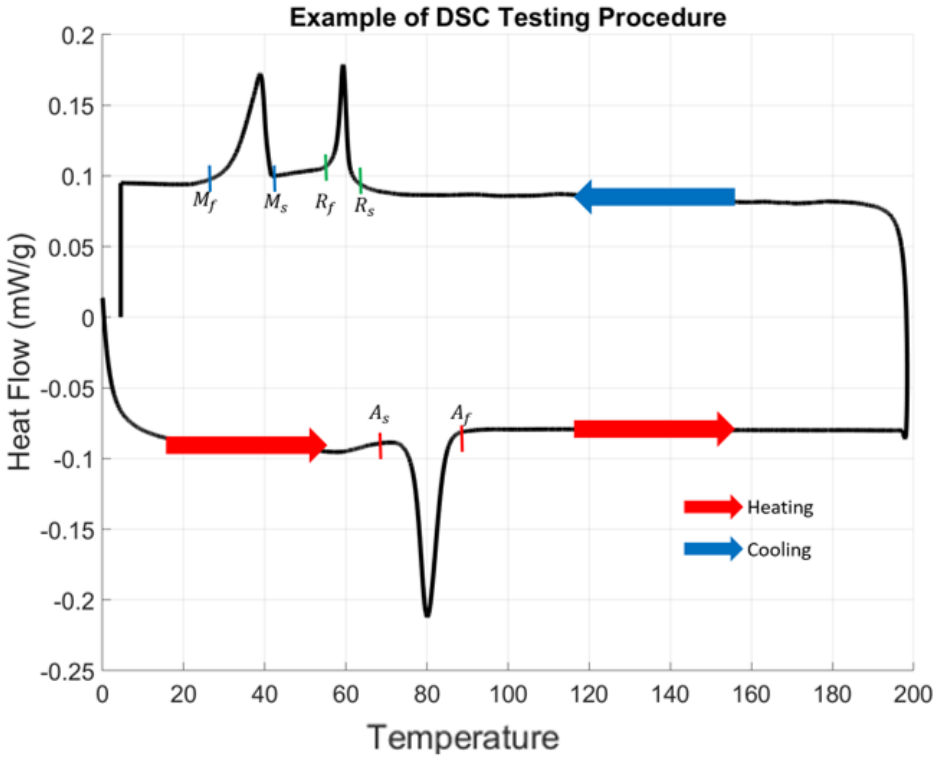

Figure 63: DSC Testing Result Example

The samples were initially in the as-drawn condition and then heat treated from 500-750℃ for 10 minutes and water quenched. The DSC test was performed on each pan 10 times to ensure the wire was thermally cycled enough times to become stable. The 10th cycle can be seen in Figure 64. However, it should be noted that the ASTM F2004-17 standard calls for the test sample to be cooled to a temperature of at least 30℃ below the M_f [121]. It is evident that this did not occur, resulting in the test analysis having potential inaccuracies.

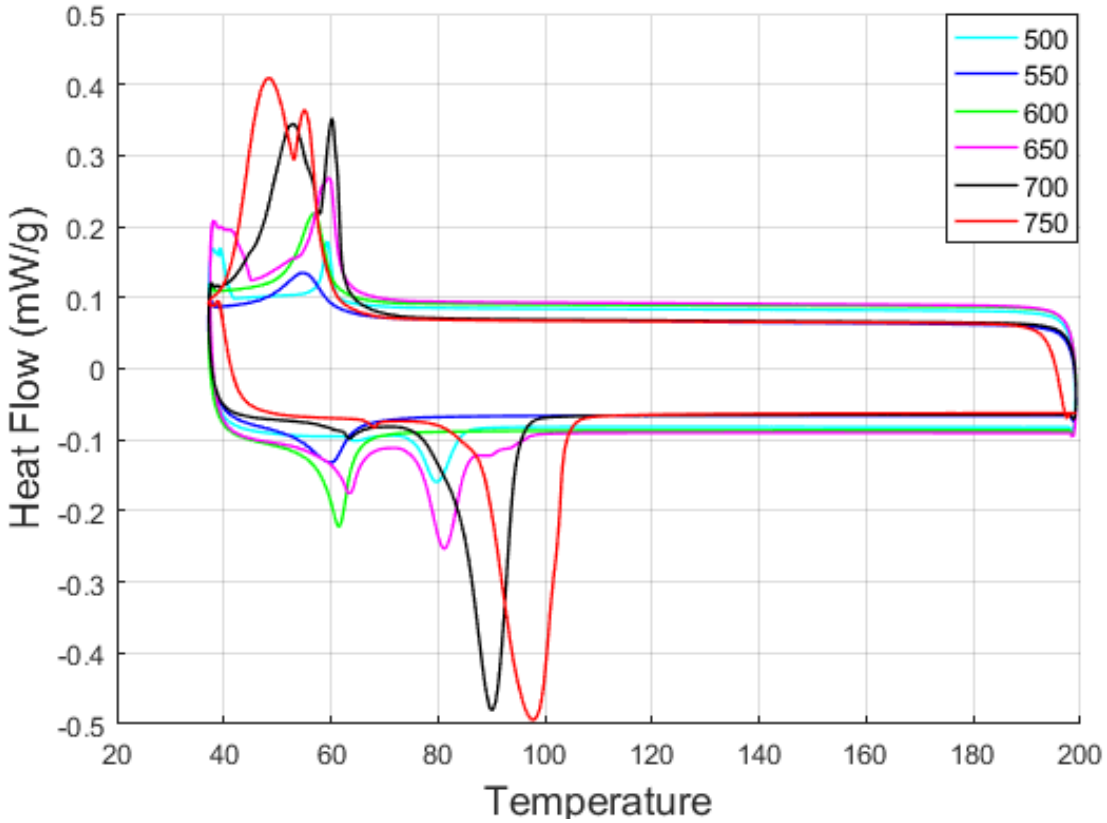

Figure 64: DSC Results for wire trained at temperatures 500-750°C testing from temperature 35°C to 200°C

Since there were potentially inaccuracies with the test above, the same pans and wire from above were used for additional cycles. The new test began at 0℃ and heated the pan to 200℃. Once the pan reached 200℃, they were Nitrogen cooled back down to 0℃. This test had a thermal ramp rate of 10℃/minute (Figure 65). This test showed similar results to the previous cyclic tests but allowed the test to fully determine the M_s and M_f temperatures.

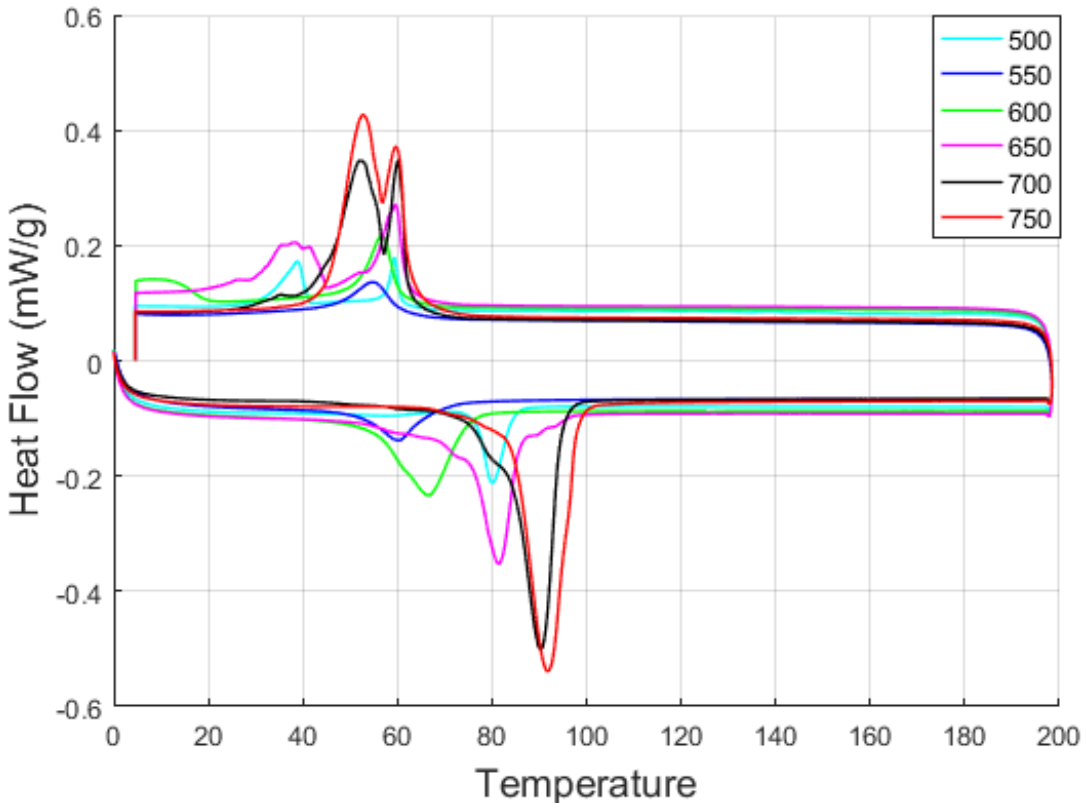

Figure 65: DSC results of wire heat treated from 500-750°C testing from 0°C to 200°C

The transformation temperature(s) of the wire were calculated by taking the "tangent" of each curve during heating and cooling. The results showed that at 550 and 600℃, there was no R-Phase present and the A_s and A_f temperature increased. It should be noted that there is some variation with the data (Figure 66), specifically as the heat-treatment temperature increases, there is no correlation between that temperature and the Martensitic start and finish temperature. The ASTM standard F2004-17 for DSC testing Nitinol wire states that the transformation temperature(s) may differ because of the effects strain and load have on the transformation. During DSC testing, there is no load or strain placed on the material. Other potential contributors to the variation to the test include: cutting the sample to its correct size as that can cause deformation to the sample, oxidation during heat treatment which changes the thermal

conductance of the sample, and a gas leak which could interfere with the thermal conductivity of the test sample. Precautions were taken when preparing the sample by using a sterilized cutting tool and the gas was monitored randomly throughout the testing procedure. Due to the challenges presented above, the results presented are the most accurate transformation temperature(s) the author could obtain for the wire heat treated from 500-750℃ and aged for 10 minutes.

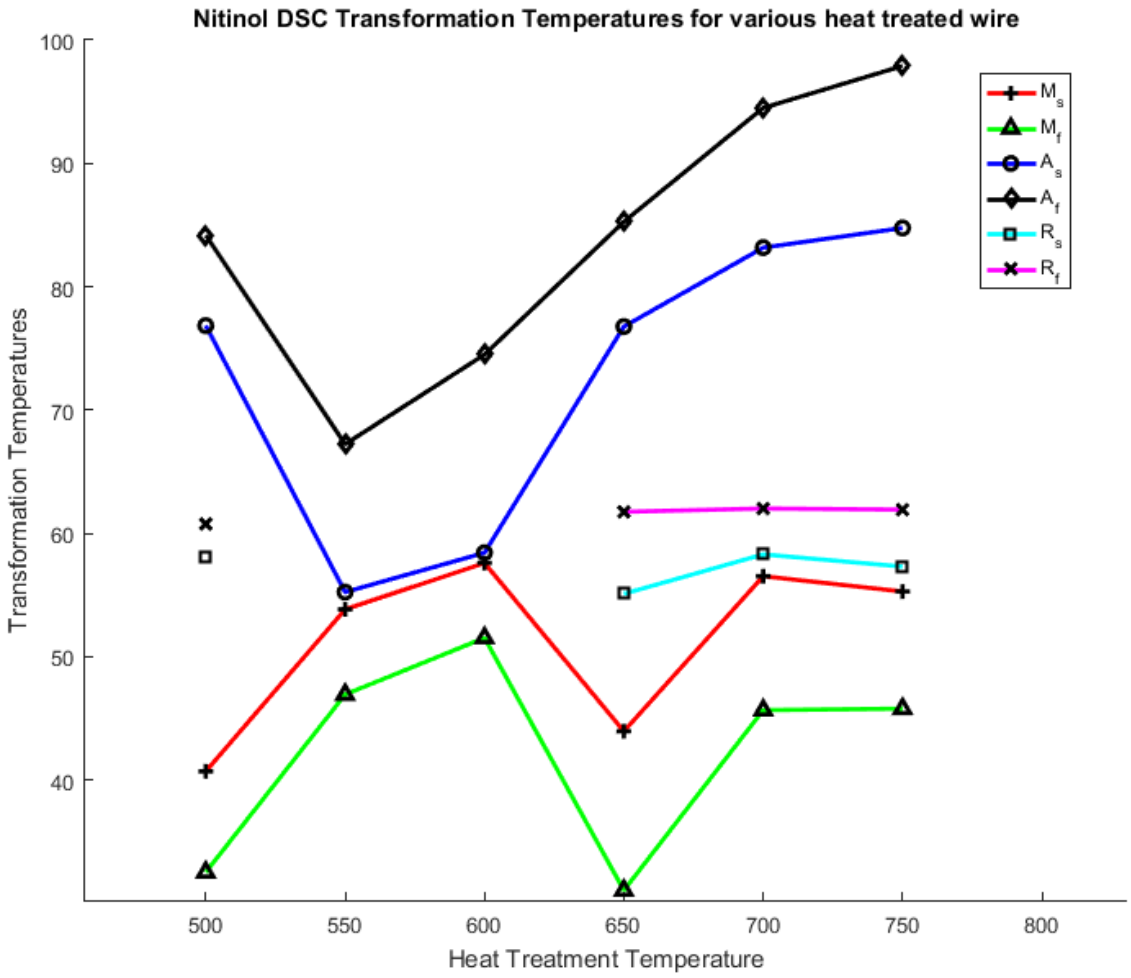

Figure 66: DSC Analysis Results on various heat-treated temperature wire

The energy the material absorbed and released was measured using DSC analysis. The energy (J/g) is measured during heating, cooling, and the R-phase (if present). The software numerically integrates the phase transformation peaks which solves for the energy the material

absorbed/released. The amount of energy absorbed/released as the material transformations through the various phases is presented in Table 6. The difference in energy during the heating and cooling cycle differ and this could be because of the unresolved sample manufacturing issues.

Table 6: Energy Absorbed during DSC analysis for wire heat treated at temperatures 500-750C and aged for 10 minutes

Temperature	Heating	R-Phase	Cooling
500℃	3.987 J/g	1.063 J/g	2.373 J/g
550℃	3.681 J/g	N/A	2.976 J/g
600℃	8.853 J/g	N/A	3.909 J/g
650℃	13.33 J/g	4.894 J/g	4.414 J/g
700℃	22.02 J/g	3.457 J/g	6.463 J/g
750℃	28.06 J/g	1.335 J/g	5.510 J/g

DSC analysis indicated that at heat treatment temperatures of 500, 650, 700 and 750℃, the R-phase was present. Also, the energy absorbed/released was extremely high for 700 and 750℃ wire. Because they are drastically different from the rest of the samples, yet relatively close to one another, only the 700℃ wire is examined further and no longer will the 750℃ be examined.

The DSC analysis results only determine the transformation temperature(s) of the wire under no load/strain and the thermal energy absorbed and released. This is not enough information to determine which heat treatment temperature will provide the most recoverable strain and stabilize the quickest. It should be noted that the author wanted to ensure that the results of the wire and fabric were as accurate as possible. It was decided that the wires would be tensile tested first and the data examined to see which temperature had the most recoverable strain and stabilized the quickest.

Tensile testing experiments using a heating and thermal chamber

The following experiments were conducted. First, a tensile test was conducted to find which heat-treatment temperature provided the wire with the most recoverable strain. Once this temperature was determined, the wire was then aged for various durations at this temperature and tensile testing was once again conducted. Finally, the woven Nitinol fabric was heat-treated at the temperature determined from the wire testing and the wire and the woven Nitinol fabrics' elastic modulus were calculated. No tests were performed that caused permanent non-recoverable deformation to the wire/fabric.

Tensile Test of a Single Nitinol Wire aged for 10 minutes at Various Temperatures

Determining which wire best fit the criteria stated above, a tensile test was performed on each wire ranging from $500 - 700℃$ in increments of 50℃.

The test performed on each wire was as follows:

1. Heat treat the wire to the desired shape-setting temperature and age for 10 minutes.
2. Upon completion of the heat treatment, quench the Nitinol wire in water immediately.
3. Place the unstrained wire in the tensile testing machine.
4. Balance the load and jog the machine down until there is 0 load ($\mp 1\ Newton$).
5. Measure the wire using calipers and record its length.
6. Reset the gage length on the machine.
7. Run one tensile testing cycle ramping up to a maximum load, followed by a ramp down to 0.

First, it is appropriate to recall what happens to the wire when it experiences the shape-memory effect i.e. when the temperature is held constant at room temperature and the stress is cycled. Initially, if the wire has not been heated above its A_f temperature, it is detwinned Martensite. However, this is not ideal, and the initial state of the material is usually twinned

Martensite. At low temperatures (below the M_f temperature), the applied stress moves the material from twinned Martensite to detwinned Martensite. Once the stress is released, the material appears to have plastically deformed. However, that is not the case and once the material is heated above its A_f temperature and cooled without any stress applied, the material transforms to twinned Martensite where it is able to recover all its strain. Hence, in the tensile tests performed at room temperature, the material appears to have plastically deformed, until heated and cooled in which the strain is recovered, and the next cycle of tests is performed. The general cycle in which the shape memory effect follows can be seen in Figure 67.

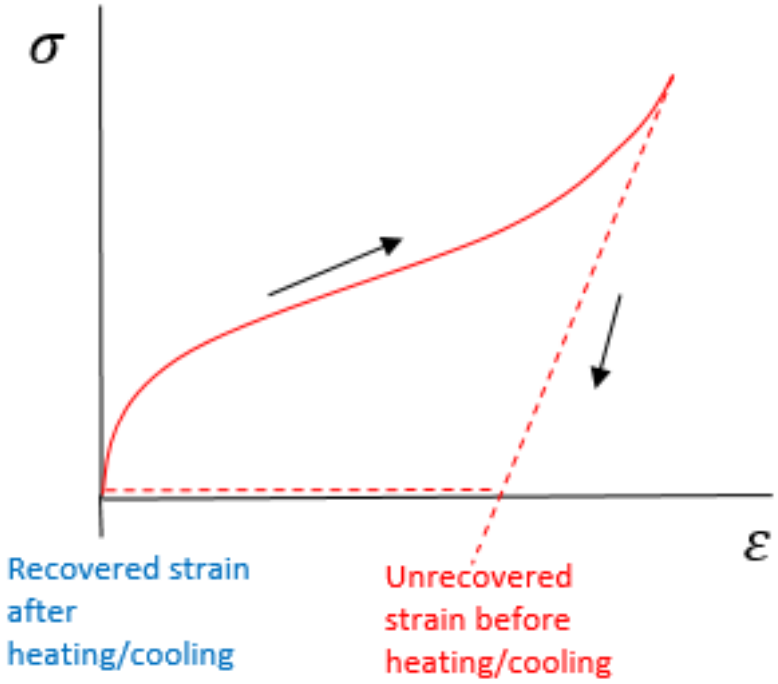

Figure 67: General Shape-Memory path for Nitinol wire and fabric

During the initial test, each wire was heat treated for exactly 10 minutes and quenched in room temperature water. Upon quenching, the wires were placed inside of the thermal chamber with the chamber door open. It can be assumed that the wires, when initially placed in the

thermal chamber, were detwinned Martensite due to the stress applied during the heating and quenching process. The predetermined maximum tensile stress was 550 MPa. The first few cycles after heat treatment cause the shape memory behavior to be extremely high, meaning the recoverable strain is a lot higher than it will be once the material stabilizes. It can be concluded that the deformation characteristics change drastically throughout the first few cycles performed on the material, therefore the results in Figure 68 are just to demonstrate the high recoverable strain the initial cycles provide.

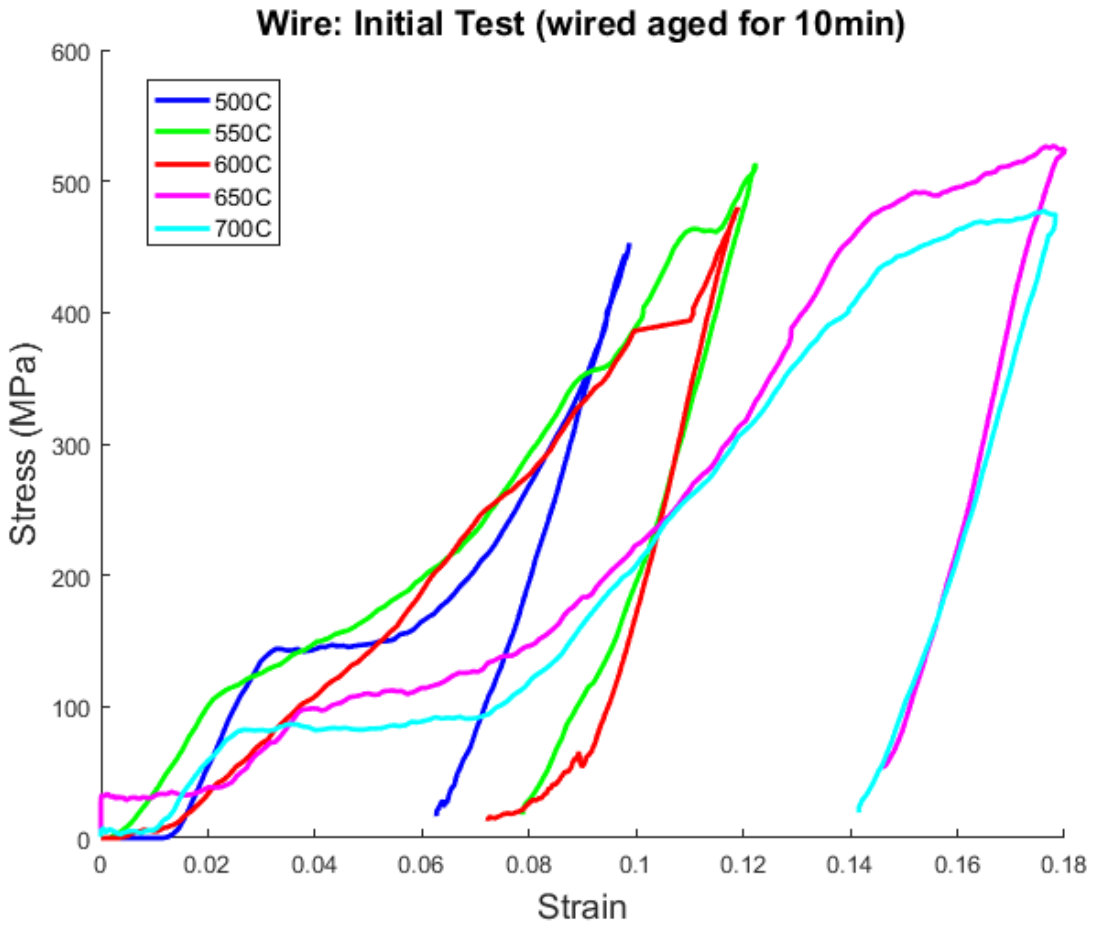

Figure 68: Initial wire cycle for wire heat treated at 500-700C and aged for 10 minutes

After the initial cycle, the wires started in the detwinned Martensite phase. However, to recover more strain, they must begin in twinned Martensite and this is sought to be the initial testing condition. To do this, the following additional steps were followed:

8. Ensure the wire is not under load/stress, close the thermal chamber and heat the wire to 150℃ (past the A_f temperature).
9. Open the thermal chamber and allow the wire, machine, and vises to cool back to room temperature, while ensuring that there is no load on the wire.
10. Repeat steps 4-9 as stated above until the wire becomes stabilized.

Once stabilization occurs, the stress-strain curve will be the same every cycle after that. The amount of cycles it took each wire to stabilize ranged from 6-10 cycles. This test was performed multiple iterations to different wires to ensure accuracy. It can be observed that the wire heat treated at 700℃ acted as if it was super-elastic once stabilized (Figure 69). The wire heat treated at 600℃ was found to have the most recoverable strain.

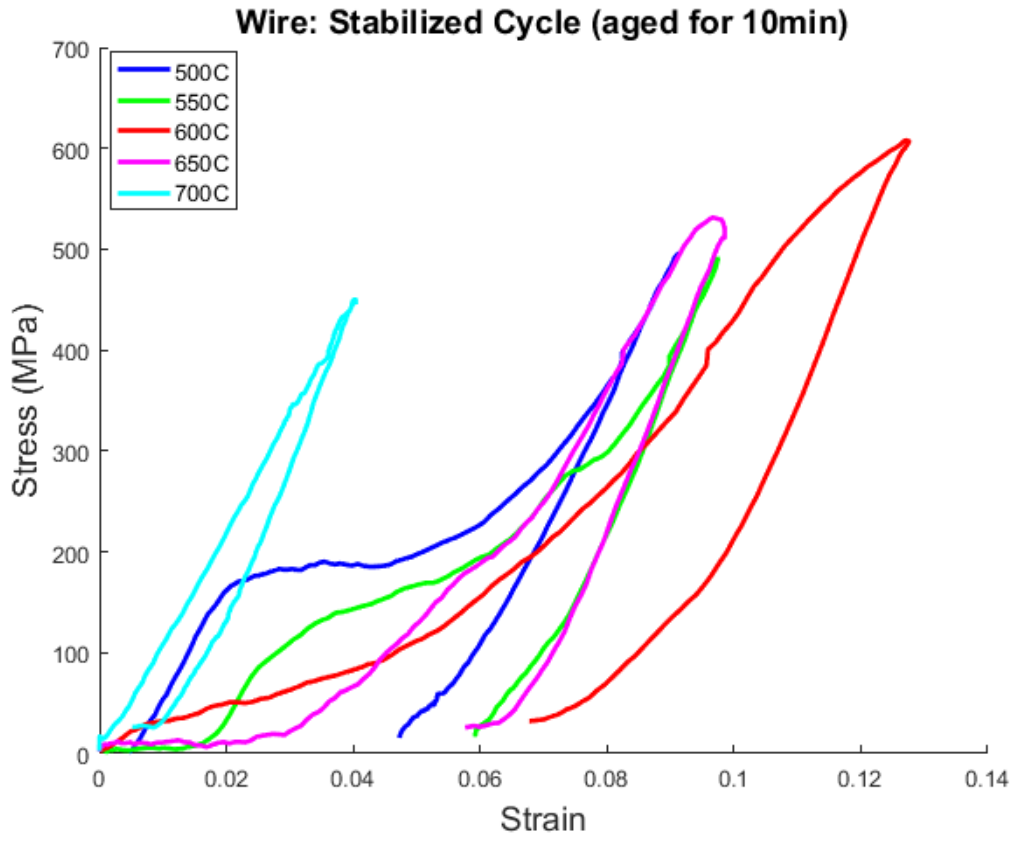

Figure 69: Tensile Test results of single wire stabilized at temperatures 500-700C aged for 10 minutes

The wire that was heat treated at 600℃ had no presence of the R-phase as observed by DSC analysis (Figure 70). It also has the most recoverable strain upon stabilization. Therefore, 600℃ was chosen as the temperature to train the wire and fabric.

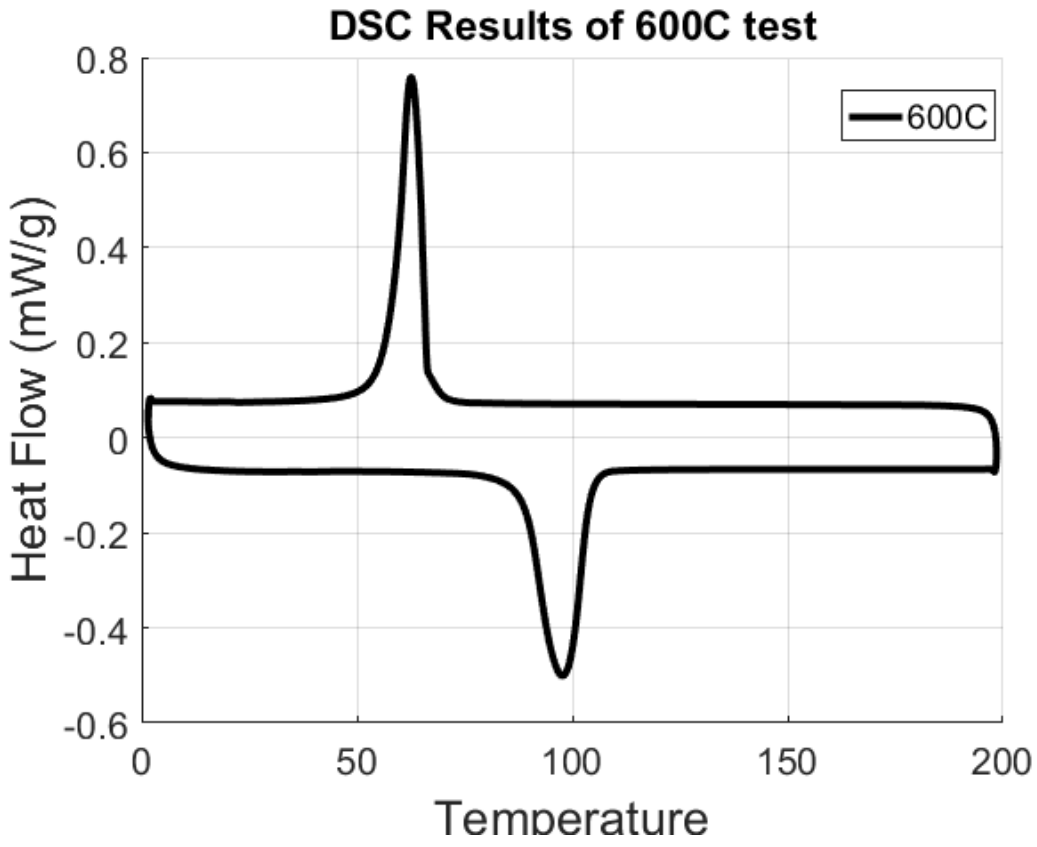

Figure 70: DSC Results of heat treated wire at 600C

Effects of Aging Time

After determining that the desired heat treatment temperature was 600℃, a new heat treatment was performed. The wires were heat treated at a constant 600℃, but their aging time was altered, ranging from 10-30 minutes (Table 7).

Table 7: Heat Treatment Performed at Constant temperature with various aging times

Heat Treatment (℃)	Aging Time	Process	Technique Used
600℃	10 minutes	Water Quenched	DSC Test
600℃	15 minutes	Water Quenched	DSC Test
600℃	20 minutes	Water Quenched	DSC Test
600℃	25 minutes	Water Quenched	DSC Test
600℃	30 minutes	Water Quenched	DSC Test

Upon completion of the heat treatment stated above, DSC analysis was performed on the samples. The results showed that as the aging time increased, the transformation temperature(s) also increased. It can also be seen that there is an increase in the energy absorption when comparing the wire aged for 10 minutes and the wire aged for 30 minutes (Figure 71).

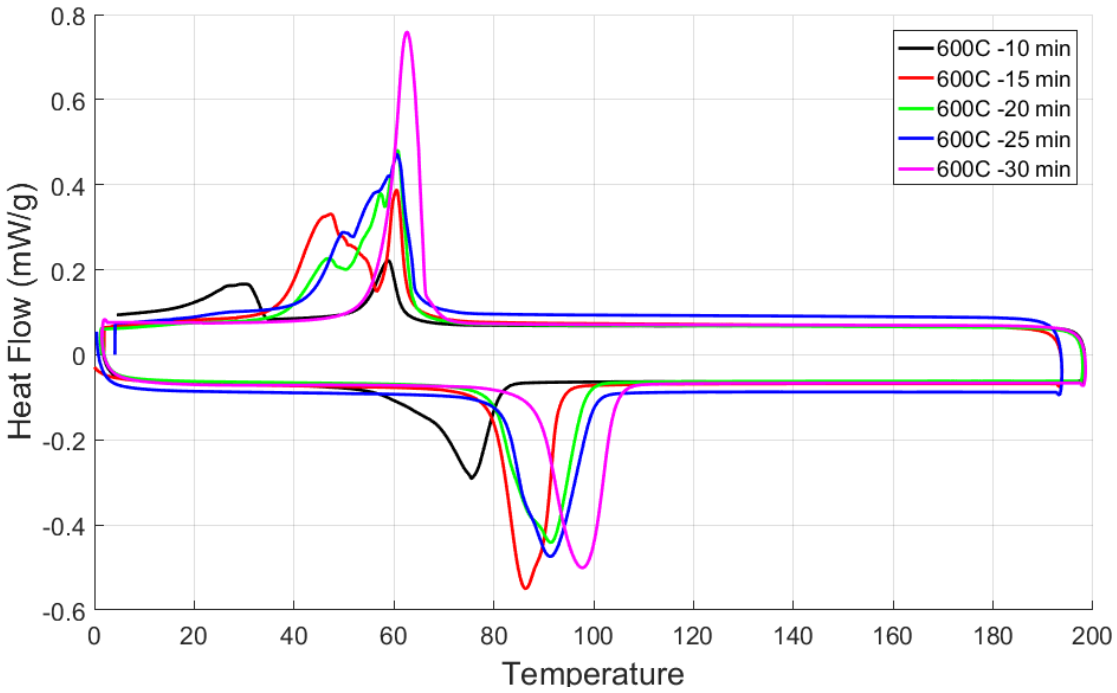

Figure 71: DSC analysis on heat treated wire at 600℃ and aged from 10-30 minutes

After DSC analysis revealed the aged wires transformation temperature(s) and energy absorption, the same tensile testing process used above to stabilize the wire was conducted on each aged wire. The 600℃ heat treated wire that had been aged for 10 minutes can be seen to stabilize after the 6th cycle (Figure 72). A tensile test was performed in which the wire was loaded to 550 MPa to ensure no non-recoverable permanent deformation occurred to the wire.

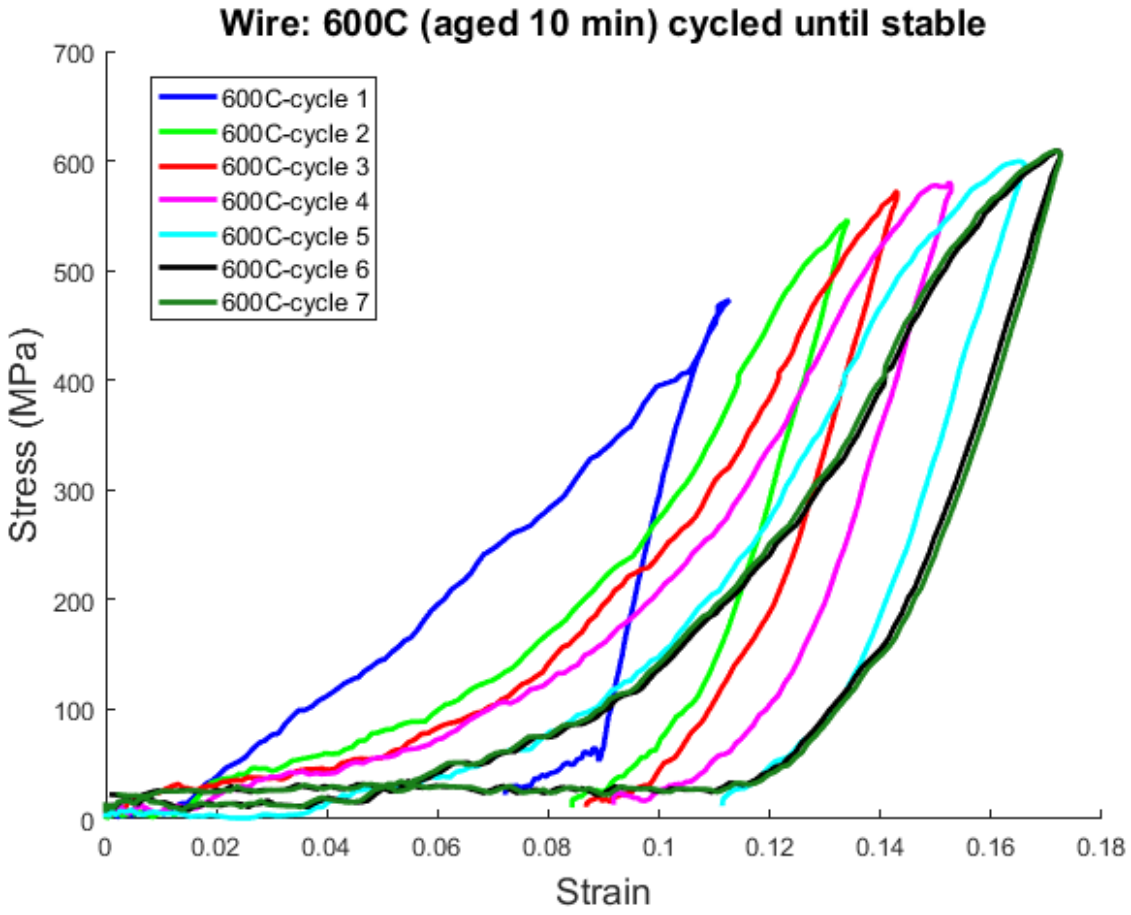

Figure 72: Stress-strain stabilization of single wire heat treated at 600C and aged for 10 min

The same process used for the stabilization of the wire aged at 10 minutes was also conducted to the wires aged at the remaining durations (Table 8).

Table 8: Cycle Number until stabilization for wire heat treated at 600C and aged for various times

Heat treatment	Aging Time	Cycles until Stabilization
600℃	10 minutes	6
600℃	15 minutes	7
600℃	20 minutes	6
600℃	25 minutes	5
600℃	30 minutes	4

Once each aged wire stabilized, they were graphed on a stress-strain curve to illustrate the recoverable strain of the various aging times (Figure 73).

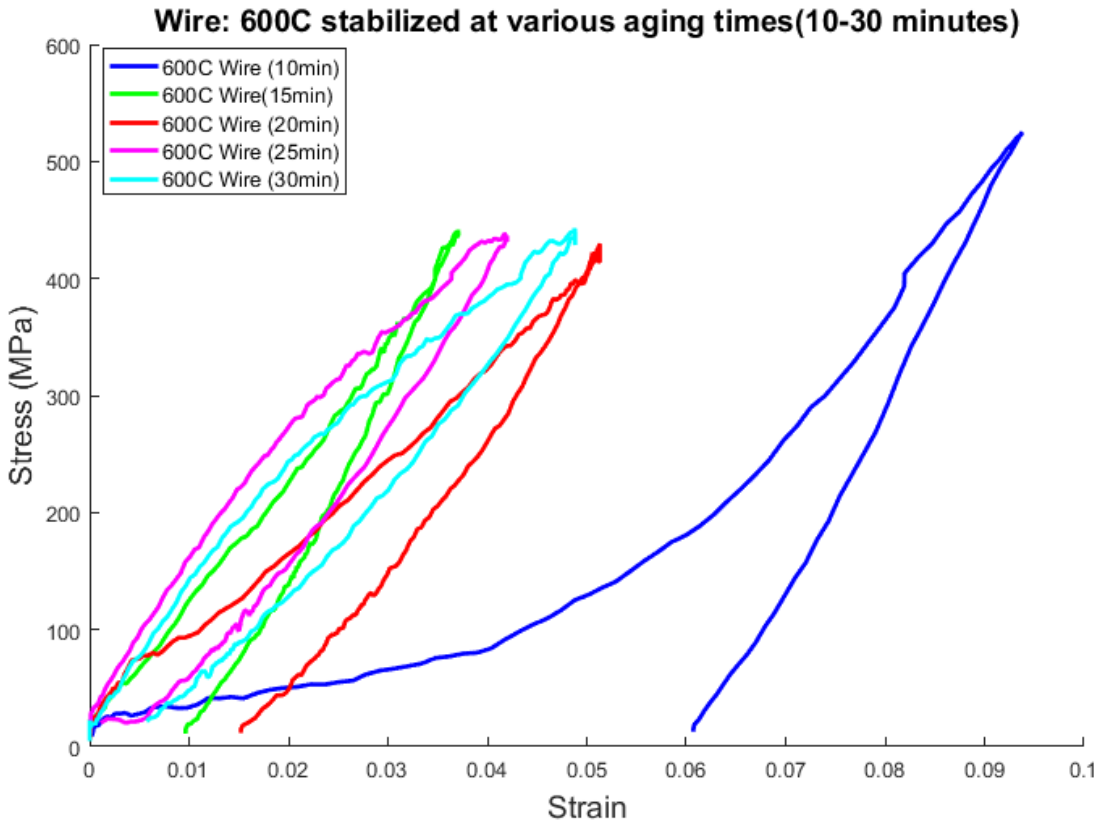

Figure 73: Stabilized stress-strain curve for wire treated at 600C and aged for various times (10-30min)

There is no obvious trend in the recoverable strain of the wire to the aging time besides that the aging time of 10 minutes illustrates the most recoverable strain.

The experimental elastic modulus of the wire (E_L) was determined by fitting a line to the stabilized data when the material was in tension. After the single wires became stabilized, the elastic modulus was measured. During testing, the wire was loaded to 550 MPa, which is far less than the wires plastic deformation region and therefore ensured the wires would only experience recoverable elastic deformation. The elastic modulus of the aged wires at room temperature were found for three different cycles and are presented in Table 9.

Table 9: Experimental Elastic Modulus of Single Wire (600C) aged at various times for three cycles

	Cycle 1	**Cycle 2**	**Cycle 3**
10 minutes	26.55 GPa	28.74 GPa	29.05 GPa
15 minutes	31.91 GPa	32.64 GPa	32.88 GPa
20 minutes	22.76 GPa	23.55 GPa	25.75 GPa
25 minutes	22.07 GPa	22.564GPa	23.24 GPa
30 minutes	17.04 GPa	18.96 GPa	19.75 GPa

The elastic modulus of the cycles of a single Nitinol wire tested at room temperature were compared (Figure 74). As the cycle increased, the elastic modulus did as well. In general, the elastic modulus decreased as the aging time increased, peaking at 15 minutes aging time.

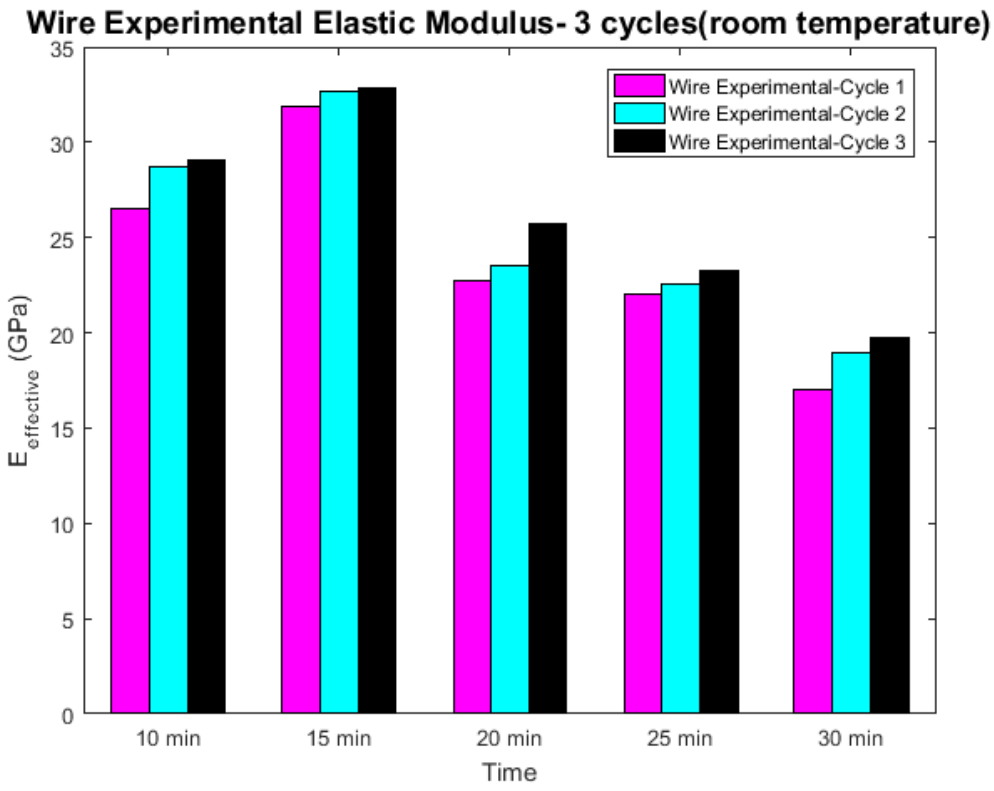

Figure 74: Elastic Moduli of Single Wire tested at room temperature for various aging times and cycles

Aged Wire Testing with the Super-elastic Effect

Upon completion of the tests at room tempeature, it was necessary to test the material at various temperatures which would allow the material to experience the super-elastic effect. For this effect, when no stress is applied, the material is in the Austenite state. When stress is initally applied, the material elastically deforms and upon further application of stress, it appears the material plastically deforms as the stress induces a transformation from Austenite to Martensite. However, once the stress is released, the material 'un-plastically' deforms and the crystals shift back to Austenite which allows the material to recover all of its strain. The temperature during the super-elastic effect remains constant throughout the experiment. The general loading and unloading cycle for a wire/fabric experiencing the super-elastic effect can be seen in Figure 75.

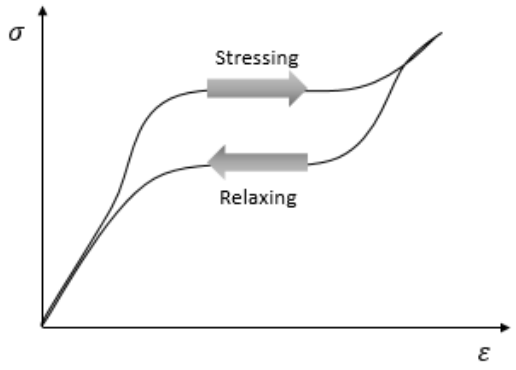

Figure 75: Super-elastic loading path for Nitinol Wire and Fabric

It should be noted that the A_f temperature for all aging times was just below 100℃ which means samples tested at 100℃ in the thermal chamber were in the Austenite phase. It is fair to also assume that the samples tested at 150 and 200℃ were in initally in the Austenite phase. The tensile test that was performed on the wire at the various testing temperatures showed extremely simlar results and the test performed at 200℃ can be seen in Figure 76.

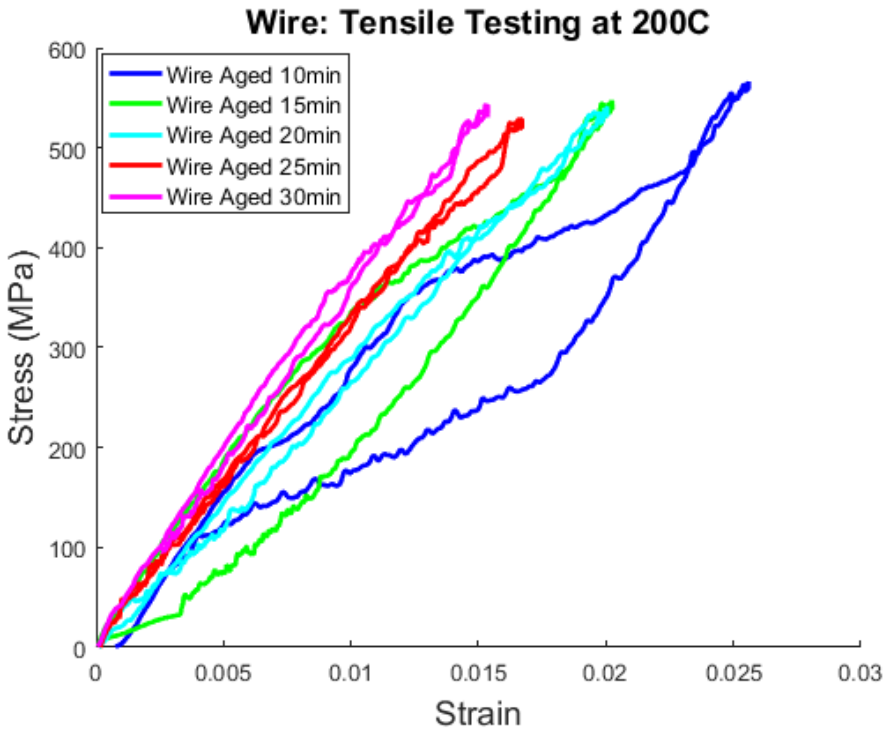

Figure 76: Tensile Testing Results of aged wire at 200C

Upon conclusion of the tensile tests, the elastic modulus of the wire was calculated by taking the slope of the straighest portion during loading. The various thermal chamber temperature elastic modulus results conducted on the wire are shown in Figure 77.

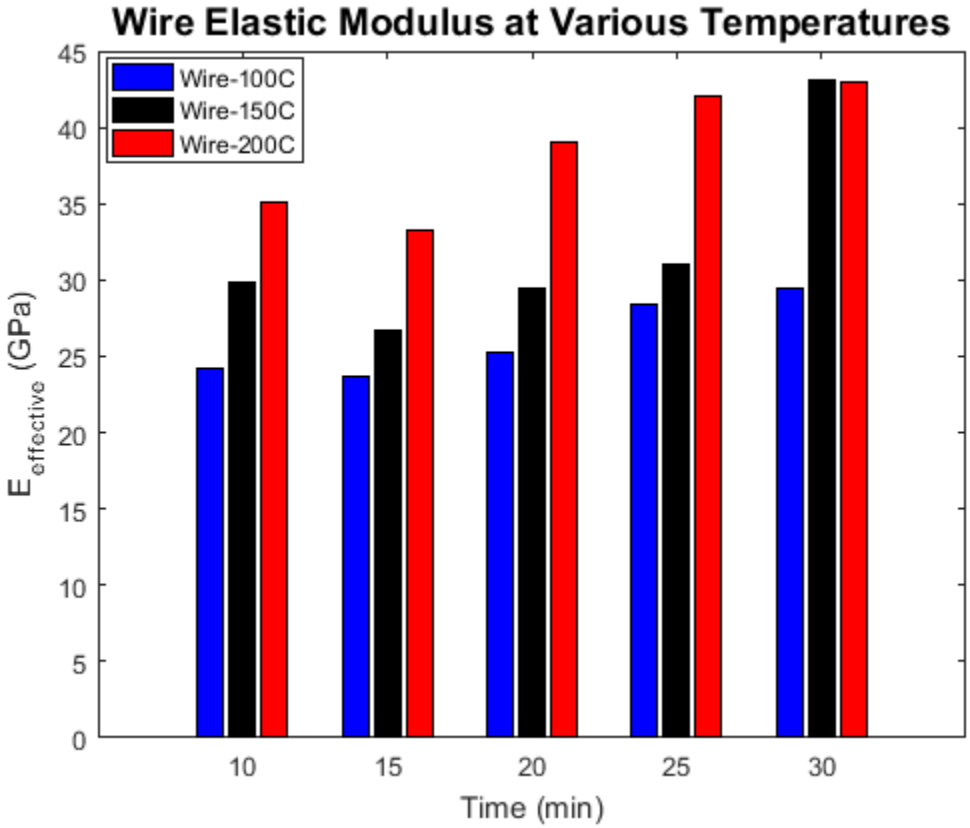

Figure 77: Elastic Modulus of wire at various temperatures

As shown from the results presented above, the wire's elastic modulus decreases as the aging time increases when tested at room temperature. However, when the material is tested at the range of 100-200℃, the elastic modulus generally increases as the aging time increases. Also, the elastic modulus increases as the temperature increases.

Effect of Aging time on Woven Nitinol Fabric

The same heat treatment was conducted on the woven Nitinol fabric for the various aging times. Since 600℃ was determined to be the best heat treatment temperature, the fabric was only heat treated at this temperature. The fabric was placed inside of the thermal chamber and the same testing procedure used on the wire was used on the fabric (Figure 78).

Figure 78: Woven Nitinol fabric inside of the thermal chamber on the tensile testing machine

Although it took the wire many cycles to stabilize, the fabric stabilized after 2 cycles for all aging times. The fabric was loaded to 450MPa to ensure no permanent plastic deformation occurred and the results of the stabilization cycle for 10-minute aging duration is shown in Figure 79. The beginning of the test that displays an odd behavior is a result of de-crimping in the fabric.

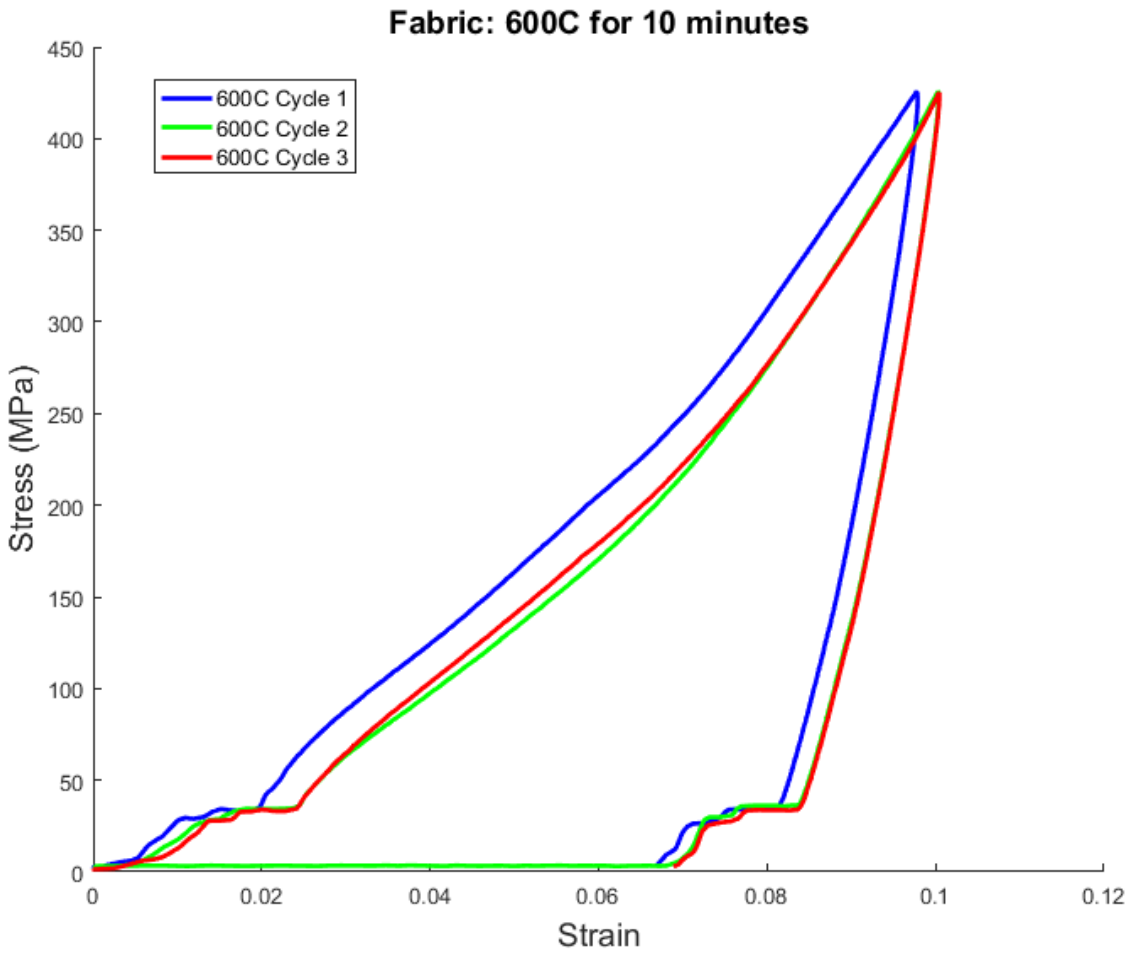

Figure 79: Stabilization Cycling for Fabric aged at 10 minutes

A trend for the fabric can be seen: as the aging time increased, the amount of recoverable strain decreased (Figure 80). For the aging times of 25 and 30 minutes, the material recovers almost all its strain upon completion of the tensile test at room temperature. For the aging time of 10 minutes, the recoverable strain is the largest. It should also be noted that both the fabric and the wire increase the amount of recoverable strain until they are stabilized.

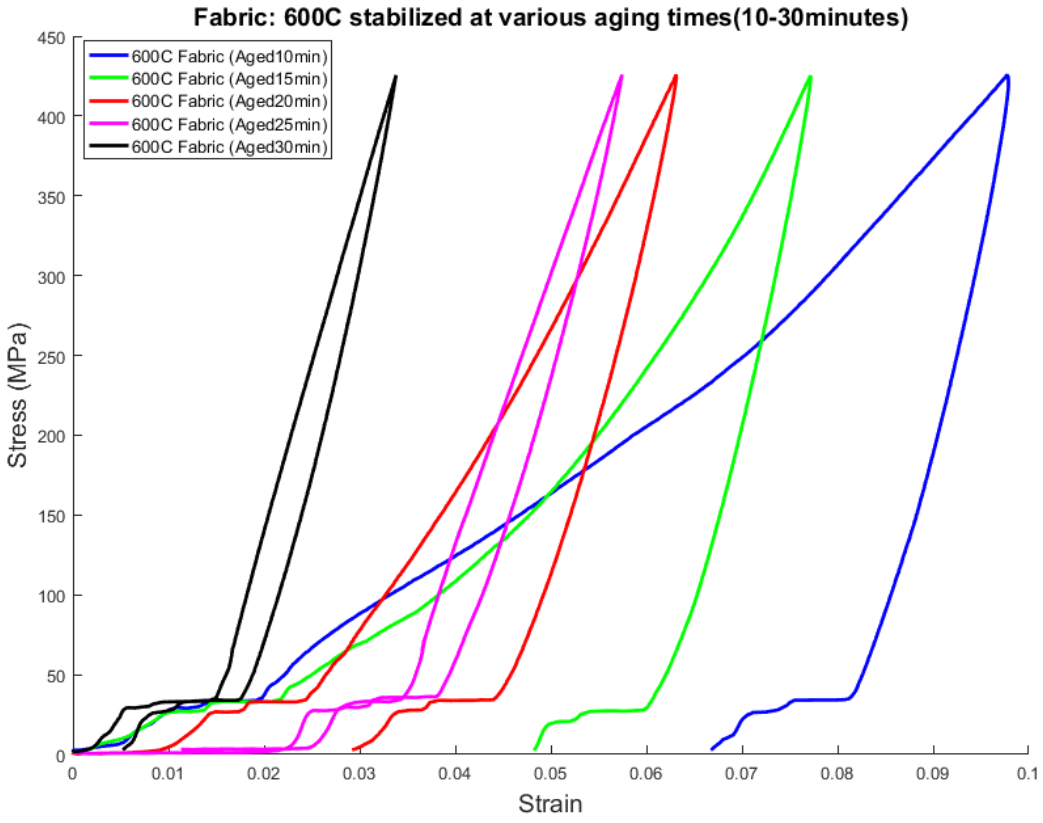

Figure 80: Tensile test of fabric at various aging times tested at room temperature

Upon completion of the room temperature test, it was imperative to test the fabric at various temperatures to see the effects phase change has on the model. It should be noted that the A_f temperature for all aging times was just below 100℃ which means samples tested at 100℃ may or may not have been in the Austenite phase. It is fair to assume that the samples tested at 150 and 200℃ were in the Austenite phase throughout the experiment. The various thermal chamber temperatures conducted on the fabric are shown in Figure 81, Figure 82, and Figure 83.

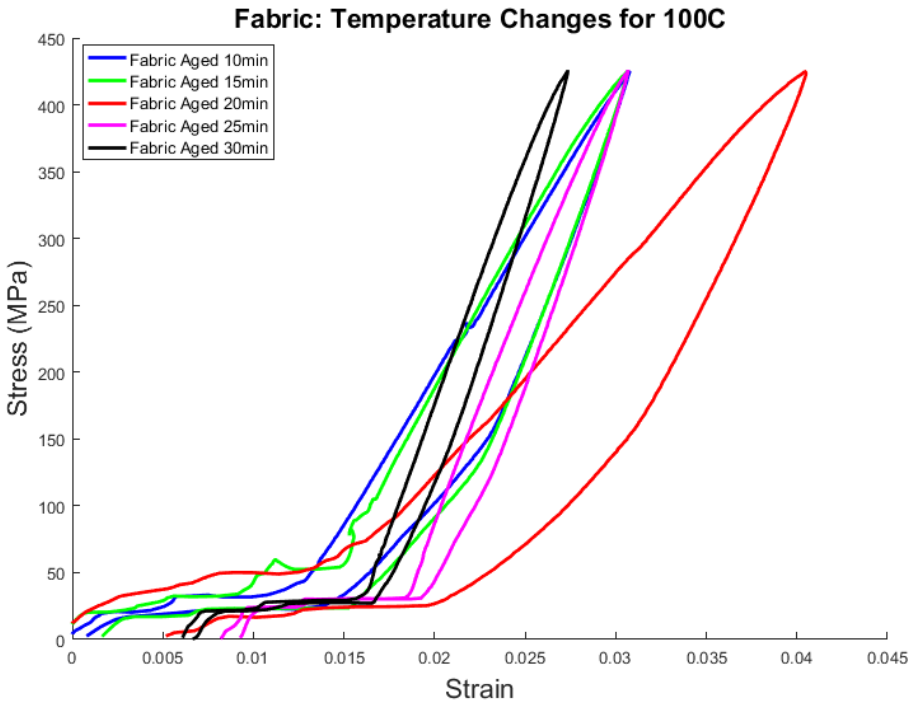

Figure 81: Fabric tensile test results at 100C

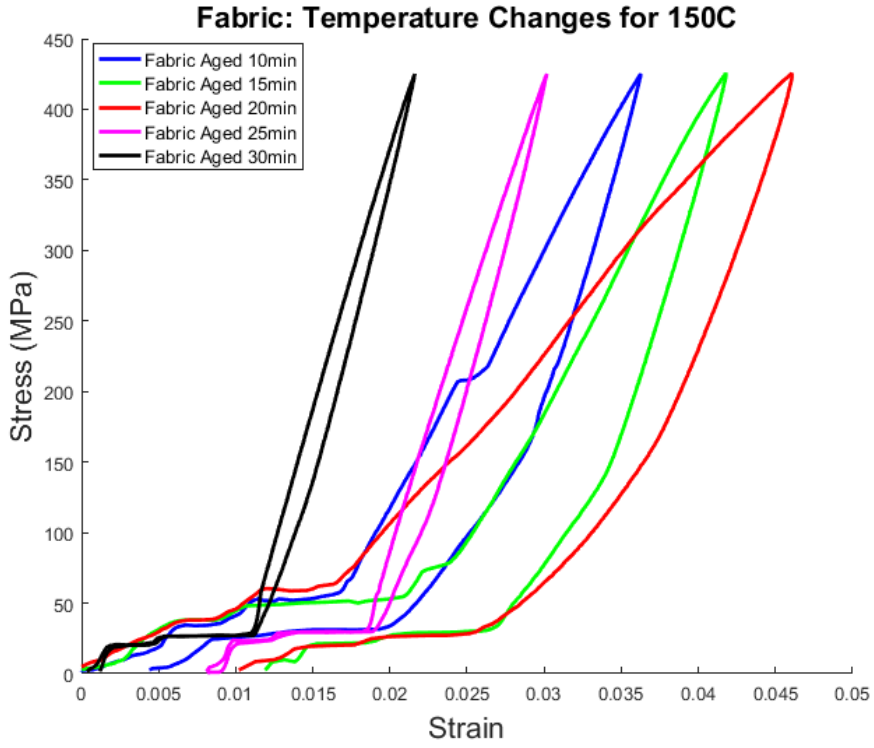

Figure 82: Fabric tensile test results at 150C

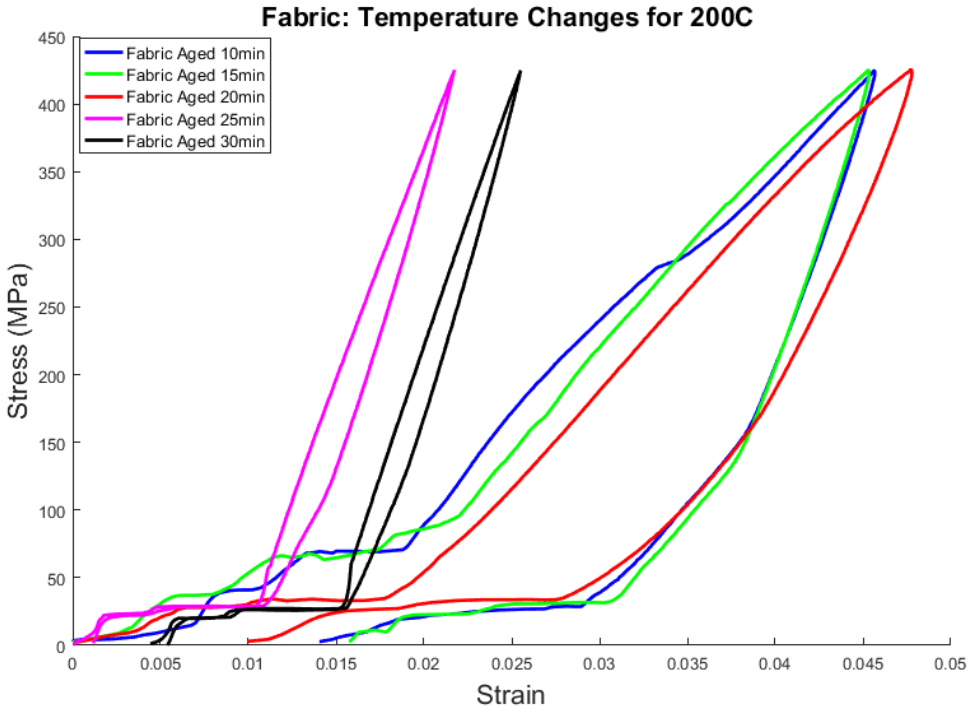

Figure 83: Fabric tensile test results at 200C

Experimental and Predicted Elastic Modulus for Woven Nitinol Fabric

The area of the fabric was measured by using the unit cells height (h), the wires diameter (d), and the amount of wires in the warp direction ($wires_{warp}$).

$$A_{fabric} = h(wires_{warp}d)$$

The fabrics' elastic modulus was determined by fitting a line to the stabilized data when the material was in tension. The test was also conducted with three cycles and can be seen in Table 10.

Table 10: Experimental Elastic Modulus of Fabric at room temperature for various aging times

	Cycle 1	Cycle 2	Cycle 3
10 minutes	6.762 GPa	6.846 GPa	6.969 GPa
15 minutes	6.957 GPa	7.014 GPa	7.048 GPa
20 minutes	6.004 GPa	6.032 GPa	6.159 GPa
25 minutes	5.610 GPa	5.666 GPa	5.720 GPa
30 minutes	4.905 GPa	5.069 GPa	5.267 GPa

The elastic moduli of the cycles of woven Nitinol fabric tested at room temperature were compared (Figure 84). As the cycle increased, the elastic modulus did as well. In general, the elastic modulus decreased as the aging time increased. Both the wire and the woven Nitinol fabric follow the same trend when tested at room temperature.

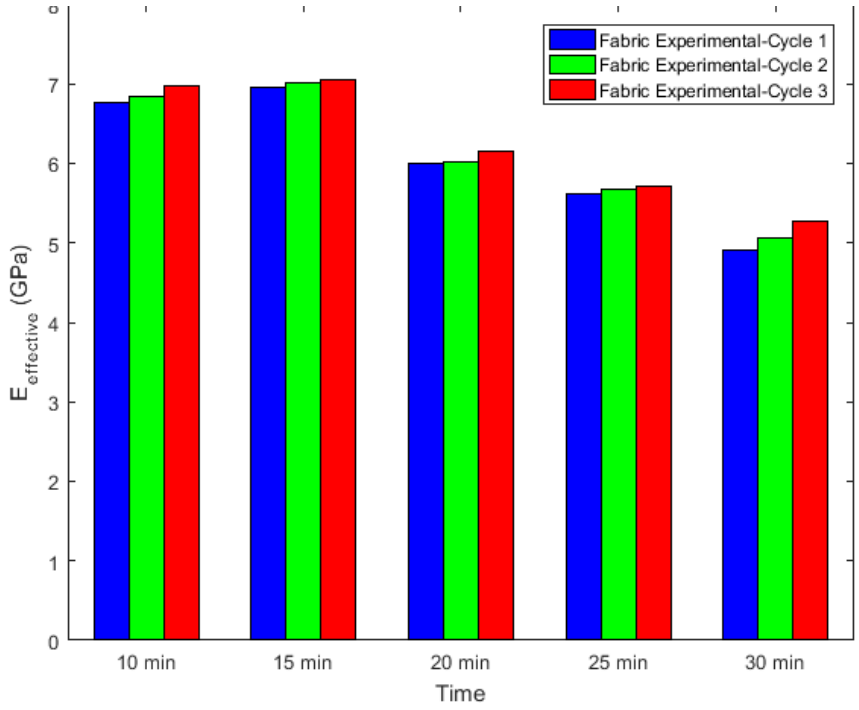

Figure 84: Elastic Moduli of fabric tested at room temperature for various aging times and cycles

The model developed in Chapter 4 was utilized to predict the elastic modulus of the fabric at various temperatures. It takes the single wire's elastic modulus and uses it to predict the elastic modulus of the fabric based on the fabrics geometry, to include the unit cell length, width, height, and the slope of the warp yarn.

$$E_a = \frac{\pi}{12}\left(\frac{E_L}{d} + \frac{E_L cos^2(\alpha)}{g}\right)$$

The predicted elastic modulus is compared to the experimental and the percent error between the samples is calculated. The samples experimental and predicted results are shown in Figure 85 and show that overall, the model has an 8.54% error on average across all aging times.

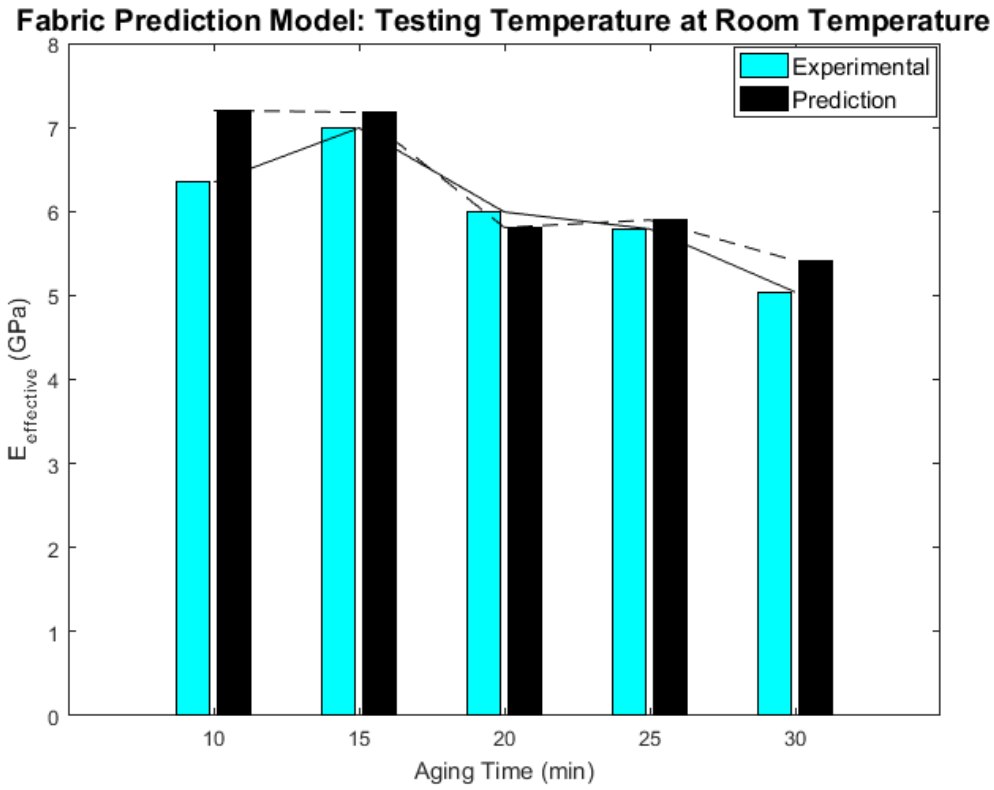

Figure 85: Fabric Prediction Model for room temperature fabric -cycle 1

The single wires elastic modulus was used to predict the fabric elastic modulus at the various aging times and thermal cycles (Table 11).

Table 11: Fabric Prediction Model Results for 100C, 150C, and 200C fabric

	100C		**150C**		**200C**	
Aging Time	**Predicted**	**Experimental**	**Predicted**	**Experimental**	**Predicted**	**Experimental**
10 min	6.19 GPa	6.641 GPa	7.61 GPa	6.938 GPa	8.96 GPa	9.534 GPa
15 min	6.05 GPa	6.122 GPa	6.82 GPa	7.176 GPa	8.48 GPa	9.985 GPa
20 min	6.45 GPa	7.148 GPa	7.50 GPa	7.816 GPa	9.95 GPa	8.413 GPa
25 min	7.25 GPa	7.674 GPa	7.92 GPa	8.242 GPa	10.71 GPa	10.376 GPa
30 min	7.53 GPa	7.621 GPa	10.99 GPa	10.851 GPa	10.96 GPa	11.347 GPa

Those results were then input into a simulation and the models accuracy was calculated. The 200C model had an error of 8.45%. The 150C model had an error of 4.09% and the 100C model had an error of 5.03%. All of the fabric prediction models for the various thermal chamber temperatures can be seen in Figure 88, Figure 87, and Figure 86.

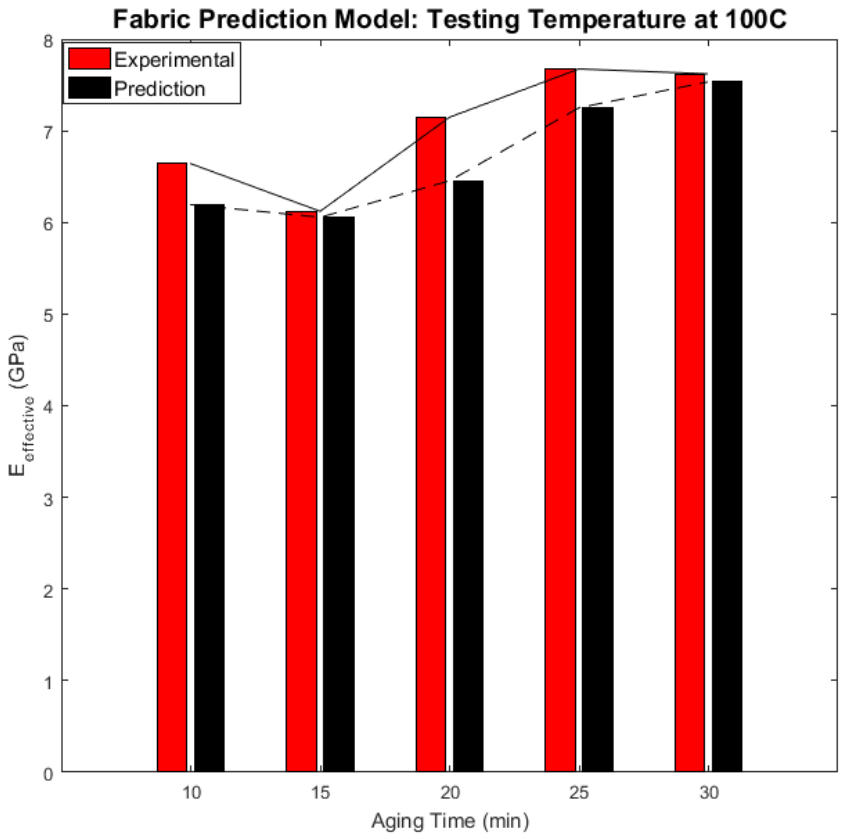

Figure 86: Fabric Prediction model for 100C

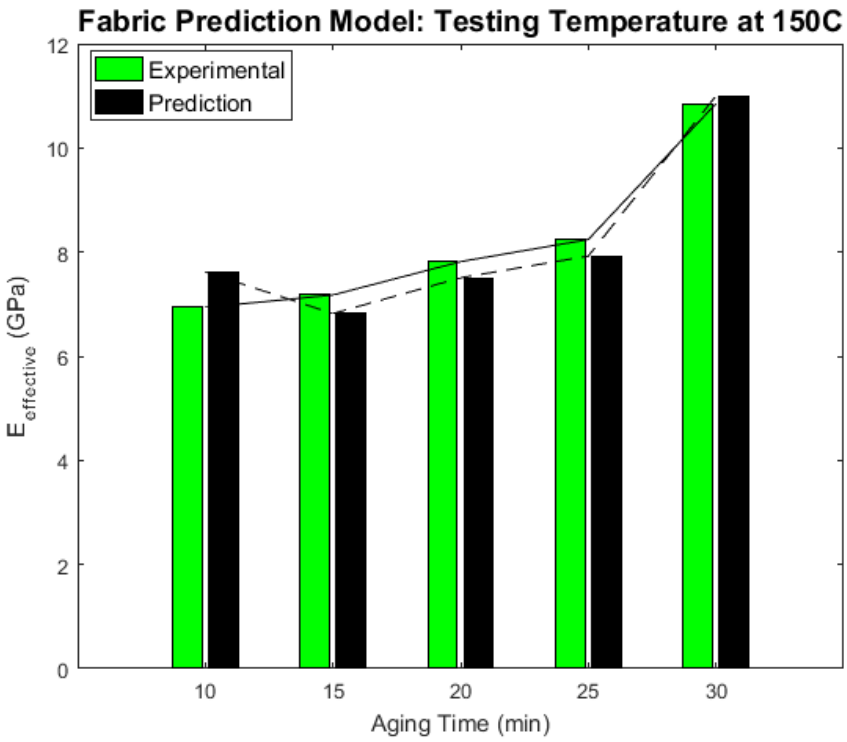

Figure 87: Fabric Prediction model for 150C

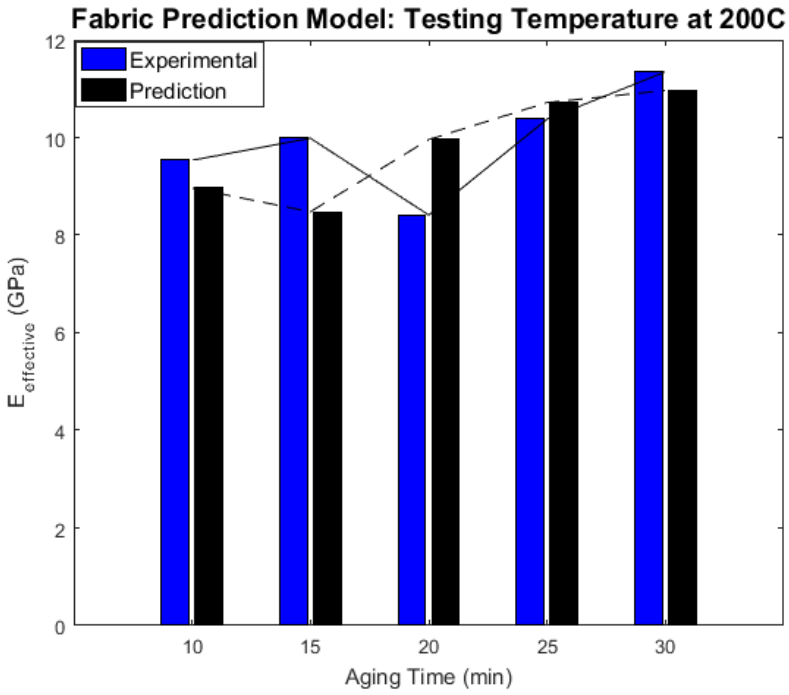

Figure 88: Fabric Prediction model for 200C

Proof of Concept Experimental Heating System vs. Thermal Chamber

Finally, testing was conducted on a wire and Nitinol woven fabric aged for 10 minutes at 600℃ using the proof of concept experimental heating system. These results are compared to those of a thermal chamber at the same aging time and temperature. The tests performed in the proof of concept experimental heating system were only tested for temperatures 100, 150, and 200℃ and the results can be seen in Figure 89. The model using the proof of concept experimental heating system had a 19.89% error overall. When comparing the model using the proof of concept experimental heating system to the model using the thermal chamber, there is a 23.01% error overall.

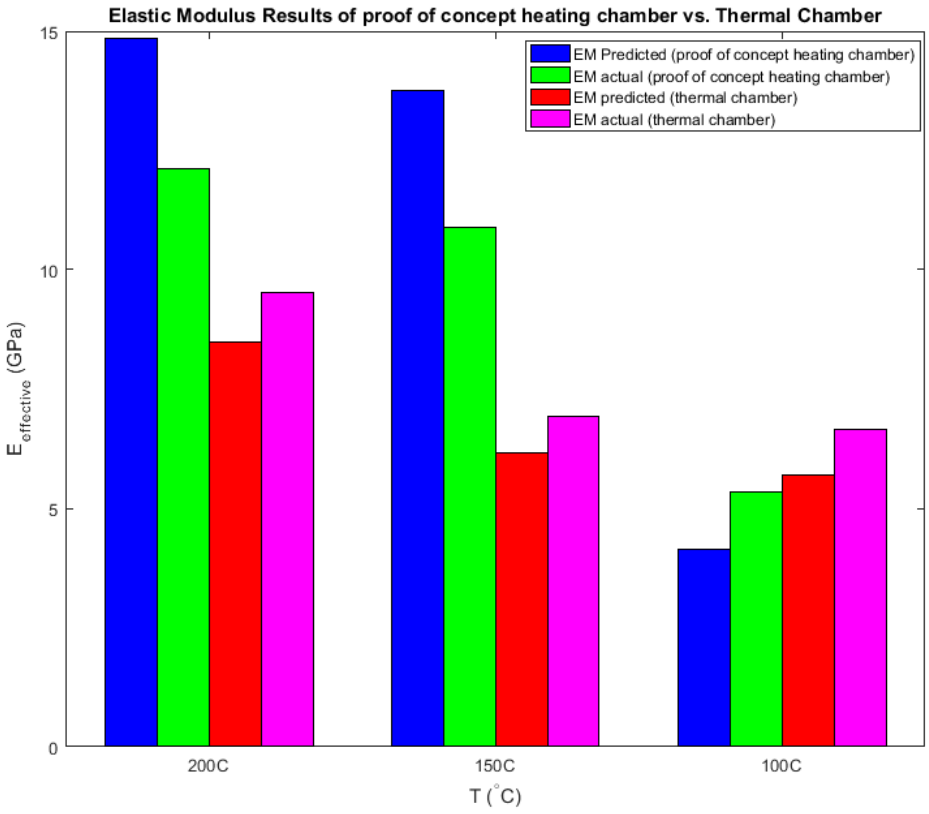

Figure 89: Results of using the proof of concept experimental heating system vs. the Thermal Chamber at Various Testing Temperatures for Wire and Fabric heat treated at 600C for 10 minutes

When the material is in the Austenite phase, the proof of concept experimental heating system predicted the elastic modulus to be way higher than it was. When the material was potentially in the Martensite phase, the model predicted the elastic modulus to be a lot smaller than it was (Figure 90).

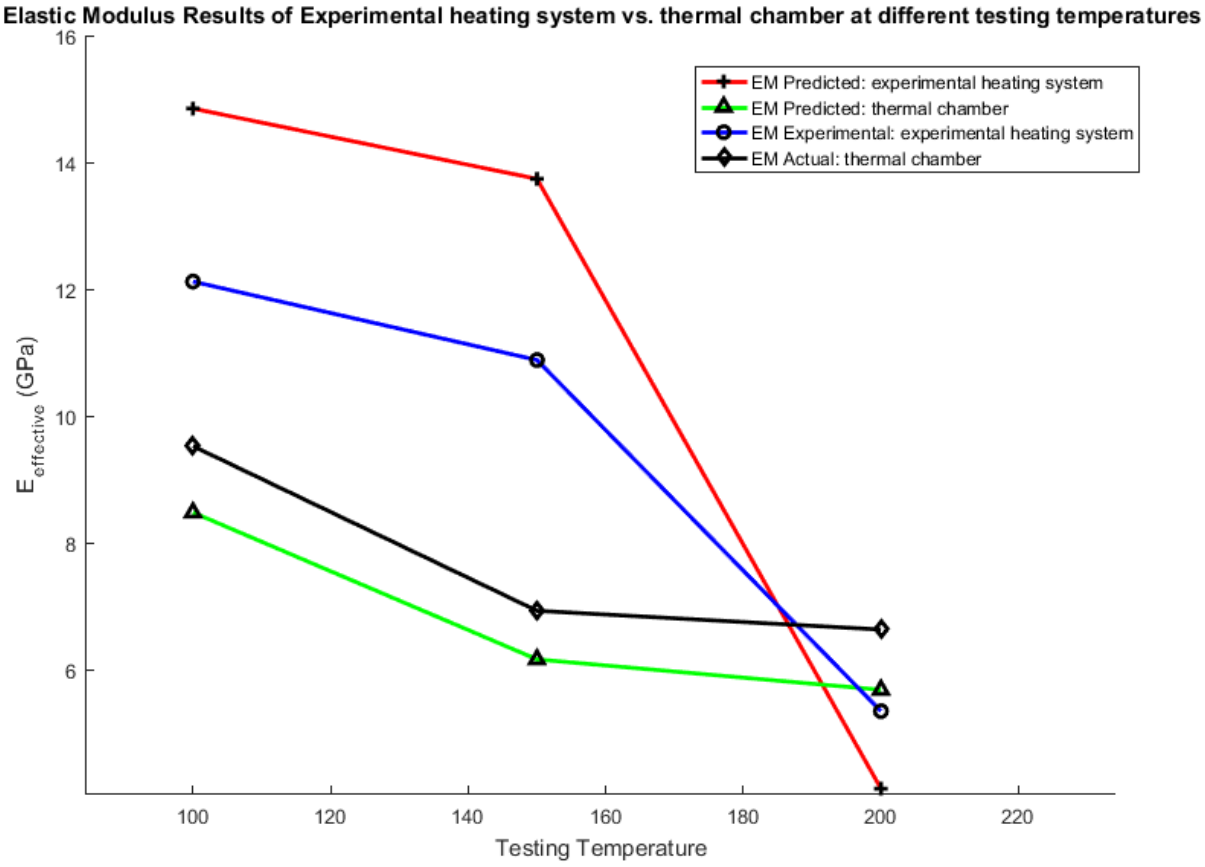

Figure 90: Elastic Modulus results of experimental heating system vs. thermal chamber at various testing temperatures

Conclusion

Through DSC testing, the testing temperatures at and below 450℃ did not demonstrate a full shape-set, therefore they were no longer tested. Additional DSC analysis was conducted on wires heat treated from 500-700℃ and their transformation temperatures found. The testing

temperatures of the 550 and 600℃ wire demonstrated no presence of the R-phase. However, that was not enough information to determine which temperature should be used to see the results of aging. An initial tensile test was conducted on the wires heat treated at those temperatures and it was concluded that the testing temperature of 600℃ showed the most amount of recoverable strain.

Upon this determination, the wires were then aged for various durations from 10-30 minutes in 5-minute intervals. The fabric was also heat treated at this temperature and aged for the same time periods. It was found that the wire took a lot longer to stabilize than the fabric did. Once the wire and fabric were stabilized, both were tested once again ranging from testing temperatures of room temperature to 200℃. From these results, the elastic modulus was calculated, and the results of the single wire were used to predict the elastic modulus of the fabric at those temperatures. Ultimately it has been concluded that using the thermal chamber provides more accurate results when testing the wire and fabric at various temperatures. Additionally, the elastic modulus decreased as the aging time increased when the testing temperature was room temperature and the elastic modulus increased as the testing temperature was 100-200℃. Finally, the model proved to be accurate across all temperatures and aging times tested and averages a 6.53% error throughout the testing process.

Chapter 8

Discussion and Conclusion

This work presents the first known woven Nitinol fabric. This fabric is modeled using composite and woven fabric analysis. The model accurately predicts the elastic behavior of woven Nitinol fabric. Various Nitinol wires and woven Nitinol fabric are aged, and heat treated for different durations and temperatures. The transformation temperature(s) of the Nitinol wire used in the woven fabric is found using DSC analysis. Once the correct heat treatment process is chosen, the single wire and woven Nitinol fabric are tested, and elastic moduli determined. It has been concluded that the elastic modulus of wire in the Martensite phase is smaller than the elastic modulus in the Austenite phase. Additionally, the fabric model created proved to be accurate across all temperatures and aging times tested and averaged a 6.45% error throughout the testing process. The potential sources of error include: using too large of a load cell when testing the wire as it demonstrated a lot of noise throughout the test, not choose the correct slope to calculate the elastic modulus, and not cycling the wires enough times, even though they showed stabilization.

Throughout the manufacturing and testing process, there were difficulties experienced throughout. First, gaining access to a thermal chamber was extremely difficult. Secondly, the tensile testing machine did not have a smaller load cell which would have been better when testing the wires. Third, having to weave the fabric using the Narrow Fabric Weaving Machine without any prior knowledge about weaving. Finally, not having the proper equipment to perform a proper DSC test for Nitinol wire.

Although there were difficulties, many things went well throughout this thesis. First, it was proven by hand weaving that it was indeed possible to weave Nitinol fabric together, thus paving

the way for future research. Secondly, the thermal chamber provided an excellent source of heating and made the testing run a lot smoother. Third, learning about weaving, DSC testing, and Nitinol has provided a base-line for future research to come.

Future research should be conducted using a thermal chamber while thermally cycling the temperature and holding the stress constant. Additionally, testing using the cooling function of the furnace should be conducted to ensure accuracy of the experimental data. Some of the errors of the results initially occurred during the DSC test as the results varied drastically as the samples were tested. This could be corrected by having the proper equipment to prepare the samples. Wire that has a pre-determined transformation temperature(s) should be used to guarantee accuracy throughout the testing process.

References

[1] W. Buechler, J. Gilfrich and R. Wiley, "Effect of low-temperature phase changes on the mechanical properties of alloys near composition.," pp. 34:1475-7, 1963.

[2] M. Wu and L. Schetky, "Industrial Applications for shape memory alloys," in *In: International conference on shape memory and superelastic technologies*, Pacific Grove, California , 2000, pp. 171-82.

[3] A. Sofla, S. Meguid, K. Tan and W. Yeo, "Shape morphing of aircraft wing: Status and challenges," *Materials and Design,* vol. 31, pp. 1284-1292, 2010.

[4] C. Tuna, J. Solomon, D. Jones and M. Hartmann, "Object shape recognition with artificial whiskers using tomographic reconstruction," in *IEEE International Conference on Acoustics, Speech and Signal Processing*, Kyoto, 2012.

[5] G. Lewis, "Materials, Fluid Dynamics, and Solid Mechanics Aspects of Coronary Artery Stents: A State-of-the-Art Review," *Wiley Periodicals, Inc.*, vol. 1, pp. 569-590, 2007.

[6] I. Kutlucinar, "Aircraft with shape memory alloys for retractable landing gear". United States of America Patent 6,938,416 B1, 6 September 2005.

[7] G. Bunget and S. Seelecke, "Actuator placement for a bio-inspired bone-joint system based on SMA," in *SPIE Smart Structures and Materials*, San Diego, 2009.

[8] J. Colorado, A. Barrientos, C. Rossi, J. Bahlman and K. Breuer, "Corrigendum: Biomechanics of smart wings in bat robot: morphing wings using SMA actuators," *Bioinspirations and Biomimetics,* vol. 7, pp. 1-16, 2012.

[9] D. Levi, N. Kusnezov and G. Carman, "Smart Materials Applications for Pediatric Cardiovascular Devices," *International Pediatric Research Foundation, Inc,* vol. 63, no. 4, pp. 552-558, 2008.

[10] M. Tawfik, J. Ro and C. Mei, "Thermal post-buckling and aeroelastic behaviour of shape memory alloy reinforced plates," *Smart Materials and Structures,* vol. 11, pp. 297-307, 2002.

[11] B. Trimmer, A. Takesian, B. Sweet, C. Rogers, D. Hake and D. Rogers, "Caterpillar locomotion: a new model for soft-bodied climbing and burrowing robots," in *7th International Symposium on Technology and the Mine Problem*, Monterey, 2006.

[12] W. Wang, S. Cooper and S. Eberhardt, "Use of a nitinol gooseneck snare to open an incompletely expanded over-the-wire stainless steel Greenfield filter," *American Roentgen Ray Society* , vol. 172, pp. 499-500, 1999.

[13] T. Lambert, A. Gurley and D. Beale, "Heat Transfer Modelling and Bandwidth Determination of Shape Memory Alloy Actuators in Robotic Applications," in *Early Career Technical Conference* , Birmingham , 2016.

[14] A. Gurley, T. Lambert, D. Beale and R. Broughton, "Robust Self-Sensing in NiTi Actuators Using a Dual Measurement Technique," in *ASME 2016 Conference on Smart Materials, Adaptive Structures and Intelligent Systems*, Stowe, Vermont, 2016.

[15] T. Lambert, A. Gurley and D. Beale, "SMA actuator material model with self-sensing and sliding-mode control; experiment and multibody dynamics model," *Smart Materials and Structures,* vol. 26, no. 3, 2017.

[16] J. M. M. Components, "Nitinol," Johnson Matthey Medical Components, 2018. [Online]. Available: http://jmmedical.com/nitinol/64/Wire.html. [Accessed 21 September 2018].

[17] K. R. Labs, "Nitinol Springs," Kellogg's Research Labs, 2015. [Online]. Available: https://www.kelloggsresearchlabs.com/Nitinol/Nitinol-springs. [Accessed 21 September 2018].

[18] T. Medical, "Quick Wire and Tubing," Tegra Medical , [Online]. Available: https://www.tegramedical.com/purchase-wiretubing/. [Accessed 21 September 2018].

[19] Indiamart, "Nitinol Sheet," IndiaMart, 2018. [Online]. Available: https://www.indiamart.com/proddetail/nitinol-sheet-10864800388.html. [Accessed 21 September 2018].

[20] J. Matthey, "Nitinology: Advancing the Science of Nitinol," Jan 2018. [Online]. Available: http://jmmedical.com/nitinol.html. [Accessed 20 Feb 2018].

[21] A. Ölander, "An electrochemical investigation of solid cadmium-gold alloys," *Am Chem Soc,* vol. 54, pp. 3819-3833, 1932.

[22] L. Vernon, "Process of manufactoring articles of thermoplastic synthetic resins". United States of America Patent 2234993, 1941.

[23] G. Kauffman and I. Mayo, "The Story of Nitinol: The Serendipitous Discovery of the Memory Metal and Its Applications," *The Chemical Educator* , vol. 2, no. 2, pp. 1-21, 1997.

[24] D. Hartl and D. Lagoudas, "Aerospace applications of shape memory alloys," *Proc Inst Mech Eng, Part G: J Aerospace ENG,* vol. 221, pp. 5535-52, 2007.

[25] D. C. Lagoudas, "Shape Memory Alloys," Springer, 2008, p. 10.

[26] C. Churchill and J. Shaw, "Shakedown Response of Conditioned Shape Memory Alloy Wire," in *Behavior and Mechanics of Multifunctional and Composite Materials,* San Diego, M.J Dapino, 2008, p. 6928.

[27] J. Uchil, K. Mohanchandra, K. Mahesh and K. Ganesha Kumara, "Thermal and electrical characterization of R-phase dependence on heat-treat temperature in Nitinol," *Physica B,* vol. 253, pp. 83-49, 1998.

[28] H. Sadiq, M. Wong, R. Al-Mahaidi and X. Zhao, "The effect of heat treatment on the recovery stresses of shape memory alloys," *Smart Materials and Structures,* vol. 19, pp. 1-7, 2010.

[29] V. Novak, P. Sittner, G. Dayananda, F. Braz-Fernandes and K. Mahesh, "Electric resistance variation of NiTi shape memory alloy wires in thermomechanical tests: Experiments and simulation," *Materials Science and Engineering,* vol. A, pp. 127-133, 2008.

[30] J. Zhang and Y. Yin, "SMA-based bionic integration design of self-sensor-actuator-structure for artificial skeletal muscle," *Elsevier,* vol. 181, pp. 94-102, 2012.

[31] J. Zhang, Y. Yin and J. Zhu, "Electrical Resistivity-Based Study of Self-Sensing Properties for Shape Memory Alloy-Actuated Artificial Muscle," *Sensors,* vol. 13, pp. 12958-12974, 2013.

[32] J. Shaw, C. Churchill and M. Iadicola, "Tips and Tricks for Characterizing Shape Memory Alloy Wire - Part 1 - Differential Scanning Calorimetry and Basic Phenomena," *Experimental Characterization of Active Materials Series,* pp. 55-62, 2008.

[33] D. Lagoudas, Shape memory alloys: Modeling and Engineering Applications, New York: Springer, 2010.

[34] T. Duerig and A. Pelton, "Ti-Ni Shape Memory Alloys," *Materials Properties Handbook: Titanium Alloys,* vol. 1, pp. 1035-1048, 1994.

[35] W. Buehler and F. Wang, "A summary of recent research on the nitinol alloys and their potential applications in ocean engineering," *Ocean Engineering,* vol. 1, pp. 105-120, 1968.

[36] K. Otsuka and C. Wayman, Shape Memory Materials, Cambridge: Cambridge University Press, 1999.

[37] W. Huang and W. Toh, "Training two-way shape memory alloy by reheat treatment," *Journal of Materials Science Letters,* vol. 19, pp. 1549-1550, 2000.

[38] D. Stöckel, "The Shape Memory Effect," EUROflex, Fremont, 2000.

[39] C. Lexcellent, S. Leclercq, B. Gabry and G. Bourbon, "The two way shape memory effect of shape memory alloys: an experimental study and a phenomenological model," *International Journal of Plasticity,* vol. 16, pp. 1155-1168, 2000.

[40] W. Huang, "Two-way behavior of a Nitinol torsion bar," in *Symposium on Smart Structures and Materials*, Newport Beach, 1999.

[41] R. Stalmans, J. Van Humbeeck and L. Delaey, "Thermomechanical cycling, two way memory and concomitant effects in Cu-Zn-Al alloys," *Acta metall. mater.,* vol. 40, no. 3, pp. 501-511, 1992.

[42] Y. Liu and P. McCormick, "Factors influencing the development of two-way shape memory in NiTi," *Acta. metall. mater.,* vol. 38, no. 7, pp. 1321-1326, 1990.

[43] R. Stalmans, J. Van Humbeeck and L. Delaey, "The two way memory effect in cooper-based shape memory alloys-Thermodynamics and mechanisms," *Acta metall. mater.,* vol. 40, no. 11, pp. 2921-2931, 1992.

[44] Z. Wei, R. Sandström and S. Miyazaki, "Shape-memory materials and hybrid composites for smart systems: Part I Shape-memory materials," *Journal of Materials Science,* vol. 33, pp. 3743-3762, 1998.

[45] F. W. M. R. P. Corp, "Fort Wayne Metals: Turning Knowledge into solutions," Fort Wayne Metals, 2018. [Online]. Available: https://www.fwmetals.com/materials/nitinol/wire/. [Accessed 20 09 2018].

[46] K. Melton and O. Mercier, "The Mechanical Properties of NiTi-based Shape Memory Alloys," *Acta Metallurgico,* vol. 29, pp. 393-398, 1981.

[47] S. Thompson, "An Overview of nickel-titanium alloys used in dentistry," *International Endodontic Journal,* vol. 33, pp. 297-310, 1999.

[48] D. Lagoudas and e. al, "Shape Memory Alloys, Part II- Modeling of polycrystals," *Mechanics of Materials,* vol. 38, pp. 430-462, 2006.

[49] M. Khan, A. Pequegnat and N. Zhou, "Multiple Memory Shape Memory Alloys," *Advanced Engineering Materials,* vol. 15, no. 5, pp. 386-393, 2013.

[50] C. Tang, W. Huang, C. Wang and H. Purnawali, "The triple-shape memory effect in NiTi shape memory alloys," *Smart Materials and Structures,* vol. 21, pp. 1-7, 2012.

[51] Sadrnezhaad, "Heat Treatment of Ni-Ti Alloy for Improvement of Shape Memory Effect," *Materials and Manufactoring Processes,* vol. 12, no. 1, pp. 107-115, 1997.

[52] J. Uchil, K. Mohanchandra, K. Mahesh and K. Ganesh Kumara, "Dilatometric and electrical resistivity measurements in various phases of Nitinol," *The International Society for Optical Engineering,* vol. 1, pp. 321-328, 1999.

[53] A. Golestaneh and J. Carpenter, "Study of the martensitic transformation in shape-memory Nitinol alloy by time-of-flight neutron diffraction techniques," *Acta Metall. Mater.*, vol. 38, no. 7, pp. 1291-1305, 1990.

[54] S. Sadrnezhaad, "Heat Treatment of Ni-Ti Alloy for Improvement of Shape Memory Effect," *Materials and Manufacturing Processes,* vol. 12, no. 1, pp. 107-115, 1997.

[55] S. Miyazaki, Y. Igo and K. Otsuka, "Effect of thermal cycling on the transformation temperatures of Ti-Ni alloys," *Acta metall. ,* vol. 34, no. 10, pp. 2045-2051, 1986.

[56] B. Li, L. Rong and Y. Li, "Porous NiTi alloy prepared from elemental powder sintering," *Journal of Materials Research,* vol. 13, no. 10, pp. 2847-2851, 1998.

[57] "The Library of Manufacturing," 2018. [Online]. Available: https://thelibraryofmanufacturing.com/index.html. [Accessed 2018 October 2018].

[58] M. P. I. Federation, "Isostatic Pressing," Metal Powder Industries Federation, 2018. [Online]. Available: https://www.mpif.org/IntrotoPM/Processes/IsostaticPressing.aspx. [Accessed 15 October 2018].

[59] K. Patil, S. Aruna and T. Mimani, "Combustion sysnthesis: an update," *Solid State & Materials Science,* vol. 6, pp. 507-512, 2002.

[60] e. a. Delgado, "Science Direct," Journal of Alloys and Compounds, 15 February 2016. [Online]. Available: https://www.sciencedirect.com/science/article/abs/pii/S0925838815314870. [Accessed 15 October 2018].

[61] F. Wang, E. DeSavage and W. Buehler, "The Irreversible Critical Range in the TiNi Transition," *Journal of Applied Physics,* vol. 39, no. 8\, pp. 2166-2175, 1968.

[62] M. Iijima, H. Ohno and I. Kawashima, "Mechanical behavior at different temperatures and stresses for superelastic nickel-titanium orthodontic wires having different transformation temperatures," *Dental Materials,* vol. 18, pp. 88-93, 2002.

[63] S. Prokoshkin and et.al, "Alloy composition, deformation temperature, pressure and post-deformation annealing effects in severely deformed Ti-NI based shape memory alloys," *Acta Materialia,* vol. 53, pp. 2703-2714, 2005.

[64] T. Todoroki and H. Tamura, "Effect of Heat Treatment after Cold Working on the Phase Transformation in TiNi Alloy," *Transactions of the Japan Institue of Metals,* vol. 28, no. 2, pp. 83-94, 1987.

[65] Dynalloy, "Flexinol Actuator Wire," 2018. [Online]. Available: http://www.dynalloy.com/flexwire_70_90.php. [Accessed 15 October 2018].

[66] S. Shabalovskaya, J. Anderegg and J. Van Humbeeck, "Critical overview of Nitinol surfaces and their modifications for medical applications," *Acta Biomaterialia,* vol. 4, pp. 447-467, 2008.

[67] T. Tadaki, Y. Nakata and K. Shimizu, "Thermal cycling effects in an Aged Ni-rich Ti-Ni Shape Memory Alloy," *Transactions of the Japan Institute of Metals,* vol. 28, no. 11, pp. 883-890, 1987.

[68] S. Wu, H. Lin and T. Chou, "A study of electrical resistivity, internal friction and shear modulus of an aged TiNi alloy," *Acta metall. mater.* , vol. 38, no. 1, pp. 95-102, 1990.

[69] M. Losertova, M. Stencek, D. Matysek, O. Stefek and J. Drapala, "Microstructure evolution of heat treated NiTi alloys," in *27th Joint Seminar Development of Materials Science in Research and Education*, Ostrava-Poruba, 2017.

[70] G. e. a. Eggeler, "On the effect of aging on martensite transformations in Ni-rich NiTi shape memory alloys," *Smart Marterials and Structures,* vol. 14, pp. 186-191, 2005.

[71] Y. Kaieda, "Fabrication of composition-controlled TiNi shape memory wire using combustion synthesis process and the influence of Ni content on phase transformation behavior," *Science and Technology of Advanced Materials,* vol. 4, pp. 239-246, 2003.

[72] D. Lagoudas and Z. Bo, "Thermomechanical modeling of polycrystalline SMAs under cyclic loading, Part II: material characterization and experimental results for a stable transformation cycle," *International Journal of Engineering Science,* vol. 37, pp. 1141-1173, 1999.

[73] S. Manchiraju and et.al, "Thermal cycling and isothermal deformation response of polycrystalline NiTi: Simulations vs. experiments," *Acta Materialia,* vol. 59, pp. 5238-5249, 2011.

[74] K. Wada and Y. Liu, "Some factors affecting the shape recovery properties of NiTi SMA," in *Structures, Structural Dynamics, and Materials Conference*, Newport, 2006.

[75] X. Wu, G. Sun and J. Wu, "The nonlinear relationship between transformation strain and applied stress for nitinol," *Materials Letters,* vol. 57, pp. 1334-1338, 2003.

[76] R. Adharapurapu, F. Jiang, J. Bingert and K. Vecchio, "Influence of cold work and texture on the high-strain-rate response of Nitinol," *Materials Science and Engineering,* vol. 527, pp. 5255-5267, 2010.

[77] S. Padula, D. Gaydosh, S. Saleeb and B. Dhakal, "Transients and Evolution in NiTi," *Experimental Mechanics,* vol. 54, pp. 709-715, 2014.

[78] N. Jones and D. Dye, "Martensite evolution in a NiTi shape memory alloy when thermal cycling under an applied load," *Intermetallics,* vol. 19, pp. 1348-1348, 2011.

[79] V. Pelosin and A. Riviere, "Effect of thermal cycling on the R-Phase and Martensitic Transformations in a Ti-Rich NiTi alloy," *Metallurgical and Materials Transactions A,* vol. 29A, pp. 1175-1180, 1998.

[80] J. Monroe and e. al, "Determining recoverable and irrecoverable contributions to accumulated strain in NiTiPd high-temperature shape memory alloy during thermomechanical cycling," *Scripta Materialia,* vol. 65, pp. 123-126, 2011.

[81] Y. Li, X. Mi and X. X. H. Yin, "Constrained recovery properies of NiTi shape memory alloy wire during thermal cycling," *Journal of Alloys and Compounds,* vol. 588, pp. 525-529, 2014.

[82] S. Islam, S. Chowdhury and S. Akter, "The Experiential Analysis of Woven Fabric for Reproduction," *Journal of Textile Science and Technology,* vol. 4, pp. 18-48, 2018.

[83] S. Heidi, "Successful Fashion Designer," Sew Heidi, 2018. [Online]. Available: https://successfulfashiondesigner.com/types-of-weave-structures/. [Accessed 27 September 2018].

[84] S. Adanur, "Fabric Manufacturing," in *Textiles, Wellington Sears Handbook of Industrial*, Lancaster, Technomic Publishing Company, Inc. , 1995, pp. 111-127.

[85] H. Otto, "Warp Let-off Means". Switzerland Patent 3,878,872, 27 September 1973.

[86] A. Wahhoud and J. Hehle, "Method and apparatus for compensating warp thread tension or elongation variations during loom shedding". Germany Patent 6,135,163, 7 December 1999.

[87] M. Kayacan, M. Dayik, O. Colak and M. Kodaloglu, "Velocity Control of Weft Insertion on Air Jet Looms by Fuzzy Logic," *Fibres and Textiles in Eastern Europe,* vol. 12, no. 3, pp. 29-33, 2004.

[88] D. Mehmet, C. Hakan and K. Cengiz, "Adaptive control of let-off system in weaving," *The Journal of The Textile Institute,* vol. 100, no. 2, pp. 186-194, 2009.

[89] Taesintex, "Heavy-Duty Narrow Fabric Needle Loom," 28 Feburary 2012. [Online]. Available: https://www.youtube.com/watch?v=6WDItC4Xc7g. [Accessed 11 November 2018].

[90] S. V. e. a. Lomov, "Meso-FE modelling of textile composites: Road map, data flow and Algorithms," *Composites Science and Technology,* vol. 67, no. 9, pp. 1870-1891, 2007.

[91] F. Peirce, "The Geometry of Cloth Structures," *Journal of the Textile Institute*, vol. 28, no. T45, pp. 43-77, 1937.

[92] T. Kang, S. Choi, S. Kim and K. Oh, "Automatic Structure Analysis and Objectives Evaluation of Woven Fabric Using Image Analysis," *Textile Research Journal,* vol. 71, no. 3, pp. 261-270, 2001.

[93] J. e. a. Crookston, "3D Textile Composite Mechanical Properties Prediction Using Automated FEA of the Unit Cell," in *16th International Conference on Composite Materials*, Kyoto, 2007.

[94] B. V. Sankar and R. V. Marrey, "Analytical Method for Micromechanics of Textile Composites," Elsevier, Gainesville, 1997.

[95] E. Morozov, "Mechanics and analysis of fabric composites and structures," *AUTEX Research Journal* , vol. 4, no. 2, pp. 60-71, 2004.

[96] Dextronix, "Nitinol Tracheal Stents," 2018. [Online]. Available: https://www.dextronix.com/products/nitinol-tracheal-stents/. [Accessed 30 October 2018].

[97] Vili, "Investigating Smart Textiles Based on Shape Memory Materials," *Textile Research Journal*, vol. 77, no. 5, pp. 290-300, 2007.

[98] S. Yi, C. Weinberg, K. Eschen and J. Abel, "Preliminary Experimental Study of the Effect of Shape Setting on Knitted SMA Stuctures," in *Smart Materials, Adaptive Structures and Intelligent Systems*, Snowbird, 2017.

[99] L. Carvalho, J. Cavalcante and J. d'Almeida, "Comparison of the Mechanical Behavior of Plain Weave and Plain Weft Knit Jute Fabric-Polyester-Reinforced Composites," *Polymer-Plastics Technology and Engineering,* vol. 45, no. 7, pp. 791-797, 2006.

[100] K. Tanaka, "A Thermomechanical Sketch of Shape Memory Effect: One-Dimensional Tensile Behavior," *Res Mechanica,* vol. 2, no. 3, pp. 59-72, 1986.

[101] C. Liang and C. Rogers, "One-dimentional thermomechanical constitutive relations for shape memory materials," *Journal of Intelligent Materials, Systems, and Structures,* vol. 1, pp. 207-234, 1990.

[102] A. Gurley, *Classifying the Development of SMA actuator Phenomenological Models from the Past 30 Years,* Auburn, AL, 2017.

[103] K. Ikuta, M. Tsukamoto and S. Hirose, "Matematical Model and Experimental Verification of Shape Memory Alloy for Designing Micro Actuator," in *Micro Elctro Mechnical Systems (MEMS '91) Proceedings. An investigation of Micro Structures, Sensors, Actuators, Machines, and Robots IEEE*, Nara, 1991.

[104] L. Brinson and M. Huang, "Simplifications and Comparisons of Shape Memory Alloy Constitutive Models," *Journal of Intelligent Material Systems and Structures,* vol. 7, pp. 108-114, 1996.

[105] A. Furst, J. Crews and S. Seelecke, "Stress, strain, and resistance behavior of two opposing shape memory alloy actuator wires for resistance based self-sensing applications," *Intelligent Material Systems and Structures,* vol. 24, no. 16, pp. 1951-1968, 2013.

[106] M. Elahinia and M. Ahmadian, "An enhanced SMA phenomenological model: II. The experimental study," *Smart Materials and Structures,* vol. 14, pp. 1309-1319, 2005.

[107] B. Jaber, S. Mehrez and O. Ghazouani, "A 1D constitutive model for shape memory alloy using strain and temperature as control variables and including martensite reorientation and asymmetric behaviors," *Smart Materials and Structures,* vol. 23, pp. 1-10, 2014.

[108] T. e. a. Lambert, "Numerical Heat Transfer Modelling of SMA actuators and model comparison," *Smart Materials, Adaptive Structures and Intelligent Systems,* pp. 1-11, 2017.

[109] N. Zotov, V. Marzynkevitsch and E. Mittemeijer, "Evaluation of kinetic equations describing the martensite-austenite phase transformation in NiTi shape memory alloys," *Journal of Alloys and Compounds,* vol. 616, pp. 385-393, 2014.

[110] W. Huang, "Modified Shape Memory Alloy Model for SMA Wire Based Actuator Design," *Journal of Intelligent Material Systems and Structures,* vol. 10, pp. 221-231, 1999.

[111] N. K. Naik and V. K. Ganesh, "Prediction of on-axes elastic properties of plain weave fabric composites," *Composites Science and Technology,* pp. 135-152, 1991.

[112] J. Hearle, P. Grosberg and S. Baker, Structural Mechanics of Fibers, Yarns, and Fabrics, New York City: John Wiley & Sons, 1969.

[113] A. Adumitroaie and E. J. Barbero, "Beyond Plain Weave Fabrics- II. Mechanical Properties," in *Composite Structures* , Morgantown, West Virginia University , 2011, pp. 1449-1462.

[114] T. Ishikawa and T. Chou, "Nonlinear Behavior of Woven Fabric Composites," *Journal of Composite Materials,* vol. 17, no. 5, pp. 399-413, 1983.

[115] T. Ishikawa and T. W. Chou, "Stiffness and Strength Behaviour of Woven Fabric Composites," *Journal of Materials Science,* pp. 17:3211-3220, 1982.

[116] M. Ito and T. Chou, "An Analytical and Experimental Study of Strength and Failure Behavior of Plain Weave Composites," *J Comp Mater,* vol. 32, no. 1, pp. 2-30, 1996.

[117] M. Ito and T. W. Chou, "Elastic Moduli and Stress Field of Plain-Weave Composites under Tensile Loading," *Composites SCience and Technology,* vol. 57, pp. 787-800, 1997.

[118] R. Naik, "Failure Analysis of Woven and Braided Fabric Reinforced Composites," *Journal of Composite Materials,* pp. 17: 2334-2363, 1995.

[119] B. e. a. Behra, Modeling of Woven Fabrics Geometry and Properties, Rijeka: Intech, 2012.

[120] V. Vasiliev and E. Morozov, Mechanics and Analysis of Composite Materials, Oxford: Elsevier, 2001.

[121] A. F2004-17, "Standard Test Method for Transformation Temperature of Nickel-Titanium Alloys by Thermal Analysis," 2017. [Online]. Available: https://doi.org/10.1520/F2004-17. [Accessed 1 September 2018].

[122] F. W. Metals, "Nitinol Wire," Fort Wayne Metals, 2018. [Online]. Available: https://www.fwmetals.com/materials/nitinol/wire/. [Accessed 15 October 2018].

[123] D. Dynamics, "neoPLC," Deft Dynamics, 2018. [Online]. Available: https://neoplc.org/. [Accessed 20 October 2018].

[124] P. Leo, T. Shield and O. Bruno, "Transient heat transfer effects on the pseudoelastic behavior of shape-memory wires," *Acta metall. mater,* vol. 41, no. 8, pp. 2477-2485, 1993.

[125] M. Zako, Y. Uetsuji and T. Kurashiki, "Finite Element Analysis of Damaged Woven Composite Materials," *Composites Science and Technology,* vol. 63, pp. 507-516, 2003.

[126] J. Whitcomb, "Three-Dimensional Stress Analysis of Plain Weave Composites," in *Composite Materials Fatigue and Fracture (Third Volume)*, Philadelphia, American Society for Testing and Materials, 1991, pp. 417-438.

[127] W. Cross, A. Kariotis and F. Stimler, "Nitinol Characterization Study," NASA, Akron, 1969.

[128] A. Teplitskiy, "Student Corner: Shape Memory Alloys," The Triz Journal, 2018. [Online]. Available: https://triz-journal.com/student-corner-the-applications-of-shape-memory-alloys/. [Accessed 15 October 2018].

[129] J. M. M. Components, "Measuring Transformation Temperatures in Nitinol Alloys," Johnson Matthey Medical Components, 2018. [Online]. Available: http://jmmedical.com/resources/211/Measuring-Transformation-Temperatures-in-Nitinol-Alloys.html. [Accessed 15 October 2018].

[130] T. Duerig, "Nitinol Ms vs Ni content," October 2 2009. [Online]. Available: https://commons.wikimedia.org/wiki/File:Nitinol_Ms_vs_Ni_content.jpg. [Accessed 15 October 2018].

[131] J. M. M. Components, "Nitinol Technical Properties," 2018. [Online]. Available: http://jmmedical.com/resources/221/Nitinol-Technical-Properties.html. [Accessed 25 October 2018].

[132] T. Sterzl and e. al, "Bistable shape memory thin film actuators," *SPIE,* vol. 101, no. 9, p. 5053, 2003.

[133] H. Tobushi, S. Hayashi, K. Hoshio, Y. Makino and N. Miwa, "Bending actuation characteristics of shape memory composite with SMA and SMP," *Intell Mater Syst Struct,* vol. 17, pp. 1075-1081, 2006.